

Nazanin Davari

Molecular modeling of ionization processes relevant for electrically insulating liquids

Thesis for the degree of Philosophiae Doctor

Trondheim, May 2015

Norwegian University of Science and Technology
Faculty of Natural Sciences and Technology
Department of Chemistry

NTNU
Norwegian University of Science and Technology

Thesis for the degree of Philosophiae Doctor

Faculty of Natural Sciences and Technology
Department of Chemistry

© Nazanin Davari

978-82-326-0938-3 (print)
978-82-326-0939-0 (digital)
1503-8181

Doctoral theses at NTNU, 2015:141

Printed by NTNU Grafisk senter

Preface

This thesis is a part of requirements for the Philosophiae Doctor degree at the Norwegian University of Science and Technology (NTNU). The thesis represents four years of my research at NTNU in 2011-2015. The research has been done under the supervision of professor Per-Olof Åstrand.

The importance of having knowledge about molecular properties of insulating materials is becoming increasingly evident when studying the mechanisms of pre-breakdown and breakdown phenomena in insulation systems. A few parameters are studied using theoretical chemistry methods such as quantum mechanics and force-field models. The thesis contains three chapters. Chapter 1 is an introduction to the electrical breakdown processes in insulating liquids and the studied molecular parameters, i.e. ionization potential, excitation energy and local electric field factor. Chapter 2 summarizes the theoretical methods for the determination of these parameters. The conclusions are given in chapter 3 and finally the papers included in the thesis are presented.

Trondheim, May 2015
Nazanin Davari

Acknowledgements

At first I would like to express my gratitude to those who contributed in conducting this research; My supervisor, Professor Per-Olof Åstrand, who has guided me thoroughly during my PhD study so that I could accomplish this work. My co-supervisor, Dr. Mikael Unge, and my former co-supervisor, Dr. Stian Ingebrigtsen, are acknowledged for their fruitful comments on the papers and in connecting this theoretical research with experiments. I kindly appreciate experimental team at SINTEF Energy, Lars E. Lundgaard and Dr. Dag Linhjell. The discussions in our bi-weekly video meetings with ABB Corporate Research in Västerås were inspiring for me in the progress of my research. I appreciate Professor Erling Ilstad for teaching electrical conductivity and breakdown phenomena which were very useful when writing the thesis.

I would like to thank Norwegian Research Council, ABB and Statnett which have been the sources of fundings. Special thanks should be given to faculty members and fellow PhD students at department of chemistry. Dr. Christopher D. Daub is thanked for his energetic and plentiful assistance and proofreading the thesis.

I would appreciate the intellectual support of people who have important role in my life; My endless gratitude to my parents for sending their warm support from a long distance and who always wish me success in life and I really thank my family members for their weekly loving phone calls.

Thanks to all my lovely friends in Trondheim for all the beautiful moments that we had together.

Finally, I would like to thank my love, Amir, whose calmness and confidence provided me a relaxed mind to focus on my research. Thank you for motivating me to work with full energy and always being by my side.

Abstract

Insulating liquids are often used as a dielectric barrier between two electrodes in high-voltage devices and may suffer a breakdown in high electric fields. Breakdown happens when a conductive plasma channel, a streamer, is created in high field regions which propagates through the barrier and bridges the gap between two electrodes. This phenomenon is influenced by the field-dependent molecular properties of the insulating liquid. Among the different properties, the molecular ionization potential (IP) and excitation energies are investigated for molecules relevant for insulating liquids. It is demonstrated how density functional theory (DFT) can be used to propose suitable molecules for the design of new insulating liquids. A model based on constrained DFT is developed for the calculation of field-dependent IP and time-dependent DFT is used to study a few lowest excitation energies in the field. For a dielectric liquid in the electric field, energy is added continuously to the liquid. The liquid releases energy by emitting heat or light in the UV/VIS region. Thus, the excitation energies of molecules in liquids may be important in the streamer experiments. The IP decreases strongly with increasing the field, while the excitation energies are weakly dependent on the field. There is a threshold field for different types of molecules that above it a two-state system consisting of the electronic ground state and the ionized state is obtained.

The local electric field is an important parameter in modeling the streamer behavior and is different from the external electric field. A force-field model is developed to calculate the response of the local field to the external field (local field factor). The local field factors are calculated for liquid benzene by combining the force-field model with the molecular dynamics simulations. The local field factor increases significantly at the absorption frequency for liquid benzene. The force-field model can also be used to calculate different dielectric properties of liquids.

List of publications

Included in the thesis:

Journal publications

1. N. Davari, P.-O. Åstrand, S. Ingebrigtsen, and M. Unge, "Excitation energies and ionization potentials at high electric fields for molecules relevant for electrically insulating liquids," *J. Appl. Phys.* 113, 143707, 2013
2. N. Davari, P.-O. Åstrand, and T. Van Voorhis, "Field-dependent ionization potential by constrained density functional theory," *Mol. Phys.* 111, 1456-1461, 2013
3. N. Davari, P.-O. Åstrand, M. Unge, L. E. Lundgaard, and D. Linhjell, "Field-dependent ionization potentials and excitation energies: Implications for electrically insulating liquids," *AIP Adv.* 4, 037117, 2014
4. N. Davari, P.-O. Åstrand, and M. Unge, "Density-functional calculations of the field-dependent ionization potential and excitation energies of aromatic molecules," *Chem. Phys.* 447, 22-29, 2015
5. N. Davari, Sh. Haghani, P.-O. Åstrand, and G. C. Schatz, "Local electric field factors by a combined charge-transfer and point-dipole interaction model," *RSC Adv.*, 5, 31594-31605, 2015
6. N. Davari, C. D. Daub, P.-O. Åstrand, and M. Unge, "Local electric field factors and dielectric properties of liquid benzene," *Manuscript*

Not included in the thesis:**Journal publications**

- Sh. Haghani, N. Davari, R. Sandnes, and P.-O. Åstrand, "Complex frequency-dependent polarizability through the $\pi \rightarrow \pi^*$ excitation energy of azobenzene molecules by a combined charge-transfer and point-dipole interaction model," *J. Phys. Chem. A* 118, 11282, 2014

Conferences in proceedings

- N. Davari, P.-O. Åstrand, M. Unge, L. E. Lundgaard, and D. Linhjell, "Field-dependent ionization potentials and excitation energies of molecules of relevance for electrically insulating liquids," IEEE Conference on Electrical Insulation and Dielectric Phenomena (CEIDP), Shenzhen, China, October 2013, DOI:10.1109/CEIDP.2013.6748207
- N. Davari, P.-O. Åstrand, and M. Unge, "Atomistic simulations of local electric field in dielectric liquids," IEEE 18th International Conference on Dielectric Liquids (ICDL), Bled, Slovenia, July 2014, DOI:10.1109/ICDL.2014.6893141
- N. Davari, P.-O. Åstrand, and M. Unge, "Field-dependent ionization potential for polyaromatic molecules," IEEE 18th International Conference on Dielectric Liquids (ICDL), Bled, Slovenia, July 2014, DOI:10.1109/ICDL.2014.6893142
- N. Davari, Sh. Haghani, and P.-O. Åstrand, "Frequency-dependent local field factors in dielectric liquids by a polarizable force field and molecular dynamics simulations", 11th international conference of computational methods in sciences and engineering (ICCMSE), Athens, Greece, March 2015, AIP proceedings, to be published

The works in papers are carried out by N. Davari and also the first draft of all manuscripts included in the thesis are written by N. Davari. The Molecular dynamics simulations in paper 6 are performed by C. D. Daub. The works are supervised by P.-O. Åstrand. The co-authors are contributed in suggesting relevant molecules to study, reading and commenting the manuscripts.

Contents

Preface	i
Acknowledgements	iii
Abstract	v
List of publications	vii
1 Introduction	1
1.1 Electrical breakdown in insulating liquids	3
1.2 Ionization potential	6
1.3 Excitation energy	11
1.4 Local electric field factor	13
2 Methodology	17
2.1 Density functional theory	19
2.1.1 Constrained density functional theory	20
2.1.2 Time-dependent density functional theory	23
2.2 Force-field models	25
2.2.1 Charge-transfer and point-dipole interaction model .	26
3 Summary and future work	33
Bibliography	37
Papers	45



Chapter 1

Introduction

1.1 Electrical breakdown in insulating liquids

Insulating materials are used in high-voltage devices such as transformers, reactors, cables, circuit breakers, etc. They are divided into different types, solid insulation, liquid insulation, gas insulation and also combinations of these as for example in oil-paper cables. Liquids are often preferred to solids since they perform a double duty, as an insulator to prevent electric current or withstand electric voltage and as a coolant to prevent overheating. Compared to gases, liquids are more dense which could result in higher breakdown voltages. In this thesis, we are interested in liquid insulations.

In high electric fields, insulating liquids may begin to conduct electricity due to dielectric breakdown. Breakdown happens at a threshold field when a conductive plasma channel, a “streamer”, bridges the gap between the two electrodes and short-circuits the voltage gap [1]. The threshold field that the liquid can withstand without breakdown is called the “dielectric strength”. Therefore, liquids with high dielectric strengths are desirable. Breakdown often causes irreversible chemical and physical changes in the liquid. Gas insulation in most cases recovers after breakdown but for the liquid, it depends on the amount of energy that is released which causes high temperatures at the breakdown site. The liquid must have a low dielectric loss in order to transport the heat through the insulation. In high-voltage systems, dielectric loss is in general the result of the generation of heat by a high current load on the conductors which increases with increasing temperature. If too much dielectric loss occurs, the applied voltage needs to be reduced in order to avoid overheating.

There are different types of insulating liquids; (i) mineral oil consisting of paraffinic hydrocarbons with the general formula of C_nH_{2n+2} , naphthenic hydrocarbons with the formula of C_nH_{2n} , and other aromatic and polyaromatic molecules, (ii) vegetable oil including triglyceride molecules and (iii) synthetic insulating liquids such as esters and silicone-based liquids. Experimental investigations are under way to study ester liquids that can be used as alternatives to mineral oil, due to their better environmental performance and biodegradability [2–4].

In high electric fields, several molecular processes may take place in insulating liquids that can affect the pre-breakdown and breakdown phenomena. Molecular ionization, electron attachment, electronic excitation, photoionization, molecular dissociation, etc. are some examples. These

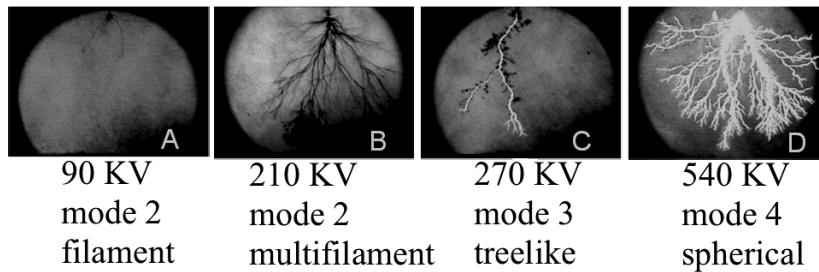


Figure 1.1: Typical streamer shapes in Exxsol in a needle-plane geometry of electrodes. Taken from Ref. [6].

processes can be studied by molecular modeling approaches. Molecular modeling includes all the theoretical and computational methods used to model the behavior of molecules. It is not only helpful in interpreting the behavior of liquids, but also in predicting and improving the performance of the liquids in their application as insulators.

It is useful to study the composition and shape of the streamer in order to better understand the breakdown phenomenon. Electrical breakdown is associated with light emission. The emitted light has been analyzed and the spectrum displays broadened hydrogen lines and vibration/rotation band profile of the diatomic carbon (C_2) molecules [5]. Figure 1.1 shows different shapes of the positive streamer in a mineral oil, Exxsol, in different applied voltages [6]. Exxsol is a well-known low aromatic content mineral oil. The images are captured just before breakdown except case A. The streamer has different shapes depending on the applied voltage and the composition of the liquid and it propagates in different modes [7,8]. The first slow mode takes place between initiation and breakdown voltages and the fast mode takes place above the breakdown levels. As shown in the figure, at 90 KV, it has a filamentary shape containing thin channels, while it is considerably changed upon increasing the voltage from 210 KV to 270 KV. The streamer is reduced to a few main branches and short-length side-branches at 270 KV, forming a tree-like shape. At 540 KV, it has a spherical shape due to a relatively large number of branches.

In the needle-plane geometries of electrodes, the electronic properties of the insulating liquids including small amounts of additives affect the properties of the streamer originating from a positive or negative voltage on the needle electrode [1,9–12]. Positive streamers initiate from the positively charged needle electrode, while negative streamers initiate from

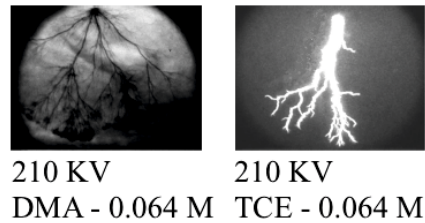


Figure 1.2: Effect of DMA and TCE on branching of the streamer in Exxsol. Taken from Ref. [6].

a negatively charged needle electrode. It has been found that electron-acceptor additives increase the velocity of negative streamers, while additives with low ionization potential (IP) speed up positive streamers [1]. Figure 1.2 shows the effect of additives on the positive streamer in Exxsol. By adding 0.064 M N,N-dimethylaniline (DMA) and 0.064 M trichloroethylene (TCE) to clean Exxsol, the streamer shape at 210 KV changes significantly as compared to clean Exxsol shown in Figure 1.1. DMA is a low-IP additive (IP=7.12 eV [paper 1]), while TCE is an electron acceptor additive that is used frequently in streamer experiments. As shown in the figure, DMA increases the branches, whereas TCE reduces the number of branches.

The IP is a field-dependent property that influences pre-breakdown and breakdown in liquids [13,14]. In a recent work, the effect of DMA on white oil (Exxsol-D140 and Marcol-52) has been studied in a long point-to-plane gap between the electrodes [15]. White oil is a highly refined and hydrogenated mineral oil free from polyaromatic compounds. It is found that DMA increases the streamer branching and velocity at low voltages. The branching spreads as voltage increases resulting in a shielding effect which reduces the electric field in front of the streamer channels. Therefore, the speed of the streamer decreases at a specific voltage.

Polyaromatic molecules have lower IPs than paraffinic and naphthenic ones and investigations have shown that they affect the breakdown processes in cyclohexane (as a base insulating liquid) by increasing the acceleration voltage of fast mode positive streamers [9]. The propagation velocity of streamers increases almost constantly as voltage increases, while above a specific voltage, i.e. acceleration voltage, the streamer velocity increases abruptly.

In addition to insulating liquids, there are several studies on the pre-breakdown and breakdown phenomena in pure water, due to its relatively high breakdown strength [16–18]. The results show that positive streamers in water with filamentary shape at lower voltages are comparable to the streamers in mineral oil at higher voltages.

Studying the behavior of molecules is important at the tip of the streamer where the local electric field is relatively high in this small volume (around a few μm^3). Molecular modeling is a valuable method for understanding the molecular behavior at small scale. In this thesis, molecular modeling via quantum chemical methods is used to study the IP of molecules relevant for insulation applications.

It has been suggested that the molecular excitation energies could affect streamer propagation [2, 13]. The influence of additives with low excitation energies has been investigated in an experimental work [2] where azobenzene and DMA were added to an ester liquid and it was shown that azobenzene causes a significant increase in the acceleration voltage in comparison with DMA, which could be the result of the low excitation energy of azobenzene (2.21 eV [paper 1]).

The molecular properties of insulating liquids that are important in breakdown processes may include ionization potential, electron affinity, excitation energy, polarizability, dissociation energy, etc. In a breakdown process, the molecules may be ionized or dissociated into ions, both of which are unfavorable phenomena, since they speed up the breakdown process. Also, the molecules can be excited which is often favorable depending on the lifetime of the excited states. Some of the molecules studied in this work are summarized in Table 1.1. A set of paraffinic, naphthenic, aromatic and ester molecules relevant for streamer experiments are included as well as a few diketones and azo dyes with relatively low excitation energies. Our purpose is to demonstrate how quantum chemical methods may be used to suggest suitable additives or base insulating liquids with respect to their IP and excitation energy.

1.2 Ionization potential

The IP of a molecule is the energy required to remove an electron from a molecule and create a cation. The definition of the IP in zero field is different from its definition in an electric field. The zero-field IP is calculated as a dissociation energy where the electron is located at an infinite

Table 1.1: Vertical gas-phase IP and lowest excitation energy (eV).

molecule	IP ¹	excitation energy ²
water	12.65 ^a	6.42 ^b
ethane	12.67 ^a	7.67 ^b
<i>n</i> -pentane	9.90 ^b	7.02 ^b
<i>n</i> -tridecane	9.41 ^a	7.08 ^a
9,10-dimethyloctadecane	8.38 ^b	6.16 ^b
<i>n</i> -eicosane	8.34 ^b	6.25 ^b
cyclohexane	10.22 ^a	7.11 ^a
ethene	10.59 ^a	6.44 ^a
1-pentene	9.33 ^b	5.65 ^b
trichloroethene	9.14 ^b	4.92 ^b
tetrakis(dimethylamino)ethene	7.49 ^b	3.77 ^b
benzene	9.63 ^a	5.41 ^a
N,N-dimethylaniline	7.12 ^b	4.00 ^b
tetramethyl-1,4-phenyldiamine	6.20 ^a	3.64 ^a
2,6-di- <i>tert</i> -butyl- <i>p</i> -cresol	7.51 ^a	4.79 ^a
flavone	8.19 ^a	3.48 ^a
pyrene	7.16 ^a	3.66 ^a
<i>p</i> -benzyltoluene	7.99 ^a	5.00 ^a
propylene carbonate	10.81 ^a	6.97 ^a
methyl butyrate	10.13 ^a	5.88 ^a
2-butenylethanoate	8.76 ^b	5.23 ^b
1,3-butenylethanoate	8.45 ^b	4.31 ^b
octylethanoate	8.78 ^b	5.35 ^b
1,3-pentenylmethanoate	8.18 ^b	4.00 ^b
glyceryltributyrate	8.45 ^b	5.09 ^b
benzil	8.62 ^a	2.89 ^a
<i>cis</i> -skew 4,4'-dihydroxybenzil	8.43 ^a	2.93 ^a
<i>trans</i> -planar 4,4'-dihydroxybenzil	8.15 ^a	2.46 ^a
2,3-heptanedione	9.03 ^a	2.69 ^a
<i>p</i> -benzoquinone	9.84 ^a	2.51 ^a
anthraquinone	9.30 ^a	2.93 ^a
<i>trans</i> -azobenzene	7.82 ^b	2.21 ^b

¹ IPs are calculated by density functional theory using ^athe B3LYP functional/cc-pVTZ basis set and ^b the PBE functional/TZP basis set.

² Excitation energies are calculated by time-dependent DFT using ^a the B3LYP functional/aug-cc-pVTZ basis set and ^b the PBE functional/aug-TZP basis set.

distance from a molecular cation,

$$IP_0 = U_{A^+} - U_A \quad (1.1)$$

where U_A and U_{A^+} are the energies of molecule A and its cation, respectively.

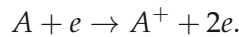
The IP in the electric field has been calculated once in a numerical approach for the hydrogen molecule and the molecular hydrogen cation using a classical theory for ionized atoms [19]. The critical fields for ionization were obtained by varying the distance between the nuclei of the molecule or the cation and the electron parallel to the external electric field. The reported critical field for ionization of a hydrogen molecule was 3.6 MV/cm with the electron at a distance of 2.34 Å.

In this thesis, to calculate the field-dependent IP a potential energy barrier needs to be determined from the interaction energy between a cation and an electron which are considered as a combined neutral system to avoid the origin dependence of the energy of an ion in an electric field. The field-dependent IP (IP_E) is defined as

$$IP_E = U_{A^{++e}} - U_A \quad (1.2)$$

where $U_{A^{++e}}$ is the potential energy barrier and U_A is the energy of molecule A in the field. The electric field decreases the energy barrier, and if the energy of an electron is greater than the energy of the barrier, the electron dissociates from the molecule. Figure 1.3 shows the interaction energy between the benzene cation and the electron as a function of the distance between them for the z -direction electric fields between 0 and 30.84 MV/cm. The interaction barrier is located closer to the cation with increasing electric field. The barrier maximum is around 20 Å at 1.03 MV/cm, while it is at around 4 Å at 30.84 MV/cm.

At high electric fields, ionization is one of the molecular processes involved in conductivity of the insulating liquids and the streamer propagation. There are different ionization mechanisms: impact ionization, photoionization and field ionization and the IP is an important parameter in all of them [13]. If the energy of an electron in the liquid is higher than the IP of the base liquid, impact ionization takes place,



In the photoionization mechanism, a photon with an energy equal to or

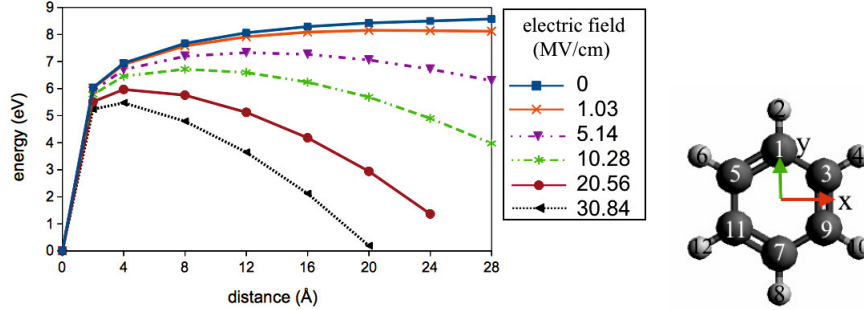


Figure 1.3: The interaction energy between the benzene cation and the electron as a function of distance in the z -direction of electric field (MV/cm) calculated by constrained DFT/B3LYP functional with the cc-pVDZ basis set. Taken from paper 4

higher than the IP of the molecule is absorbed by a molecule and an electron is released,



Field ionization is based on the tunneling phenomenon and is only dependent on the local electric field. At very high electric fields, the potential barrier becomes very thin and the electrons tunnel through the barrier instead of going over it. Either of these mechanisms may be dominant in one of the different modes of streamer propagation.

It has been shown by DFT calculations using a point-charge model that the IP decreases strongly with increasing the field [13]. In this model, an electron is regarded as a negative point charge and it has been found that the decrease of the potential barrier is proportional to the square root of the electric field, in agreement with the classical Poole-Frenkel effect describing the excitation of an electron to the conduction band at high electric fields [20],

$$IP_E = IP_0 - 2\sqrt{\frac{E}{\epsilon_r}} \quad (1.3)$$

where E is the external electric field and ϵ_r is the relative permittivity of the liquid, respectively. In the Poole-Frenkel mechanism, the electric current is due to the release of electrons from donor states within the bulk insulator. The potential barrier is lowered by the external electric field. The current, I , is proportional to

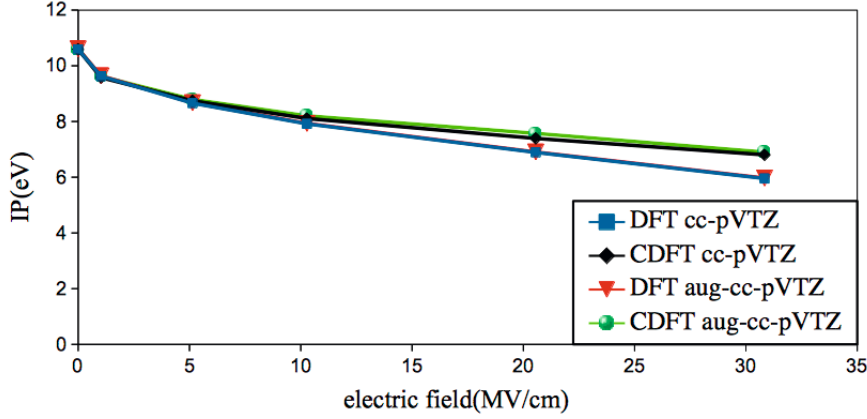


Figure 1.4: Field-dependent IP of ethene calculated by the B3LYP functional in the electric field parallel to the π -bond. Taken from paper 2.

$$I \propto I_0 e^{\frac{\beta_{PF} E^2}{k_B T}} \quad (1.4)$$

where the factor I_0 is dependent on the number of electrons involved in the conduction, the potential barrier, mobility, etc. β_{PF} is the Poole-Frenkel coefficient depending on the charge and permittivity. k_B and T are the Boltzmann's constant and temperature, respectively. In the Poole-Frenkel mechanism, the potential barrier is given as

$$U(r) = \frac{-q^2}{4\pi\epsilon_0\epsilon_r r^2} - \beta_{PF} E^{\frac{1}{2}} \quad (1.5)$$

where q is the electronic charge, ϵ_0 is the vacuum permittivity and r is the insulation thickness. Thus, the decrease of the potential barrier is equal to $\beta_{PF} E^{\frac{1}{2}}$.

In this work, constrained density functional theory (CDFT) is used to find the interaction energy barrier as shown in Figure 1.3 and afterwards the field-dependent IP is calculated from Eq. 1.2. Figure 1.4 shows the field-dependent IP of ethene in the field parallel to the π bond calculated by the CDFT method and the previous point-charge model denoted by DFT in the figure. Both methods have similar behavior up to 10 MV/cm while at fields higher than 10 MV/cm, the difference between the two methods becomes more significant.

1.3 Excitation energy

Excitation energy is an energy required to transfer an electron from the ground state to a higher energy bound state, i.e. the excited state. Ultraviolet/visible light spectroscopy is used to determine the wavelength and intensity of the electronic transitions. Theoretically, excitation energy is obtained from the poles of response function that will be explained in Section 2.1.2. Excitation energies may influence the ionization mechanisms in insulating liquids [13]. Figure 1.5 shows a sketch of possible ionization mechanisms in the field for DMA. The exact field values are not meaningful, but in general these processes may occur around the indicated field strengths as the field increases. The two excitation energies are around 4 and 5 eV, respectively, and they remain almost constant in the field, while the IP decreases strongly with increasing the field. The zero energy level indicates the ground state. In the field, there are two possible routes for a liquid to lose its added energy; (i) by emitting heat in the infrared region or (ii) light in the ultraviolet/visible light region. Excitation mechanisms are by electron impact or by photon absorption. The possible excitation/ionization processes are as follow:

1. Photoexcitation: At relatively low electric fields, the electron is excited by photon absorption. The energy of the photon is too low to cause photoionization.
2. Electron impact excitation: The energy of the electron is higher than the excitation energy of the liquid.
3. Two-step ionization process: The excited molecule can be ionized when the life-times of excited states are longer than the frequency of either electron impact or photon absorption.
4. Photoionization: The photon energy is higher than the IP of the molecule.
5. Field ionization: At very high electric fields, electron tunneling takes place.

The actual mechanism has not been recognized yet and it probably varies from liquid to liquid depending on the chemical composition of the liquid. However, it could be predicted that in general additives with low

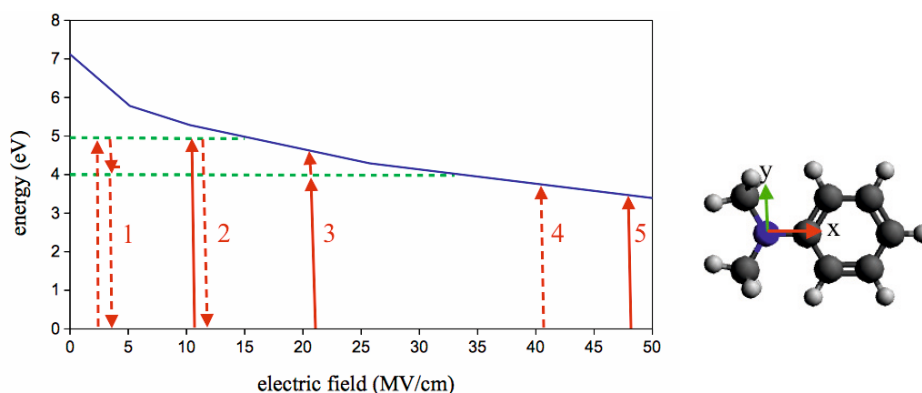


Figure 1.5: The IP and excitation energies (eV) in the field for DMA. The solid line shows the IP and the green dashed lines are the two lowest excited states. Possible ionization processes may take place that are shown by numbers. Solid arrows denote an electron impact process and dashed arrows denote light. Taken from paper 1.

excitation energies and relatively short life-times will improve the insulating properties of a liquid because they can postpone the ionization of liquid which is responsible for the electrical breakdown.

Above a threshold field the excited states are no longer available, i.e. a two-state system is obtained with the ground state and the ionized state. Due to the strong field dependence of the IP a high-energy photon may be generated in a low-field region which may lead to ionization in a high-field region.

Since the IP has a stronger field dependence, the number of available excited states decreases with increasing field which may have a strong impact on the insulating properties of the liquid. At a threshold field, different for different types of molecules, all the excited states of the molecule disappear which could be the molecular origin of different streamer modes. Figure 1.6 indicates that the lowest unoccupied molecular orbital (LUMO) of *trans*-azobenzene, π^* orbital, changes into an unbound state at fields higher than 51.4 MV/cm.

For alkanes the threshold field is lower than for esters, diketones, azo dyes and polyaromatic molecules. For molecules with many low excitation energies, e.g. azo dyes, some excited states survive at higher fields as compared to molecules with only a few relatively high excitation energies.

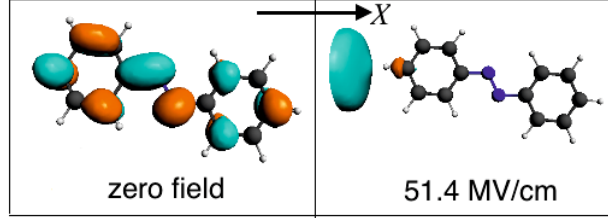


Figure 1.6: π^* orbital of *trans*-azobenzene at zero field and 51.4 MV/cm in the x -direction of the field. Taken from paper 1.

1.4 Local electric field factor

An electron avalanche may be initiated from a hot spot, i.e. a point with a relatively high local electric field. In the electron avalanche process a number of free electrons accelerate in the electric field and subsequently collide with the molecules and ionize them, releasing more electrons that can lead to the formation of a streamer and an electrical breakdown. Therefore, the local electric field is an important factor in modeling the streamer behavior as well as deducing the actual molecular IP of insulating liquids. In this thesis, molecular modeling is used to develop a model based on a force-field approach to calculate the local field response to the external field (local field factor).

When the external electric field is applied, an electronic polarization takes place in a dielectric liquid resulting in a local electric field that is different from the external field. The Lorentz approach has been used frequently as an approximate method to determine the local electric field [21]. In this approach, the local field at a certain point of a dielectric is the same as that inside a fictive sphere. However, the Lorentz model is limited to non-polar materials where it is assumed that the contribution of electric dipoles inside the sphere is zero. For the external field applied in the z -direction, E_z^{ext} , the resulting polarization, P_z , leads to a Lorentz local field defined as

$$E_z^{\text{loc}} = E_z^{\text{ext}} + \frac{4\pi}{3} P_z. \quad (1.6)$$

The macroscopic polarization is given in terms of the molecular induced dipole moments [22,23],

$$P_z = N_d \langle \mu_\alpha \rangle_z = N_d \langle \alpha_{\alpha\beta}^{\text{mol}} \rangle E_z^{\text{loc}} \quad (1.7)$$

where α and β denotes the Cartesian coordinates. N_d is the number density and $\langle \alpha_{\alpha\beta}^{\text{mol}} \rangle = \frac{1}{3}(\alpha_{xx} + \alpha_{yy} + \alpha_{zz})$ is the isotropic polarizability. Eq. 1.7 relates the macroscopic quantity, P_z , to the microscopic quantity, $\langle \alpha_{\alpha\beta}^{\text{mol}} \rangle$.

We may have different types of polarization in dielectrics:

1. Electronic polarization at ultraviolet/visible light frequencies: The electronic charge distribution is perturbed in the external field. This type of polarization is of interest in this work.
2. Atomic polarization limited to frequencies up to infrared region: The positive and negative charge centers on atoms align with the electric field resulting in deformation of atomic orbitals.
3. Orientational polarization takes place where molecules with permanent dipole moments align their dipoles with the direction of the electric field.
4. Space-charge polarization arises due to movement of charge carriers building up a continuum of charges distributed over a region of space in the bulk of the insulating liquid.

The determination of electronic polarization from an atomistic point of view requires knowledge of the local field at the atoms of the dielectric. To obtain the local field, the electrostatic energy, V_{ele} , between two multipole charge distributions of atoms I and J is given as [24]

$$V_{ele} = q_I T_{IJ}^{(0)} q_J - q_I T_{IJ,\alpha}^{(1)} \mu_{J,\alpha} + \mu_{I,\alpha} T_{IJ,\alpha}^{(1)} q_J \quad (1.8)$$

where q_I is the atomic charge and $\mu_{I,\alpha}$ is the atomic dipole moment. The higher multipole moments are disregarded. $T_{IJ}^{(0)}$ and $T_{IJ,\alpha}^{(1)}$ are the charge-charge and charge-dipole interaction tensors, respectively,

$$T_{IJ}^{(0)} = \frac{1}{R_{IJ}} \quad (1.9)$$

$$T_{IJ,\alpha}^{(1)} = \nabla_\alpha T_{IJ}^{(0)} = \frac{-R_{IJ,\alpha}}{R_{IJ}^3} \quad (1.10)$$

where $R_{IJ,\alpha} = R_{I,\alpha} - R_{J,\alpha}$ and $R_{I,\alpha}$ is the coordinate of atom I . Since $R_{IJ,\alpha} = -R_{JI,\alpha}$, we have $T_{JI} = (-1)^n T_{IJ}$, where n is the rank of the tensor.

The potential at atom I, ϕ_I , is defined as

$$\phi_I = \sum_{J \neq I}^N (T_{IJ}^{(0)} q_J - T_{IJ,\alpha}^{(1)} \mu_{J,\alpha}). \quad (1.11)$$

The electric field arising from the permanent and induced multipole moments of surrounding atoms is

$$E_{I,\alpha}^{\text{pol}} = -\nabla_{\alpha} \phi_I = \sum_{J \neq I}^N -T_{IJ,\alpha}^{(1)} q_J + T_{IJ,\alpha\beta}^{(2)} \mu_{J,\beta} \quad (1.12)$$

where $T_{IJ,\alpha\beta}^{(2)}$ is determined by

$$T_{IJ,\alpha\beta}^{(2)} = \nabla_{\beta} T_{IJ,\alpha}^{(1)} = \frac{3R_{IJ,\alpha} R_{IJ,\beta} - \delta_{\alpha\beta} R_{IJ}^2}{R_{IJ}^5}. \quad (1.13)$$

The local field at an atom is

$$E_{I,\alpha}^{\text{loc}} = E_{I,\alpha}^{\text{ext}} + E_{I,\alpha}^{\text{pol}}. \quad (1.14)$$

The calculated local field is divided into the charge contribution and the dipole contribution. The local field response to the external field (local field factor) is calculated by

$$\frac{\partial E_{I,\alpha}^{\text{loc}}}{\partial E_{I,\gamma}^{\text{ext}}} = \delta_{\alpha\gamma} + \sum_{J \neq I}^N -T_{IJ,\alpha}^{(1)} \frac{\partial q_J}{\partial E_{I,\gamma}^{\text{ext}}} + T_{IJ,\alpha\beta}^{(2)} \frac{\partial \mu_{J,\beta}}{\partial E_{I,\gamma}^{\text{ext}}}. \quad (1.15)$$

Figure 1.7 shows the local field factor of liquid benzene at hydrogen atom 2 in the y -direction of the homogenous external electric field ($E_{I,y}^{\text{ext}} = E_y^{\text{ext}}$). The static local field factor, $\partial E_{I,y}^{\text{loc}} / \partial E_y^{\text{ext}}$, is around 2.5, while at the absorption frequency it increases to around 6. The dipole contribution dominates over the charge contribution at lower frequencies, while they are comparable at the absorption frequency.

The local field model can also be used to calculate the relative permittivity and refractive index of different liquids [22]. For this purpose, the local-field model is combined with the Clausius-Mossotti equation [25]. The response of the macroscopic polarization to the external electric field gives the linear susceptibility, $\chi_{zz}^{(1)}$, used in the calculation of relative permittivity, defined as

$$\chi_{zz}^{(1)} = \frac{\partial P_z}{\partial E_z^{\text{ext}}} = \frac{N_d \langle \alpha_{\alpha\beta}^{\text{mol}} \rangle}{1 - \frac{4\pi}{3} N_d \langle \alpha_{\alpha\beta}^{\text{mol}} \rangle}. \quad (1.16)$$

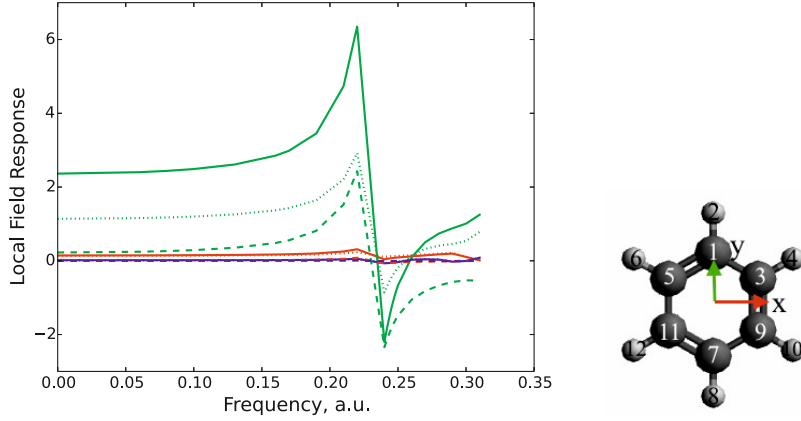


Figure 1.7: The largest local field response to the y -direction of the external field of the liquid benzene at hydrogen atom 2. The green line is $\frac{\partial E_{I,y}^{\text{loc}}}{\partial E_y^{\text{ext}}}$ and the red and blue lines are $\frac{\partial E_{I,x}^{\text{loc}}}{\partial E_y^{\text{ext}}}$ and $\frac{\partial E_{I,z}^{\text{loc}}}{\partial E_y^{\text{ext}}}$, respectively. The dashed line is the charge contribution and the dotted line is the dipole contribution. (1 a.u = 27.21 eV) Taken from paper 6.

The relative permittivity is given as

$$\epsilon = 1 + 4\pi\chi_{zz}^{(1)}. \quad (1.17)$$

The refractive index is then calculated from the square root of the relative permittivity.

To summarize, the effect of field-dependent IP, excitation energy and high local fields on the breakdown phenomenon has been discussed. The IP and excitation energy of different types of molecules are investigated to suggest suitable liquids to be used as insulators. In an insulating liquid, we should avoid hot spots where the local electric field is high since at hotspots, the probability of electrical breakdown can increase. Therefore, the linear response of the local field to the external field is studied to find the hot spots in liquids. In general, we are looking for possibilities that could reduce the risk of electrical breakdown in insulating liquids.

Chapter 2

Methodology



Molecular properties can be described by molecular modeling approaches such as quantum chemistry using molecular orbital methods and density functional theory (DFT). The basis of the molecular orbital approaches is the Hartree-Fock approximation but these approaches are usually expensive computationally for relatively large systems. DFT on the other hand is applicable to large systems, but its limitation is that the exchange-correlation part of the energy functional is not known exactly. Force-field models are rapid ways of calculating molecular properties based on atom-type-parameters and they are the standard models used in molecular dynamics simulations. In this chapter, the DFT-based methods are used to calculate the IP and excitation energies of molecules suitable for insulating liquids. Also, a force-field model is described which is used to calculate local field factors in insulating liquids.

2.1 Density functional theory

Density is a physical observable which forms the basis of DFT [26]. The DFT method is extensively used to calculate electronic ground state properties. Kohn and Sham proposed a method to evaluate the density of systems [27]. In the Kohn-Sham (KS) approach, the electrons obey a one-particle Schrödinger equation with an effective external potential. The Kohn-Sham electronic energy is written as

$$E[\rho] = \sum_{\sigma} \sum_i^{\alpha\beta} \langle \phi_{i\sigma} | -\frac{\nabla^2}{2} | \phi_{i\sigma} \rangle + \int v_{\text{ext}}(\mathbf{r})\rho(\mathbf{r})d\mathbf{r} + J[\rho] + E_{xc}[\rho] \quad (2.1)$$

where ρ is the electron density, $\phi_{i\sigma}$ is the lowest energy orbital with σ spin and $N = \sum_{\sigma} N_{\sigma}$ is the total number of electrons. J and E_{xc} are the classical coulomb energy of the interaction between the electrons,

$$J[\rho] = \frac{1}{2} \int \frac{\rho(\mathbf{r})\rho(\mathbf{r}')}{|\mathbf{r} - \mathbf{r}'|} d\mathbf{r}d\mathbf{r}' \quad (2.2)$$

and the exchange-correlation energy, respectively, and v_{ext} is the external potential. All the many-body effects are contained in the E_{xc} term which is the fundamental approximation in DFT. The local density approximation (LDA) and the generalized gradient approximation (GGA) are the standard choices of approximation methods [27].

The KS equations are as follows,

$$\left[-\frac{\nabla^2}{2} + v_{\text{ext}}(\mathbf{r}) + \int \frac{\rho(\mathbf{r}')}{|\mathbf{r}-\mathbf{r}'|} d\mathbf{r}' + v_{xc\sigma}(\mathbf{r})\right]\phi_{i\sigma} = \epsilon_{i\sigma}\phi_{i\sigma} \quad (2.3)$$

where $v_{xc\sigma}$ is the derivative of E_{xc} with respect to the density. Eq. 2.3 must be solved in a self-consistent (SC) procedure. With an initial guess of the electron density, the equations are solved to obtain a set of orbitals from which a new density is constructed. The process is repeated until the input and output densities are the same at convergence. The probability density $\rho(\mathbf{r})$ is obtained by summing the squares of the KS orbitals multiplying by their occupation numbers n_i ,

$$\rho(\mathbf{r}) = \sum_i^{\text{occ}} n_i |\phi_i(\mathbf{r})|^2. \quad (2.4)$$

The original DFT formulation can describe an electronic system at its ground state and zero temperature. Constrained DFT (CDFT) and time-dependent DFT (TDDFT) are two extensions of DFT that will be discussed further in Sections 2.1.1 and 2.1.2, respectively. In this thesis work, the CDFT and TDDFT methods are used for the calculation of the field-dependent ionization potential and excitation energies, respectively.

2.1.1 Constrained density functional theory

In CDFT, we minimize the energy of the system subject to a constraint on the electron density defined as [28]

$$\sum_{\sigma} \int w_c^{\sigma}(\mathbf{r}) \rho(\mathbf{r}) d\mathbf{r} = N_c \quad (2.5)$$

where $w_c^{\sigma}(\mathbf{r})$ acts as a weight function defining the constraint property and N_c is the constraint value. The CDFT energy functional for one constraint is

$$W[\rho, V_c] = E[\rho] + V_c \left(\sum_{\sigma} \int w_c^{\sigma} \rho(\mathbf{r}) d\mathbf{r} - N_c \right) \quad (2.6)$$

where $E[\rho]$ is the DFT energy functional (Eq. 2.1) and V_c is a Lagrange multiplier. Making W stationary under the condition that the orbitals are normalized, gives equations of the form

$$\left[-\frac{\nabla^2}{2} + v_{ext}(\mathbf{r}) + \int \frac{\rho(\mathbf{r}')}{|\mathbf{r}-\mathbf{r}'|} d\mathbf{r}' + v_{xc\sigma}(\mathbf{r}) + V_c w_c^\sigma(\mathbf{r})\right] \phi_{i\sigma} = \epsilon_{i\sigma} \phi_{i\sigma}. \quad (2.7)$$

These equations are the KS equations with the addition of the constraint potential $V_c w_c^\sigma(\mathbf{r})$ in the effective Hamiltonian. Eq. 2.7 can be solved in a SC procedure like in the KS equations. At each SC iteration, a set of input either from an initial guess or from the output of previous iterations, is used to construct the conventional KS Hamiltonian. With an initial value of V_c , $V_c w_c^\sigma(\mathbf{r})$ is added to form the full Hamiltonian. Then an optimization of V_c is carried out by,

1. Solving Eq. 2.7
2. Calculating the first derivative of W with respect to V_c to find the stationary point

$$\frac{\partial W}{\partial V_c} = \sum_{\sigma} \int w_c^\sigma \rho^\sigma(\mathbf{r}) d\mathbf{r} - N_c \quad (2.8)$$

where $\frac{\partial W}{\partial \phi_{i\sigma}} = 0$ is used. The stationary point returns the constraint in Eq. 2.5.

3. Second derivatives of W (Hessian) with respect to V_c are determined to find whether the stationary point is a maximum or minimum,

$$\frac{\partial^2 W}{\partial V_c \partial V_k} = \sum_{\sigma} \sum_i \sum_a \frac{\langle \phi_{i\sigma} | w_c^\sigma | \phi_{a\sigma} \rangle \langle \phi_{i\sigma} | w_k^\sigma | \phi_{a\sigma} \rangle}{\epsilon_{i\sigma} - \epsilon_{a\sigma}} \quad (2.9)$$

where the indices i and a go over occupied and virtual orbitals, respectively. The Hessian is nonpositive because for any V_c ,

$$\sum_{c,k} V_c \frac{\partial^2 W}{\partial V_c \partial V_k} V_k = 2 \sum_{\sigma} \sum_i \sum_a \frac{\langle \phi_{i\sigma} | w_c^\sigma | \phi_{a\sigma} \rangle^2}{\epsilon_{i\sigma} - \epsilon_{a\sigma}} \quad (2.10)$$

and since $\epsilon_{i\sigma} - \epsilon_{a\sigma} < 0$, the stationary point is a maximum.

4. V_c is updated in the last step. The optimization of V_c is complete when the constraint, i.e., Eq. 2.5, is satisfied. The obtained $\phi_{i\sigma}$ are used as input for the next SC iteration. Finally, this procedure results in the converged ground state of the constrained system [29].

By constraining the charges on molecular fragments in CDFT, long-range charge transfer (CT) states can be treated well, whereas TDDFT fails [29–31]. In TDDFT (explained in Section 2.1.2) the ground state is used as a reference state to calculate the CT states. It is problematic since the exact exchange functional is required to show the correct asymptotic behavior at long-range limits which is missing in the standard functionals. CDFT on the other hand yields the CT state directly with the CT state itself as the reference.

In addition to charge constraints, the net spin can also be constrained to obtain for example magnetic exchange couplings [32]. In this context, a complex AB is divided into two fragments A and B with spins s_A and s_B , respectively. The difference between the number of α and β electrons on A is considered as the constraint value of A and similarly the difference between the number of α and β electrons on B is the constraint value placed on B. The CDFT equations are then solved to determine the coupling strength between spins on fragments A and B.

There are a variety of population prescriptions for constraining the density in Eq. 2.5. Density based schemes, e.g. Voronoi method [33], Becke [34], Hirshfeld [35], and atomic orbital based schemes such as Mulliken [36] and Löwdin [37] can be used in CDFT. With a prescription for atomic charges in hand, one can build up the weight function, $w_c^\sigma(\mathbf{r})$. The Löwdin population scheme is used here which is an improvement upon the Mulliken method. It corrects the instability of predicted charges with increasing the size of the basis set. The total number of electrons in the Mulliken method is expressed as [36]

$$\begin{aligned} N &= \sum_j \int \psi_j^*(\mathbf{r})\psi_j(\mathbf{r})d\mathbf{r}_j = \sum_j \sum_{r,s} \int c_{jr}\phi_r^*(\mathbf{r}_r)c_{js}\phi_s(\mathbf{r}_s)d\mathbf{r}_j \\ &= \sum_j \left(\sum_r c_{jr}^2 + \sum_{r \neq s} c_{jr}c_{js}S_{rs} \right) \end{aligned} \quad (2.11)$$

where ϕ_r and ϕ_s are the atomic orbital basis functions, c_{jr} are coefficients of the basis function in the molecular orbital ψ_j and $S_{rs} = \int \phi_r^*\phi_s d\mathbf{r}$ is the overlap matrix. The first term can be thought of as electrons belonging to the particular atom, while the second term causes problems since there is no single best way to divide the shared electrons between the two atoms. Mulliken suggests splitting the shared density 50:50. In this work, the Löwdin approach is used in which the atomic orbital basis functions are

transformed into an orthonormal set of basis functions prior to the population analysis. Therefore, the transformation eliminates the overlap term, S .

When diffuse basis functions are involved, it is recommended to use density-based prescriptions such as Becke instead of Löwdin [38]. The number of electrons on an atom in the Becke approach is

$$N = \int w^{Becke}(\mathbf{r})\rho(\mathbf{r})d\mathbf{r}. \quad (2.12)$$

The space is partitioned into cells where w^{Becke} is nearly unity inside cells consisting of all points closest to the atom and zero outside.

In this work, we show how CDFT can be used as a model for the interaction between an electron and a molecule. In our model, the electron is represented by a ghost atom, i.e. basis functions are added to an expansion center without a nuclear charge, and the charge of this ghost atom is constrained to -1 . The total system, the electron and the molecular cation, are kept neutral. The spin of the electron and total system are constrained to a doublet and singlet spin states, respectively. By varying the distance between the ghost atom and the cation, we obtain an accurate picture of the interaction energy between the departing electron and the cation in the presence of the electric field.

2.1.2 Time-dependent density functional theory

For the calculation of photoabsorption spectra, TDDFT is used here where the external potential is weak [39]. Therefore, the induced change in the density is determined by “linear response theory”. The key quantity in linear response theory is the response function, $\chi(\mathbf{r}, \mathbf{r}', t - t')$, defined as

$$\chi(\mathbf{r}, \mathbf{r}', t - t') = \frac{\delta\rho(\mathbf{r}, t)}{\delta v_{ext}(\mathbf{r}', t')}. \quad (2.13)$$

Introducing a small change to the external potential leads to a small perturbation to the unperturbed Hamiltonian, H^0 , given as

$$H(t) = H^0 + \delta H(t) \quad (2.14)$$

where δH can be written in frequency space, ω , as

$$\delta H(t) = \frac{1}{2\pi} \int e^{-i\omega t} \delta v_{ext}(\mathbf{r}, \omega) \rho(\mathbf{r}) d\mathbf{r} d\omega \quad (2.15)$$

The unperturbed time-dependent ground state is given as

$$|\Psi^0(t)\rangle = e^{-iE_0t} |\Psi_0^0\rangle \quad (2.16)$$

while in the first-order perturbation theory, the time-dependent wavefunction can be written as

$$|\Psi(t)\rangle = e^{-iE_0t} |\Psi_0^0\rangle + \sum_{j \neq 0} a_j(t) e^{-iE_jt} |\Psi_j^0\rangle \quad (2.17)$$

where E_0 and E_j are the energies of the ground state and the excited state j , respectively. The first term is $|\Psi^0(t)\rangle$ and the second term gives a mixture of components resulting from the unperturbed time-dependent excited states. The time-dependent coefficients, $a_j(t)$, are given by

$$\begin{aligned} a_j(t) &= -i \int_{-\infty}^t e^{i\omega_{0j}t'} \langle \Psi_j^0 | \delta H(t') | \Psi_0^0 \rangle dt' \\ &= \frac{-1}{2\pi} \int \delta v_{ext}(\mathbf{r}', \omega) \langle \Psi_j^0 | \rho(\mathbf{r}') | \Psi_0^0 \rangle \frac{e^{i(\omega_{0j}-\omega)t}}{\omega_{0j}-\omega} d\omega d\mathbf{r}' \end{aligned} \quad (2.18)$$

where $\omega_{0j} = E_j - E_0$. The change of the density resulting from the time-dependent perturbation is defined as

$$\delta\rho(\mathbf{r}, t) = \langle \Psi(t) | \rho(\mathbf{r}) | \Psi(t) \rangle - \langle \Psi^0(t) | \rho(\mathbf{r}) | \Psi^0(t) \rangle. \quad (2.19)$$

Inserting Eqs. 2.16, 2.17 and 2.18 into Eq. 2.19 and switching to frequency space gives

$$\begin{aligned} \delta\rho(\mathbf{r}, \omega) &= - \int \delta v_{ext}(\mathbf{r}', \omega) \sum_{j \neq 0} \left(\frac{\langle \Psi_j^0 | \rho(\mathbf{r}') | \Psi_0^0 \rangle \langle \Psi_0^0 | \rho(\mathbf{r}') | \Psi_j^0 \rangle}{\omega_{0j} - \omega} \right. \\ &\quad \left. + \frac{\langle \Psi_0^0 | \rho(\mathbf{r}') | \Psi_j^0 \rangle \langle \Psi_j^0 | \rho(\mathbf{r}') | \Psi_0^0 \rangle}{\omega_{0j} + \omega} \right) d\mathbf{r}'. \end{aligned} \quad (2.20)$$

The change in the density with respect to the change in the external potential gives the response function

$$\begin{aligned} \frac{\delta\rho(\mathbf{r}, \omega)}{\delta v_{ext}(\mathbf{r}', \omega)} = \chi(\mathbf{r}, \mathbf{r}', \omega) &= - \sum_{j \neq 0} \left(\frac{\langle \Psi_j^0 | \rho(\mathbf{r}') | \Psi_0^0 \rangle \langle \Psi_0^0 | \rho(\mathbf{r}') | \Psi_j^0 \rangle}{\omega_{0j} - \omega} \right. \\ &\quad \left. + \frac{\langle \Psi_0^0 | \rho(\mathbf{r}') | \Psi_j^0 \rangle \langle \Psi_j^0 | \rho(\mathbf{r}') | \Psi_0^0 \rangle}{\omega_{0j} + \omega} \right). \end{aligned} \quad (2.21)$$

Finally, the excitation energies of the system can be derived from the poles of the response function.

In the Kohn-Sham system, the response function is

$$\chi_{KS}(\mathbf{r}, \mathbf{r}', t - t') = \frac{\delta\rho(\mathbf{r}, t)}{\delta v(\mathbf{r}', t')}. \quad (2.22)$$

The linear change of the KS potential, $\delta v(\mathbf{r}, t)$, is obtained as

$$\delta v(\mathbf{r}, t) = \delta v_{ext}(\mathbf{r}, t) + \int \frac{\delta\rho(\mathbf{r}', t)}{|\mathbf{r} - \mathbf{r}'|} d\mathbf{r}' dt' + \int f_{xc\sigma\sigma'}(\mathbf{r}, \mathbf{r}', t - t') \delta\rho(\mathbf{r}', t') d\mathbf{r}' dt' \quad (2.23)$$

where $f_{xc\sigma\sigma'}(\mathbf{r}, \mathbf{r}', t - t')$ is the exchange-correlation (xc) kernel given as

$$f_{xc\sigma\sigma'}(\mathbf{r}, \mathbf{r}', t - t') = \frac{\delta v_{xc}(\mathbf{r}, t)}{\delta\rho(\mathbf{r}', t')}. \quad (2.24)$$

The relation between the response functions of the Kohn-Sham system and the interacting electron system is found by the Dyson equation [39],

$$\chi(\mathbf{r}, \mathbf{r}', \omega) = \chi_{KS}(\mathbf{r}, \mathbf{r}', \omega) + \int \chi_{KS}(\mathbf{r}, \mathbf{r}_1, \omega) \left(\frac{1}{|\mathbf{r}_1 - \mathbf{r}_2|} + f_{xc\sigma\sigma'}(\mathbf{r}_1, \mathbf{r}_2, \omega) \right) \chi(\mathbf{r}_2, \mathbf{r}', \omega) d\mathbf{r}_1 d\mathbf{r}_2. \quad (2.25)$$

To evaluate the response function, an approximate xc kernel is required. The simplest solution is to ignore the effect of xc functional which is called the random phase approximation (RPA).

2.2 Force-field models

Force-field models describe the electrostatic interactions between particles as a function of interparticle distances. As a simple example, the Lennard-Jones potential energy, V_{LJ} , is described as [40],

$$V_{LJ}(R) = 4\epsilon \left[\left(\frac{\sigma}{R} \right)^{12} - \left(\frac{\sigma}{R} \right)^6 \right] \quad (2.26)$$

where R is the distance between two particles and ϵ and σ are the model parameters describing the potential well and the distance at which the interparticle potential is zero, respectively. These parameters can be fitted

to reproduce experimental or quantum chemical data. The R^{-12} term describes the short-range repulsive interaction while the R^{-6} term describes the long-range attraction interactions.

The standard force-field models are pairwise additive force fields describing electrostatic interactions in terms of fixed atomic charges and as such the polarization effects are missing in their formalisms. Polarizable force-field models are important when a molecule is polarized by its surroundings in a dielectric medium [41]. In polarizable force fields, the charge distribution is varied depending on the dielectric medium. The point-dipole interaction model (PDI) [42–46] and the nonmetallic electronegativity equalization model (EEM) [47–49] are examples of methods used to account for polarization. In the PDI model, the atomic polarizability is included as an atom-type parameter. The molecular polarizability, $\alpha_{\alpha\beta}$, is defined as

$$\mu_{\alpha}^{ind} = \alpha_{\alpha\beta} E_{\beta}^{ext} \quad (2.27)$$

where μ_{α}^{ind} is the induced dipole moment, E_{β}^{ext} is the external electric field and α and β denote the Cartesian coordinates. In EEM, the charge flows between atoms until the electronegativities of the atoms are equal. The atomic electronegativity and chemical hardness are atom-type parameters in this model. EEM and PDI are the basis of the charge-transfer and point-dipole interaction (CT-PDI) model explained in the following section.

2.2.1 Charge-transfer and point-dipole interaction model

The CT-PDI model is explained here in detail since the equations are not given in the papers included in the thesis.

The EEM potential is given as

$$V^{EEM} = \sum_I^N (\chi_I^* + \varphi_I^{ext}) q_I + \frac{1}{2} \sum_I^N \eta_I^* q_I^2 + \frac{1}{2} \sum_{I,J \neq I}^N q_I T_{IJ}^{(0)} q_J \quad (2.28)$$

where q_I is the atomic charge, χ_I^* is the atomic electronegativity, η_I^* is the atomic chemical hardness, φ_I^{ext} describes the external electrostatic potential at atom I and $T_{IJ}^{(0)} = 1/R_{IJ}$, where R_{IJ} is the distance between atoms I and J . In the CT-PDI model the EEM potential is modified as follows

$$V^{qq} = \sum_{I,K>I}^N (\chi_{IK} + \varphi_{IK}^{\text{ext}}) q_{IK} + \frac{1}{2} \sum_{I,K>I,J,M>J}^N q_{IK} T_{IK,JM}^{(0)} q_{JM} \quad (2.29)$$

where V^{qq} is the charge-charge interaction energy, $\chi_{IK} = \chi_I^* - \chi_K^*$, $\varphi_{IK}^{\text{ext}} = \varphi_I^{\text{ext}} - \varphi_K^{\text{ext}}$, $T_{II}^{(0)} = \eta_I^*$ and $T_{IK,JM}^{(0)}$ is defined as

$$T_{IK,JM}^{(0)} = T_{IJ}^{(0)} - T_{KJ}^{(0)} - T_{IM}^{(0)} + T_{KM}^{(0)}. \quad (2.30)$$

The modifications are listed as,

1. The atom-atom charge-transfer (AACT) method is adopted, where atomic charges are replaced by charge-transfer terms, q_{IK} [50],

$$q_I = \sum_K^N q_{IK} \quad (2.31)$$

Inserting Eq. 2.31 to 2.28 and using $R_{IJ,\alpha} = -R_{JI,\alpha}$, Eq. 2.29 is obtained.

2. A Gaussian charge distribution $\rho_I(r_i)$ is used for each atom instead of point charges [51,52],

$$\rho_I(r_i) = q_I \left(\frac{\Phi_I^*}{\pi} \right)^{\frac{3}{2}} e^{-\Phi_I^* r_i^2} \quad (2.32)$$

where r_i is an electronic coordinate and Φ_I^* is the width of the Gaussian distribution, an atom-type parameter of the model. The interaction between two Gaussian charge distributions is written as [52]

$$\tilde{V} = q_I \tilde{T}_{IJ}^{(0)} q_J = \frac{q_I q_J}{\tilde{R}_{IJ}} \quad (2.33)$$

where \tilde{R}_{IJ} is a modified distance, $\tilde{T}_{IJ}^{(0)} = 1/\tilde{R}_{IJ}$, given by the regular error function $\tilde{R}_{IJ} = R_{IJ}/\text{erf}(\sqrt{a_{IJ}}R_{IJ})$, and a_{IJ} is

$$a_{IJ} = \frac{\Phi_I^* \Phi_J^*}{\Phi_I^* + \Phi_J^*}. \quad (2.34)$$

3. An approximation of the error function is considered in the CT-PDI model [52,53],

$$\tilde{R}_{IJ} = \sqrt{R_{IJ}^2 + \frac{\pi}{4a_{IJ}}} \quad (2.35)$$

which has the same limiting behavior at $R_{IJ} \rightarrow 0$ and $R_{IJ} \rightarrow \infty$ as when $\tilde{R}_{IJ} = R_{IJ}/\text{erf}(\sqrt{a_{IJ}}R_{IJ})$.

4. EEM has a limitation regarding the charge transfer over large distances [50,54], i.e. the charge-transfer is not zero between two particles at infinite separation. Two approximations to Eq. 2.30 are imposed:
(i) In the three-particle case,

$$\tilde{T}_{IK,IM}^{(0)} = \eta_I^* - \tilde{T}_{KI}^{(0)} - \tilde{T}_{IM}^{(0)} + \tilde{T}_{KM}^{(0)}, \quad I = J \text{ and } K \neq M \quad (2.36)$$

the chemical hardness, η_I^* , is modified as [55]

$$\eta_I^* \rightarrow \eta_I^* S_{IK}^{-\frac{1}{2}} S_{IM}^{-\frac{1}{2}} g_{I,KM}, \quad I = J \text{ and } K \neq M \quad (2.37)$$

where $g_{I,KM}$ is a function of the two distances, R_{IK} and R_{IM} , describing a resistance to charge flow in the molecule, given as [56]

$$g_{I,KM} = (g_{0,I}^*)^2 g_{0,K}^* g_{0,M}^* H_{I,KM}(\Delta_{I,KM}) + (g_{1,I}^*)^2 g_{1,K}^* g_{1,M}^* (1 - H_{I,KM}(\Delta_{I,KM})) \quad (2.38)$$

where $g_{0,I}^*$ and $g_{1,I}^*$ are atom-type parameters and $H_{I,KM}$ is a smooth step function,

$$H_{I,KM}(\Delta) = \frac{1}{2}(1 + \tanh(C_{I,KM}\Delta_{I,KM})) \quad (2.39)$$

$C_{I,KM} = (C_I^*)^2 C_K^* C_M^*$, where C_I^* and R_I^* are atom-type parameters and $\Delta_{I,KM} = R_{IK} - (R_I^* + R_K^*) + R_{IM} - (R_I^* + R_M^*)$. In Eq. 2.37, S_{IK} is,

$$S_{IK} = e^{-a_{IK}(R_{IK} - R_I^* - R_K^*)^2}. \quad (2.40)$$

- (ii) In the two-particle case, $K = M$ and $I = J$, for a large separation distance $\tilde{T}_{IK,IM}^{(0)}$ becomes $\eta_I^* + \eta_K^* - 2\tilde{T}_{IK}^{(0)}$ and the modification of the chemical hardness in $\tilde{T}_{IK,IK}^{(0)}$ is introduced as [55]

$$(\eta_I^* + \eta_K^*) \rightarrow (\eta_I^* + \eta_K^*) S_{IK}^{-1} \quad (2.41)$$

The EEM problem for the two-particle system is thus solved by considering Eq. 2.41, whereas Eq. 2.37 addresses the “long-chain” problem, i.e. an energy cost is added for charge transport in an extended system.

In the PDI model, atomic polarizabilities couple with each other in an external electric field through the atomic induced dipole moments and the molecular polarizability is obtained by considering atomic polarizabilities as atom-type parameters. The PDI potential is defined as [55]

$$V^{\mu\mu} = \frac{1}{2} \sum_I^N \mu_{I,\alpha} (\alpha_{I,\beta\alpha})^{-1} \mu_{I,\beta} - \frac{1}{2} \sum_I^N \sum_{K \neq I}^N \mu_{I,\alpha} \tilde{T}_{IK,\alpha\beta}^{(2)} \mu_{K,\beta} - \sum_I^N E_{I,\alpha}^{\text{ext}} \mu_{I,\alpha} \quad (2.42)$$

where $V^{\mu\mu}$ is the dipole-dipole interaction energy, $\alpha_{I,\beta\alpha}$ is the atomic polarizability and $E_{I,\beta}^{\text{ext}}$ is the external electric field at atom I . $\tilde{T}_{IJ,\alpha}^{(1)}$ and $\tilde{T}_{IJ,\alpha\beta}^{(2)}$ are obtained from the derivations of $\tilde{T}_{IJ}^{(0)}$ with respect to R_{IJ} [56],

$$\tilde{T}_{IJ,\alpha}^{(1)} = \frac{\partial \tilde{T}_{IJ}^{(0)}}{\partial R_{IJ,\alpha}} = -\frac{R_{IJ,\alpha}}{\tilde{R}_{IJ}^3} \quad \text{and} \quad \tilde{T}_{IJ,\alpha\beta}^{(2)} = \frac{\partial \tilde{T}_{IJ,\alpha}^{(1)}}{\partial R_{IJ,\beta}} = \frac{3R_{IJ,\alpha} R_{IJ,\beta}}{\tilde{R}_{IJ}^5} - \frac{\delta_{\alpha\beta}}{\tilde{R}_{IJ}^3}, \quad (2.43)$$

where the Einstein summation convention is used for repeated subscripts. In the CT-PDI model, $\alpha_{I,\beta\alpha}$ is modified to include the chemical surroundings [56,57],

$$\alpha_{I,\beta\alpha} = \alpha_I^* (\delta_{\beta\alpha} + x_I^* (1 - G_{I,\beta\alpha})) \quad (2.44)$$

where α_I^* and x_I^* are atom-type parameters describing the isotropic and anisotropic parts of the atomic polarizability, respectively, and $G_{I,\beta\alpha}$ is

$$G_{I,\beta\alpha} = \frac{3}{\text{Tr}(\Gamma_I)} \Gamma_{I,\beta\alpha} \quad (2.45)$$

where $\Gamma_{I,\beta\alpha}$ is expressed by

$$\Gamma_{I,\beta\alpha} = \sum_{J \neq I}^N \alpha_J^* S_{IJ} \frac{R_{IJ,\beta} R_{IJ,\alpha}}{R_{IJ}^2}. \quad (2.46)$$

Here, $R_{IJ,\beta}R_{IJ,\alpha}/R_{IJ}^2$ gives the correct rotational properties of $\alpha_{I,\beta\alpha}$.

The charge-dipole interaction energy $V^{q\mu}$ in the CT-PDI model is written as [55]

$$V^{q\mu} = \sum_{I,J}^N q_I \tilde{T}_{IJ,\alpha}^{(1)} \mu_{J,\alpha} = \sum_{I,K>I,J}^N q_{IK} \tilde{T}_{IK,J,\alpha}^{(1)} \mu_{J,\alpha} \quad (2.47)$$

where $\tilde{T}_{IK,J,\alpha}^{(1)} = \tilde{T}_{IJ,\alpha}^{(1)} - \tilde{T}_{KJ,\alpha}^{(1)}$.

In the CT-PDI model, the Lagrangian including the kinetic energies for $q_{IK}(t)$ and $\mu_I(t)$ [58] as well as the potential energies provides a set of coupled linear equations and the frequency-dependent polarizability is calculated by solving the linear response equations. The charge-transfer terms and the atomic dipole moments are assumed to oscillate with the same frequency, ω , as the external electric field, $E_{J,\alpha}^{\text{ext}} = \text{Re} (E_{J,\alpha}^{(\omega)} e^{i\omega t})$, and electrostatic potential, $\varphi_{IJ}^{\text{ext}} = \text{Re} (\varphi_{IJ}^{(\omega)} e^{i\omega t})$, so that $q_{IK} = \text{Re} (q_{IK}^{(0)} + q_{IK}^{(\omega)} e^{i\omega t})$ and $\mu_{I,\alpha} = \text{Re} (\mu_{I,\alpha}^{(0)} + \mu_{I,\alpha}^{(\omega)} e^{i\omega t})$.

The Lagrangian, L , of the system is expressed by [58]

$$L = K^q + K^\mu - (V^{qq} + V^{q\mu} + V^{\mu\mu}) \quad (2.48)$$

where K^q and K^μ are the kinetic energies of atomic charges and atomic dipole moments, respectively. The kinetic energy K^q associated with the oscillations of charges is given by [56]

$$K^q = \frac{1}{2} \sum_{I,K>I}^N (c_I^{q*} + c_K^{q*}) R_{IK}^2 (\dot{q}_{IK})^2 \quad (2.49)$$

where \dot{q}_{IK} is the time-derivative of the charge-transfer term and c_I^{q*} and c_K^{q*} are atom-type parameters. The kinetic energy K^μ of the oscillating atomic dipole moments is given as [58]

$$K^\mu = \frac{1}{2} \sum_I^N c_I^{\mu*} (\dot{\mu}_I)^2 \quad (2.50)$$

where $\dot{\mu}_I$ is the time derivative of μ_I , and $c_I^{\mu*}$ is an additional atom-type parameter.

The Lagrangian equations to be solved are

$$\frac{\partial}{\partial t} \left(\frac{\partial L}{\partial \dot{q}_{IK}} \right) - \frac{\partial L}{\partial q_{IK}} = 0 \quad ; \quad \frac{\partial}{\partial t} \left(\frac{\partial L}{\partial \dot{\mu}_I} \right) - \frac{\partial L}{\partial \mu_I} = 0 \quad (2.51)$$

The final equations are written in a matrix form as [56,59]

$$\left\{ \begin{pmatrix} \tilde{T}_{M \times M}^{(0)} & \tilde{T}_{M \times 3N}^{(1)} \\ \tilde{T}_{M \times 3N}^{(1)t} & -\tilde{T}_{3N \times 3N}^{(2)} \end{pmatrix} - \omega^2 \begin{pmatrix} C_{M \times M}^q & 0 \\ 0 & C_{3N \times 3N}^\mu \end{pmatrix} \right\} \begin{pmatrix} q_{M \times 1} \\ \mu_{3N \times 1} \end{pmatrix} = \begin{pmatrix} -\varphi_{M \times 1} \\ E_{3N \times 1} \end{pmatrix} \quad (2.52)$$

where M and N are the number of bonds and atoms, respectively. The elements of $\tilde{T}^{(0)}$, $\tilde{T}^{(1)}$ and $\tilde{T}^{(2)}$ are $\tilde{T}_{SP, JM}^{(0)}$, $\tilde{T}_{SP, K, \beta}^{(1)}$ and $\tilde{T}_{IK, \alpha \beta}^{(2)}$ ($\tilde{T}_{II, \alpha \beta}^{(2)} = (\alpha_{I, \beta \alpha})^{-1}$), respectively. C^q is a diagonal matrix in which one element is $(c_J^{q*} + c_M^{q*})R_{JM}^2(1 - \frac{i}{2\omega}(\gamma_J^{q*} + \gamma_M^{q*}))\delta_{SJ}\delta_{PM}$, while the C^μ matrix element is $c_K^{\mu*}(1 - i\gamma_K^{\mu*}/\omega)\delta_{IK}\delta_{\alpha\beta}$.

The dissipations are included by replacing ω^2 with $\omega^2 - i\frac{1}{2}(\gamma_I^{q*} + \gamma_K^{q*})\omega$ and $\omega^2 - i\gamma_I^{\mu*}\omega$ in the diagonal matrix in which γ_J^{q*} and $\gamma_K^{\mu*}$ are dissipation parameters for charges and dipoles, respectively [58]. Thus, q has the elements $q_{JM}^{(\omega)}$ and μ has the elements given by $\mu_{K, \beta}^{(\omega)}$. On the right-hand side of Eq. 2.52, the elements of φ and E are $\varphi_{SP}^{(\omega)}$ and $E_{I, \alpha}^{(\omega)}$, respectively. For a homogeneous electric field, $E_{I, \alpha}^{(\omega)}$ is $E_\alpha^{(\omega)}$ and $\varphi_{SP}^{(\omega)} = -(R_{S, \alpha} - R_{P, \alpha})E_\alpha^{(\omega)}$. Finding the derivative of Eq. 2.52 with respect to a homogeneous external electric field gives the molecular polarizability obtained as [56]

$$\alpha_{\alpha\beta}(\omega) = \frac{\partial \mu_\alpha^{(\omega)}}{\partial E_\beta^{(\omega)}} = \sum_{I, M > I}^N R_{IM, \alpha} \frac{\partial q_{IM}^{(\omega)}}{\partial E_\beta^{(\omega)}} + \sum_I^N \frac{\partial \mu_{I, \alpha}^{(\omega)}}{\partial E_\beta^{(\omega)}}. \quad (2.53)$$

The two terms on the right hand side of Eq. 2.53 gives the charge-transfer and dipole contributions to the polarizability, respectively. $\frac{\partial q_{IM}^{(\omega)}}{\partial E_\beta^{(\omega)}}$

and $\frac{\partial \mu_{I, \alpha}^{(\omega)}}{\partial E_\beta^{(\omega)}}$ are used in the calculation of local field factors. The local field factor (Eq. 1.15) in terms of charge-transfer terms is given as

$$\frac{\partial E_{I, \alpha}^{\text{loc}}}{\partial E_{I, \gamma}^{\text{ext}}} = \delta_{\alpha\gamma} + \sum_{J \neq I, M > J}^N -(T_{IJ, \alpha}^{(1)} - T_{IM, \alpha}^{(1)}) \frac{\partial q_{JM}}{\partial E_{I, \gamma}^{\text{ext}}} + \sum_{J \neq I}^N T_{IJ, \alpha \beta}^{(2)} \frac{\partial \mu_{J, \beta}}{\partial E_{I, \gamma}^{\text{ext}}}. \quad (2.54)$$

Chapter 3

Summary and future work



The general problem of electrical breakdown in insulating liquids is introduced in Chapter 1 and Chapter 2 summarizes the methodologies used to calculate molecular properties of insulating liquids. These properties are field-dependent IP and field-dependent excitation energies. To study the IP in the field, the point-charge model based on DFT is used which is described in **paper 1** and a new model is developed in **paper 2** which is based on CDFT and applied to different types of molecules (**paper 3**). A limitation of the CDFT model is resolved in **paper 4** and we extend the model to larger aromatic molecules. The excitation energies of molecules are also investigated in papers 1-4. Some of the general conclusions of papers 1-4 are as follows:

- Different types of molecules behave differently in the field.
- The IP decreases strongly in the field, while the excitation energies remain relatively constant.
- Due to the significant decrease of the IP in the field, the number of available excited states decreases with increasing field.
- At a threshold field, all the excited states of the molecule vanish and change into unbound states.

The vanishing of the excited states in the field may be the origin of different modes of the streamer propagation. In general, we have proposed that molecules with low IPs and low excitation energies show the most promise for streamer experiments.

The local field factor is also discussed in Chapter 1. **Paper 5** represents a model to calculate the static and frequency-dependent local field factors of the benzene and azobenzene dimers as initial model systems. In **paper 6**, the applicability of the model to much larger systems such as aggregates of molecules is investigated by combining it with a molecular dynamics simulation of liquid benzene which is used in breakdown experiments [60,61]. The local field model is partitioned into a charge term and a dipole term, determining the contribution of each term in the local field factor. Some of the conclusions of paper 5 and 6 are as follows:

- The local field factor increases significantly at the absorption frequency.
- The local field factor is dependent on the intermolecular distance.

- The charge contribution is smaller than the dipole contribution at frequencies below absorption, while at the absorption frequency they are comparable.
- At atoms, the charge and dipole terms may add up to give a large local field factor or they may to a large extent cancel each other and results in a small local field factor at the absorption frequency.

The local field model developed in this thesis can be applied to different liquids to obtain their dielectric properties.

The thesis work is limited to the study of a few molecular processes in insulating liquids using molecular modeling. To better understand the pre-breakdown and breakdown phenomena, it is required to consider more possible processes and further studies may be performed to connect the modeling results to experiments both qualitatively and quantitatively.

There are some potentially alternative approaches to the field-dependent IP model presented in this work. A useful approach that can be used in future work is applying continuum wavefunctions developed for studying photoionization spectra [62,63].

The excitation energies are calculated by the TDDFT method using standard functionals. For excitation energies close to the ionization threshold, the calculations need to be extended to use long-range corrected (LC) functionals which are more accurate at long distances [64,65]. The LC functionals may give the actual number of excited states with energies below the IP in zero field as well as the actual decrease in the number of excited states in the field.

The parameters of the local-field model need to be improved by extending the set of molecules to provide a generic set of optimized parameters for all studied molecules rather than several system-specific sets. Adding higher-order terms such as hyperpolarizabilities and atomic quadrupole moments improves the physics of the model and provides a useful tool for the calculation of numerous optical properties used in breakdown experiments.

Bibliography

- [1] J. C. Devins, S. J. Rzed, and R. J. Schwabe, "Breakdown and prebreakdown phenomena in liquids," *J. Appl. Phys.*, vol. 52, pp. 4531–4545, 1981.
- [2] M. Unge, S. Singha, N. V. Dung, D. Linhjell, S. Ingebrigtsen, and L. E. Lundgaard, "Enhancements in the lightning impulse breakdown characteristics of natural ester dielectric liquids," *Appl. Phys. Lett.*, vol. 102, p. 172905, 2013.
- [3] Q. Liu and Z. D. Wang, "Streamer characteristic and breakdown in synthetic and natural ester transformer liquids under standard lightning impulse voltage," *IEEE Trans. Dielect. Elect. Insul.*, vol. 18, pp. 285–294, 2011.
- [4] C. T. Duy, O. Lesaint, A. Denat, and N. Bonifaci, "Streamer propagation and breakdown in natural ester in high voltage," *IEEE Trans. Dielect. Elect. Insul.*, vol. 16, pp. 1582–1594, 2009.
- [5] P. Bårmann, S. Kröll, and A. Sunesson, "Spectroscopic measurements of streamer filaments in electric breakdown in a dielectric liquid," *J. Phys. D: Appl. Phys.*, vol. 29, pp. 1188–1196, 1996.
- [6] N. V. Dung, H. K. Høidalen, D. Linhjell, L. E. Lundgaard, and M. Unge, "Influence of impurities and additives on positive streamers in paraffinic model oil," *IEEE Trans. Dielect. Elect. Insul.*, vol. 19, pp. 1593–1603, 2012.
- [7] O. Lesaint and G. Massala, "Positive streamer propagation in large oil gaps. experimental characterization of propagation modes," *IEEE Trans. Dielect. Elect. Insul.*, vol. 5, pp. 360–370, 1998.

- [8] L. Lundgaard, D. Linhjell, G. Berg, and S. Sigmond, "Propagation of positive and negative streamers in oil with and without pressboard interfaces," *IEEE Trans. Dielect. Elect. Insul.*, vol. 5, pp. 388–395, 1998.
- [9] O. Lesaint and M. Jung, "On the relationship between streamer branching and propagation in liquids: influence of pyrene in cyclohexane," *J. Phys. D: Appl. Phys.*, vol. 33, pp. 1360–1368, 2000.
- [10] S. Ingebrigtsen, H. S. Smalø, P.-O. Åstrand, and L. E. Lundgaard, "Effects of electron-attaching and electron-releasing additives on streamers in liquid cyclohexane," *IEEE Trans. Dielect. Elect. Insul.*, vol. 16, pp. 1524–1535, 2009.
- [11] S. Ingebrigtsen, L. E. Lundgaard, and P.-O. Åstrand, "Effects of additives on prebreakdown phenomena in liquid cyclohexane: II. streamer propagation," *J. Phys. D: Appl. Phys.*, vol. 40, pp. 5624–5634, 2007.
- [12] Ø. Hestad, H. S. Smalø, P.-O. Åstrand, S. Ingebrigtsen, and L. E. Lundgaard, "Effects of N,N-dimethylaniline and trichloroethene on prebreakdown phenomena in liquid and solid *n*-tridecane," *IEEE Trans. Dielect. Elect. Insul.*, vol. 18, pp. 1886–1896, 2011.
- [13] H. S. Smalø, Ø. Hestad, S. Ingebrigtsen, and P.-O. Åstrand, "Field dependence on the molecular ionization potential and excitation energies compared to conductivity models for insulation materials at high electrical fields," *J. Appl. Phys.*, vol. 109, p. 073306, 2011.
- [14] J. Jadidian, M. Zahn, N. Lavesson, O. Widlund, and K. Borg, "Effect of impulse voltage polarity, peak amplitude, and rise time on streamers initiated from a needle electrode in transformer oil," *IEEE Trans. Plasma Sci.*, vol. 40, pp. 909–918, 2012.
- [15] N. V. Dung, H. K. Høidalen, D. Linhjell, L. E. Lundgaard, and M. Unge, "Effects of reduced pressure and additives on streamers in white oil in long point-plane gap," *J. Phys. D: Appl. Phys.*, vol. 46, p. 255501, 2013.
- [16] J. Sidney Clements, M. Sato, and R. H. Davis, "Prebreakdown phenomena and chemical reactions using a pulsed high-voltage discharge in water," vol. IA-23, pp. 224–235, 1987.

- [17] J. Nietro-Salazar, O. Lesaint, and A. Denat, "Transient current and light emission associated to the propagation of pre-breakdown phenomena in water," in *IEEE conference on electrical insulation and dielectric phenomena (CEIDP)*, pp. 542–545, 2003.
- [18] I. V. Timoshkin, M. J. Given, M. P. Wilson, R. A. Fouracre, and S. J. MacGregor, "Impulse breakdown of liquid water," in *IEEE conference on electrical insulation and dielectric phenomena (CEIDP)*, (West Lafayette, IN), pp. 1–3, 2010.
- [19] M. B. Smirnov and V. P. Kraĭnov, "Critical fields for ionization of the hydrogen molecule and the molecular hydrogen ion," *J. Exp. Theor. Phys.*, vol. 85, pp. 447–450, 1997.
- [20] L. A. Dissado and J. C. Fothergill, *Electrical Degradation and Breakdown in Polymers*. IEE Material and Devices series 9, London, United Kingdom: Peter Peregrinus Ltd., 1992.
- [21] C. Kittel, *Introduction to solid state physics*. New York: Wiley, 4 ed., 1971.
- [22] J. D. Jackson, *Classical Electrodynamics*. New York: John Wiley and Sons, 2 ed., 1975.
- [23] C. J. F. Böttcher, *Theory of Electric Polarization*, vol. 1. Amsterdam, Netherlands: Elsevier, 2 ed., 1973.
- [24] A. D. Buckingham, "Permanent and induced molecular moments and long-range intermolecular forces," *Adv. Chem. Phys.*, vol. 12, pp. 107–142, 1967.
- [25] L. Jensen, P.-O. Åstrand, and K. V. Mikkelsen, "Microscopic and macroscopic polarization in C₆₀ fullerene clusters as calculated by an electrostatic interaction model," *J. Phys. Chem. B*, vol. 108, pp. 8226–8233, 2004.
- [26] P. Hohenberg and W. Kohn, "Inhomogeneous electron gas," *Phys. Rev.*, vol. 136, pp. B864–B871, 1964.
- [27] R. G. Parr and W. Yang, *Density-functional theory of atoms and molecules*. Oxford University Press, New York, 1989.

- [28] P. H. Dederichs, S. Blügel, R. Zeller, and H. Akai, "Ground states of constrained systems: Application to cerium impurities," *Phys. Rev. Lett.*, vol. 53, pp. 2512–2515, 1984.
- [29] Q. Wu and T. Van Voorhis, "Direct optimization method to study constrained systems within density-functional theory," *Phys. Rev. A*, vol. 72, p. 024502, 2005.
- [30] Q. Wu and T. Van Voorhis, "Constrained density functional theory and its application in long-range electron transfer," *J. Chem. Theory Comput.*, vol. 2, pp. 765–774, 2006.
- [31] T. Kowalczyk, Z. Lin, and T. Van Voorhis, "Fluorescence quenching by photoinduced electron transfer in the Zn^{2+} sensor Zinpyr-1: A computational investigation," *J. Phys. Chem. A*, vol. 114, p. 10427, 2010.
- [32] I. Rudra, Q. Wu, and T. Van Voorhis, "Predicting exchange coupling constants in frustrated molecular magnets using density functional theory," *Inorg. Chem.*, vol. 46, pp. 10539–10548, 2007.
- [33] G. F. Voronoi, "Nouvelles applications des parametres continus a la theorie des formes quadratiques," vol. 134, pp. 198–287, 1908.
- [34] A. D. Becke, "A multicenter numerical integration scheme for polyatomic molecules," *J. Chem. Phys.*, vol. 88, p. 2547, 1988.
- [35] F. L. Hirshfeld, "Bonded-atom fragments for describing molecular charge densities," *Theor. Chim. Acta*, vol. 44, p. 129, 1977.
- [36] R. S. Mulliken, "Electron population analysis on LCAO-MO molecular wave functions. I," *J. Chem. Phys.*, vol. 23, pp. 1833–1840, 1955.
- [37] P.-O. Löwdin, "On the non-orthogonality problem connected with the use of atomic wave functions in the theory of molecules and crystals," *J. Chem. Phys.*, vol. 18, p. 365, 1950.
- [38] B. Kaduk, T. Kowalczyk, and T. Van Voorhis, "Constrained density functional theory," *Chem. Rev.*, vol. 112, pp. 321–370, 2012.
- [39] M. A. L. Marques and E. K. U. Gross, "Time-dependent density functional theory," *Ann. Rev. Phys. Chem.*, vol. 55, pp. 427–455, 2004.

- [40] J. E. Lennard-Jones, "On the determination of molecular fields," *Proc. Roy. Soc. Lond. A*, vol. 106, pp. 463–477, 1924.
- [41] T. A. Halgren and W. Damm, "Polarizable force fields," *Curr. Opinion Struct. Biol.*, vol. 11, pp. 236–242, 2001.
- [42] L. Silberstein, "Molecular refractivity and atomic interaction," *Phil. Mag.*, vol. 33, pp. 92–128, 1917.
- [43] L. Silberstein, "Molecular refractivity and atomic interaction. II," *Phil. Mag.*, vol. 33, pp. 521–533, 1917.
- [44] J. Applequist, J. R. Carl, and K.-F. Fung, "An atom dipole interaction model for molecular polarizability. Application to polyatomic molecules and determination of atom polarizabilities," *J. Am. Chem. Soc.*, vol. 94, pp. 2952–2960, 1972.
- [45] J. Applequist, "An atom dipole interaction model for molecular optical properties," *Acc. Chem. Res.*, vol. 10, pp. 79–85, 1977.
- [46] K. A. Bode and J. Applequist, "A new optimization of atomic polarizabilities in halomethanes, aldehydes, ketones, and amides by way of the atom dipole interaction model," *J. Phys. Chem.*, vol. 100, pp. 17820–17824, 1996.
- [47] W. J. Mortier, K. van Genechten, and J. Gasteiger, "Electronegativity equalization: applications and parametrization," *J. Am. Chem. Soc.*, vol. 107, pp. 829–835, 1985.
- [48] A. K. Rappé and W. A. Goddard III, "Charge equilibration for molecular dynamics simulations," *J. Phys. Chem.*, vol. 95, pp. 3358–3363, 1991.
- [49] H. A. Stern, G. A. Kaminski, J. L. Banks, R. Zhou, B. J. Berne, and R. A. Friesner, "Fluctuating charge, polarizable dipole, and combined models: Parameterization from ab initio quantum chemistry," *J. Phys. Chem. B*, vol. 103, pp. 4730–4737, 1999.
- [50] R. Chelli, P. Procacci, R. Righini, and S. Califano, "Electrical response in chemical potential equalization schemes," *J. Chem. Phys.*, vol. 111, pp. 8569–8575, 1999.

- [51] D. Bakowies and W. Thiel, "Hybrid models for combined quantum mechanical and molecular mechanical approaches," *J. Phys. Chem.*, vol. 100, pp. 10580–10594, 1996.
- [52] L. Jensen, P.-O. Åstrand, A. Osted, J. Kongsted, and K. V. Mikkelsen, "Polarizability of molecular clusters as calculated by a dipole interaction model," *J. Chem. Phys.*, vol. 116, pp. 4001–4010, 2002.
- [53] G. A. van der Velde, *A realistic Coloumb potential. MD and MC on water*. France: CECAM, H. J. C. Berendsen ed., 1972. 38-39.
- [54] L. Jensen, P.-O. Åstrand, and K. V. Mikkelsen, "An atomic capacitance-polarizability model for the calculation of molecular dipole moments and polarizabilities," *Int. J. Quant. Chem.*, vol. 84, pp. 513–522, 2001.
- [55] H. S. Smalø, P.-O. Åstrand, and L. Jensen, "Nonmetallic electronegativity equalization and point-dipole interaction model including exchange interactions for molecular dipole moments and polarizabilities," *J. Chem. Phys.*, vol. 131, p. 044101, 2009.
- [56] H. S. Smalø, P.-O. Åstrand, and A. Mayer, "Combined nonmetallic electronegativity equalization and point-dipole interaction model for the frequency-dependent polarizability," *Mol. Phys.*, vol. 111, p. 1470, 2013.
- [57] R. R. Birge, G. A. Schick, and D. F. Bocian, "Calculation of molecular polarizabilities using a semiclassical Slater-type orbital-point dipole interaction (STOPDI) model," *J. Chem. Phys.*, vol. 79, pp. 2256–2264, 1983.
- [58] A. Mayer, P. Lambin, and P.-O. Åstrand, "An electrostatic interaction model for frequency-dependent polarizability: methodology and applications to hydrocarbons and fullerenes," *Nanotechnology*, vol. 19, p. 025203, 2008.
- [59] S. Haghani, N. Davari, R. Sandnes, and P.-O. Åstrand, "Complex frequency-dependent polarizability through the $\pi \rightarrow \pi^*$ excitation energy of azobenzene molecules by a combined charge-transfer and point-dipole interaction model," *J. Phys. Chem. A*, vol. 118, pp. 11282–11292, 2014.

- [60] H. Yamashita and H. Amano, "Prebreakdown phenomena in hydrocarbon liquids," *IEEE Trans. Elect. Insul.*, vol. 23, pp. 739–750, 1988.
- [61] J. H. Tortai, N. Bonifaci, and A. Denat, "Back to results insulating properties of some liquids after an electrical arc," *IEEE Trans. Dielect. Elect. Insul.*, vol. 9, pp. 3–9, 2002.
- [62] H. Bachau, E. Cormier, P. Decleva, J. E. Hansen, and F. Martín, "Applications of *b*-splines in atomic and molecular physics," *Rep. Prog. Phys.*, vol. 64, pp. 1815–1942, 2001.
- [63] D. Toffoli, M. Stener, G. Fronzoni, and P. Decleva, "Convergence of the multicenter B-spline DFT approach for the continuum," *Chem. Phys.*, vol. 276, pp. 25–43, 2002.
- [64] B. M. Wong and T. H. Hsieh, "Optoelectronic and excitonic properties of oligoacenes: Substantial improvements from range-separated time-dependent density functional theory," *J. Chem. Theory Comput.*, vol. 6, pp. 3704–3712, 2010.
- [65] L. Kronik, T. Stein, S. Rafaely-Abramson, and R. Baer, "Excitation gaps of finite-sized systems from optimally tuned range-separated hybrid functionals," *J. Chem. Theory Comput.*, vol. 8, pp. 1515–1531, 2012.

Papers



Paper 1

Excitation energies and ionization potentials at high electric fields for molecules relevant for electrically insulating liquids

Nazanin Davari, Per-Olof Åstrand, Stian Ingebrigtsen and Mikael Unge

Journal of Applied Physics, 113, 143707 (2013)



Excitation energies and ionization potentials at high electric fields for molecules relevant for electrically insulating liquids

N. Davari,¹ P.-O. Åstrand,^{1,a)} S. Ingebrigtsen,² and M. Unge³

¹*Department of Chemistry, Norwegian University of Science and Technology (NTNU), NO 7491 Trondheim, Norway*

²*Department of Electric Power Engineering, SINTEF Energy Research, NO 7491 Trondheim, Norway*

³*ABB Corporate Research, SE 72178 Västerås, Sweden*

(Received 1 February 2013; accepted 21 March 2013; published online 10 April 2013)

The electric-field dependence of the molecular ionization potential and excitation energies is investigated by density-functional theory calculations. It is demonstrated that the ionization potential has a strong field dependence and decreases with increasing field. The excitation energies depend weakly on the field and the number of available excited states decreases with increasing field since the ionization potential has a stronger field dependence. Above a specific field, different for each molecule, a two-state model is obtained consisting of the electronic ground state and the ionized state. Implications for streamer propagation and electrically insulating materials are discussed. © 2013 American Institute of Physics. [<http://dx.doi.org/10.1063/1.4800118>]

I. INTRODUCTION

Insulating liquids are often used as a part of the dielectric barrier between two conductors in high-voltage equipment and may suffer a dielectric breakdown in high electric fields.^{1–6} Breakdown happens when a conductive plasma channel, a streamer, is created in the high field regions which propagates through the entire dielectric barrier and bridges the gap between two conductors. This phenomenon is influenced by the molecules properties in the insulating liquid. Electrons are the main charge carriers in dielectrics at high fields and the concentration of free electrons depends on the ionization potential (IP) and the excitation energies of the molecules.⁷

Although experimental studies on pre-breakdown and breakdown phenomena are extensive,^{8–11} corresponding theoretical investigations on a molecular level are sparse. In the needle-plane electrode geometries, the properties of the streamer originating from a positive or negative voltage on the needle electrode depend on the electronic properties of the insulating liquids including small amounts of additives.^{12–22} There are different ionization mechanisms such as impact ionization, photoionization, and field ionization.⁷ If the energy of an electron in the liquid is higher than the IP of the base liquid, impact ionization takes place. In the photoionization mechanism, a photon with an energy equal to or higher than the IP of the molecule is absorbed by a molecule and an electron is released. Field ionization is based on a tunneling phenomenon and is only dependent on the local electric field. Either of these mechanisms may be dominant in one of the different modes of streamer propagation.^{23,24} The first slow mode takes place between initiation voltages and breakdown of the streamer and the fast mode takes place above the breakdown levels. The IP is an important factor in all ionization mechanisms and the IP must be viewed as a field-dependent property.⁷ In this work, the hypothesis is that at high electric

fields, the excitation energy is also an important factor in the transition to fast mode streamer propagation.

In a previous work,⁷ it was realized that the IP had a strong dependence on the electric field, whereas the excitation energies (the lowest excitation energy was included in Ref. 7) had a relatively weak dependence on the electric field for the molecules included in the study. With an applied high voltage, energy is continuously added to the insulating liquid and there are two main routes for the liquid to release this energy, by emitting light or heat. That the number of available excited states decreases with increasing field, since the IP has a stronger field dependence may have a strong impact on the insulating properties of the liquid. It is, however, a complex process as sketched in Figure 1 with many possible effects on streamer initiation and propagation. As indicated in Figure 1, we may have excitation by electron impact or by photon absorption. In general, excitation is a preferred process for an insulating liquid since light is emitted to the surroundings, but in some cases, the life-time of the excited state is long compared to the frequency of either electron impact or photon absorption processes and a two-step ionization process may be obtained. With increasing field, the number of available excited states decreases. If an excited state that is important for the insulation suddenly vanishes since the field is increased, it may have dramatic effects on streamer initiation and propagation. It is here hypothesized that the vanishing of an important excited state may be the cause for the change in the mode of a streamer, which is presently characterized by the measured speed of the streamer without a detailed mechanistic explanation. We also note that above some field a region is reached where excited states are no longer available, i.e., a two-state model is obtained with the ground state and the ionized state.⁷ The strong field dependence on the IP also gives a new perspective on photoionization since a high-energy photon may be generated in a low-field region which may lead to ionization in a high-field region. We are presently not in a position to deduce which of these processes that are critical and it will

^{a)}Electronic mail: per-olof.astrand@ntnu.no

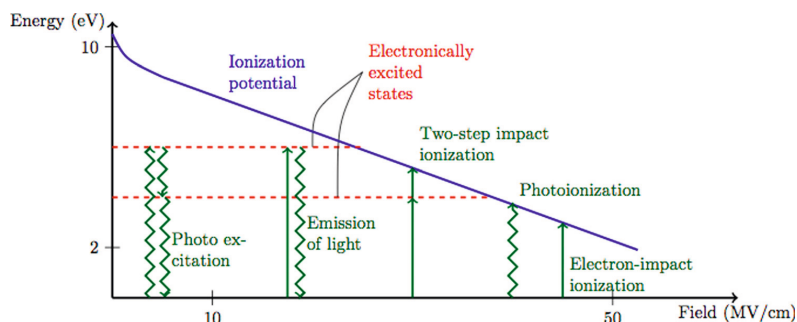


FIG. 1. A sketch of different possible ionization processes in the field for an insulating molecule. Each process can happen at different fields and the processes have been placed in the graph with a purpose of a clear presentation. Field ionization is not included since it is a pure statistical process. The scales, both for energy and the electric field, are only indicative. Solid arrows denote an electron impact process and wavy arrows denote light.

probably vary from liquid to liquid depending on the chemical composition of the liquid. As a starting point, this work is restricted to the calculation of the field-dependent excitation energies and ionization potentials for a set of relevant molecules to illustrate that various molecules behave quite differently.

II. THEORY

A. Field-dependent model of the ionization potential

The IP of a molecule A in the presence of an electric field is defined by⁷

$$IP = U_{A^+} + V_{e^-} - U_A, \quad (1)$$

where U_{A^+} is the energy of a cation, V_{e^-} is the interaction energy between an electron placed at a position R relative to the cation in the field, and U_A is the energy of the molecule in the electric field. The energy of the cation in an electric field is dependent on the choice of origin since an ion is accelerated by the force of an electric field. But if the cation and electron are considered as a combined neutral system ($A^+ + e^-$), the total energy will be origin-independent. In our model,⁷ the electron is regarded as a negative point charge and the interaction energy between the electron at position R and the molecular cation is calculated. In practice, the point charge is placed at a certain distance from a chosen atom of the cation and the distance between the point charge and the cation is varied along the direction of the field. The total energy of the combined system at the maximum of the energy, U_{max} , along the escaping path of the electron is used to calculate the IP. It has been found that the choice of the atom from which the electron is pulled out has a small effect on the IP.⁷ In the following, a detailed description of the model is given with one of the studied molecules as an example. An electric field of 5.14–102.8 MV/cm is applied to glyceryltributyrate (GTB) (see Figure 2) in the positive x , y , and z directions. The point charge is positioned at distances 2–22 Å from the origin shown in Figure 2.

At each electric field, the point charge distance from the cation is varied in the opposite direction of the field and the interaction energy is plotted against the position of the point charge. Figures 3(a) and 3(b) show the interaction energy between GTB cation and the point charge in $E_z = 20.56$ and 77.1 MV/cm, respectively. The maximum position of the

point charge relative to the cation at the fields 20.56 and 77.1 MV/cm are 10.0 and 4.0 Å, respectively.

The IP is calculated as

$$IP = U_{max} - U_A \quad (2)$$

and the IP of GTB becomes 5.94 and 4.04 eV at $E_z = 20.56$ and 77.1 MV/cm, respectively.

The validation of the model has been performed by comparison with the classical results of IP for the fields below 30 MV/cm.⁷ In high electric fields, conductivity of the insulating materials increases because of the increase in the number of free charge carriers. The high-field conductivity in the bulk material can be explained by the classical Poole-Frenkel mechanism with the following equation:²⁵

$$\sigma(E) = \sqrt{N_{eff} N_d} \mu e^{-\frac{IP_0}{2k_B T}} e^{-\frac{\sqrt{E}}{k_B T \sqrt{\epsilon_r}}}, \quad (3)$$

where N_{eff} is the effective density of states in the conduction band, N_d is the number density of the molecules, μ is the mobility of free electrons in the conduction band, ϵ_r is the relative permittivity of the material, IP_0 is the IP of molecules at zero field, and E is the electric field. From Eq. (3), it is assumed that the IP of a molecule depends on the square root of the electric field

$$IP = IP_0 - 2\sqrt{\frac{E}{\epsilon_r}}. \quad (4)$$

This functional form of the field dependence of the IP has been reported in previous experimental works^{26,27} and computational work.⁷

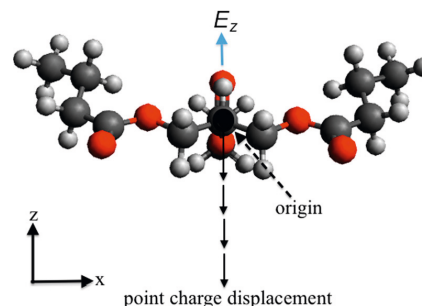


FIG. 2. The position of a point charge with respect to the GTB cation in z direction of the electric field.

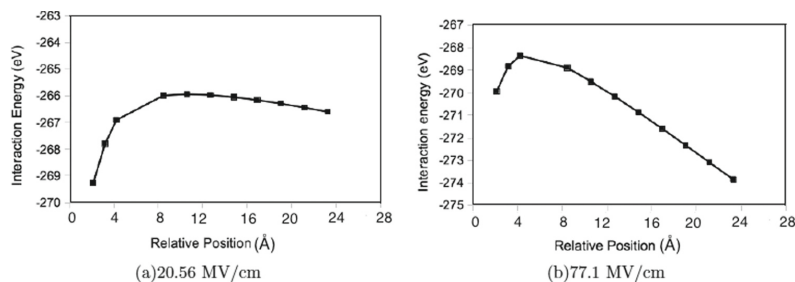


FIG. 3. The interaction energy between the GTB cation and the point charge in the different positions in z direction of the electric field.

B. Field-dependent excitation energies

In this work, we will focus on the calculation of the excitation energies in an electric field. For this purpose, time-dependent density functional theory (TDDFT)²⁸ was used to calculate the 20 lowest singlet-singlet excitation energies for each molecule. Although TDDFT has become the standard tool for calculating excitation energies, it also has several shortcomings.²⁹ The accuracy of TDDFT may vary depending on the choice of exchange correlation functionals, especially in the description of high-lying Rydberg states, the excited states of long-range charge-transfer systems, and double or higher order excitations.^{30,31} The exchange correlation potential generated by approximate standard functionals such as the local density approximation (LDA) and the generalized gradient approximation (GGA) decays too rapidly in contrast to the slow asymptotic decay of the true electrostatic potential. Thus, these functionals provide poor results when the excitation energies get close to the ionization threshold.³² In the field, the excited states become more diffuse and it is shown in Sec. IV that some of the excitation energies remain in higher fields with energies close to the IP. This might be the result of using different models for the calculation of IP compared with the excitation energy and also the deficiency of the local exchange correlation functional in the interpretation of diffuse excited states in high fields.

It is important to identify if an excited state is a bound or unbound state at high electric fields since there is a transition from bound to unbound of some of the excited states. As the field increases, some of the excited states change into ionized states. Figure 4 shows the lowest unoccupied molecular orbital (LUMO) for *trans*-azobenzene (TAB) in the electric field of $E_x = 0$ and 51.4 MV/cm. The LUMO which is the π^* orbital of the azo bond is unbound at $E_x = 51.4$ MV/cm. For each molecule in this study, it will be shown that at high electric fields some of the excited states change into ionized

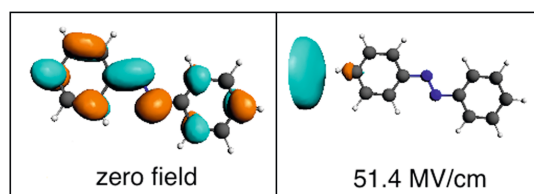


FIG. 4. π_{azo}^* at $E_x = 0$ and $E_x = 51.4$ MV/cm for TAB.

unbound states. Since excited states become more diffuse in an electric field, an augmented basis set is used that results in a better description of the excitation energies in a high field.

III. COMPUTATIONAL DETAILS

All the calculations are done using the ADF software package.^{33,34} The geometry optimizations of all the molecules are performed using the PBE³⁵ functional with the augmented triple-zeta polarization (TZP) basis set^{36,37} and the optimized geometries of ground states are used for the calculation of vertical IP and excitation energies in the electric field. The electric field is between 0 and 102.8 MV/cm which is beyond the range of interest in the streamer propagation process. The unrestricted open shell method is applied for the optimization of the molecular cation. For each molecule, the 20 lowest singlet-singlet excitation energies are calculated by TDDFT method with the same functional and basis set. The field-dependent IP was calculated as described in Ref. 7.

IV. RESULTS

Figure 5 shows the molecules chosen for this study: TAB, GTB, trichloroethylene (TCE), *N,N*-dimethylaniline (DMA), tetrakis (dimethylamino) ethylene (TDAE), and 9,10-dimethyloctadecane (DMOD). DMA and TCE are selected because of the previous experimental studies on additives applied in streamer experiments.^{20–22,38} It was found that the IP of the additives has a significant effect on pre-breakdown phenomena and propagation.²⁰ For this reason, TDAE is chosen since it is an organic amino compound with a very low IP compared with other organic molecules.³⁹ TAB has a low singlet-singlet excitation energy at 2.21 eV (Ref. 40) which may represent a relevant property to be used as an additive. DMOD has the potential to be used as a base insulating liquid because of its desirable physical properties such as high viscosity indices, good thermal and oxidative stabilities, and low toxicity.⁴¹ GTB is an ester molecule with some advantages as a base insulating liquid. Ester liquids are used as insulating liquids in high voltage applications. In addition to good biodegradability properties, they have a much higher fire point compared to mineral oils.^{42,43} In this section, the effect of the electric field on the IP and the 20 lowest excitation energies are studied. The electric field is applied on the positive direction for all the molecules. The excitations surviving at high electric field are studied in more detail.

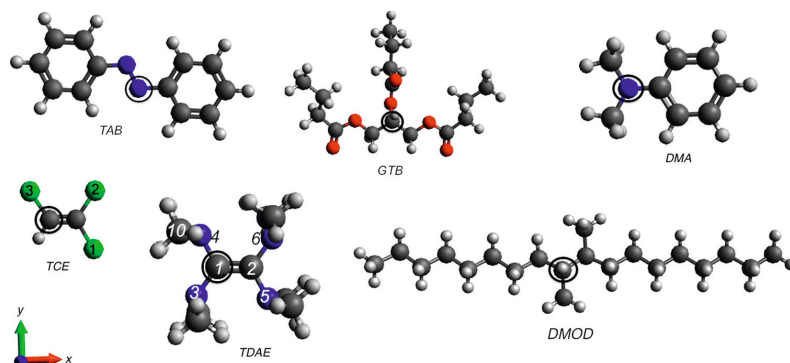


FIG. 5. Structure of molecules in the coordinate system indicated in the left corner. The origin of the coordinate system for each molecule is shown by a circle.

A. *trans*-azobenzene

Figure 5 shows how TAB is placed in the coordinate system. The geometrical parameters are in good agreement with the experimental structure⁴⁴ with typical errors within 0.03 Å and 1.0° which indicates the coplanarity of azo bond with the phenyl rings. The x and y directions are the in-plane and z is the out-of-plane electric field, respectively. Figure 6 shows the IP and excitation energies in the x , y , and z directions of the electric field, respectively. The experimental $\pi \rightarrow \pi^*$ excitation energy is 3.54 eV (Ref. 45) compared to our calculated value of 3.36 eV. Applying an electric field facilitates ionization processes, i.e., as the electric field increases, the IP becomes smaller. The reduction of IP is a little more significant for E_x which is the direction through the two phenyl rings and also some of the excitation energies are reduced in magnitude in this direction. This is reasonable since the π orbitals are extended in the x direction.

The excitation energies remain almost constant in the field but for E_x some of them decrease slightly. To understand these variations, the MOs that are involved in these excitations are inspected. The MOs show that the excitations at $E < 25.7$ MV/cm are the same as in zero field. The reduction of some of the excitation levels mainly originate from two reasons: some MOs tend to be more delocalized as the field

increases and second, the contributions of various transitions to some excitations change significantly which result in lowering of the excitation energies as exemplified below.

For E_x , the symmetry of the molecule is broken. At $E_x = 61.7$ MV/cm, six excitations exist. The first excitation is from the lone pairs of the nitrogen atoms (n_{azo}) to the π^* orbital of the azo bond (π_{azo}^*). Figure 6(a) shows that this excitation remains constant in the field and disappears at $E_x > 61.7$ MV/cm. The reason is that π_{azo}^* changes into an ionized state (see Figure 4).

The second excitation in TAB is π_{azo} to π_{azo}^* with a minor contribution of the π orbitals of the benzene rings, π_b , to π_{azo}^* . As the field increases, the contribution of π_b to π_{azo}^* becomes greater. Since the latter transition is lower in energy than the former, a deduction in the second excitation energy is observed. The third excitation at $E_x = 61.7$ MV/cm is n_{azo} to π_b^* and the fourth one is π_b to π_{azo}^* . The last two excitations are transitions between π_b and π_b^* .

The other in-plane field, E_y , is slightly less effective than E_x because the excitations remain constant by increasing the field mainly since E_x includes a polarization from one phenyl ring to the other. The first excitation (n_{azo} to π_{azo}^*) survives also at the higher fields. At $E_y = 51.4$ MV/cm, there are four other excitations. The first three of these excitations are

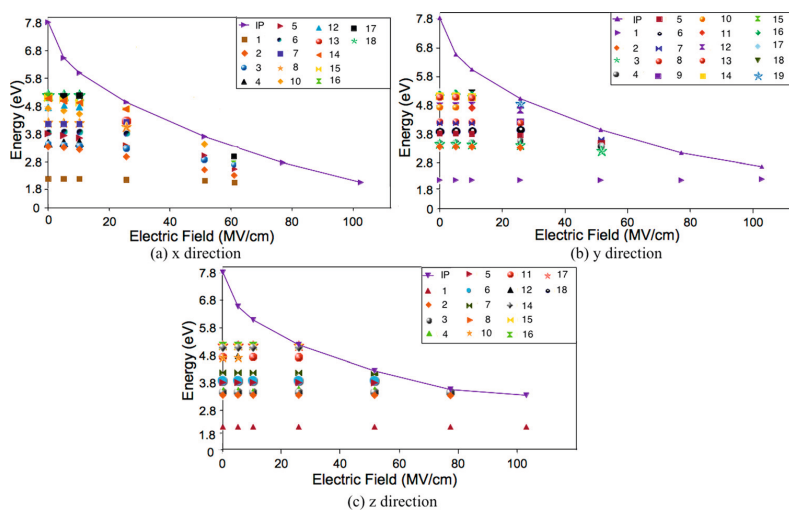


FIG. 6. The ionization potential and the excitation energies (eV) in different directions of the electric field for TAB. The solid line shows the IP and the dots are the excitation energies.

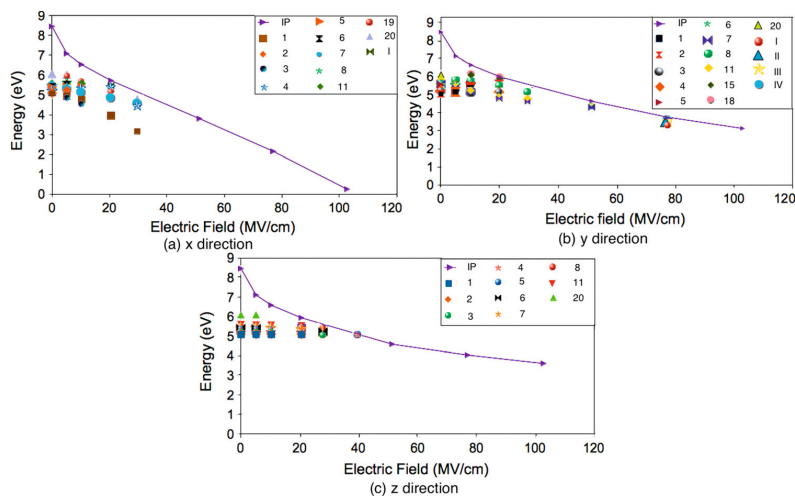


FIG. 7. The variation of the ionization potential and the excitation energies (eV) in different directions of the electric field for GTB. The solid line shows the IP and the dots are the excitation energies.

mainly composed of transition from π_b to π_{azo}^* , π_{azo} to π_{azo}^* with a little contribution of π_b to π_{azo}^* and π_{azo} to π_{azo}^* , respectively. The last one is contributed equally from π_{azo} to π_b^* and π_b to π_{azo}^* . The excitations in the out-of-plane field, E_z , also remain constant and these excitations are almost similar to the zero field. There are seven, four, and one excitations at 51.4, 77.1, and 102.8 MV/cm, respectively. The first excitation remains also at 102.8 MV/cm. At 77.1 MV/cm, the second, third, and fourth excitations have the same energy and are mainly composed of transitions π_{azo} and π_b to π_{azo}^* with different contributions. At 51.4 MV/cm, there are three other excitations that two of them are degenerate and from n_{azo} to π_b^* and the last one is mostly contributed from the π orbital of benzene rings including the nitrogen atoms (π_{ba}) to π_{azo}^* .

At some electric fields, there are a few excitation energies that lie very close to the IP. These excitation energies are likely the result of the different models for calculating the IP and the excitation energies and the deficiencies in these models, and should probably be above the IP.

B. Glyceryltributyrate

The central carbon atom in GTB is chosen as the origin (see Figure 5 for the coordinate system). For E_x , the IP decreases sharply and it approaches zero at $E_x > 100$ MV/cm (see Figure 7). The ground state of the molecule changes at $E_x > 100$ MV/cm, consequently the electronic properties of the molecule is different compared with $E_x < 100$ MV/cm.

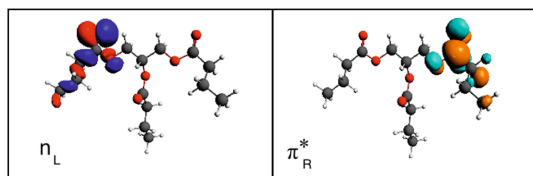


FIG. 8. The first excitation at $E_x = 31.0$ MV/cm for GTB (L refers to the left chain and R refers to the right chain).

GTB is more sensitive to the direction of the electric field than the other molecules and the electric field is able to shift the order of the excited states.

It is observed that some of the excitation energies decrease in E_x . At $E_x > 31.0$ MV/cm, the excited states change into ionized states. Four excitations are observed at 31 MV/cm. Only one of the carbonyl π^* orbitals of side chains remains bound (π_R^* : R refers to the right chain), whereas the others are ionized at this field. The first excitation is from the lone pairs of the oxygen atoms of the left chain (n_L) to the π_R^* orbital (Figure 8).

The second excitation is from the lone pairs of oxygen atom in the middle chain (n_m) to the π_R^* orbital. The third and fourth excitations are from the lone pairs of side oxygen atoms, n_L and n_R , to π_R^* orbital. For E_y , some of the excitation energies increase slightly. The molecular orbitals of these excitations are almost different from the molecular orbitals in zero field. As an example, the molecular orbitals of the

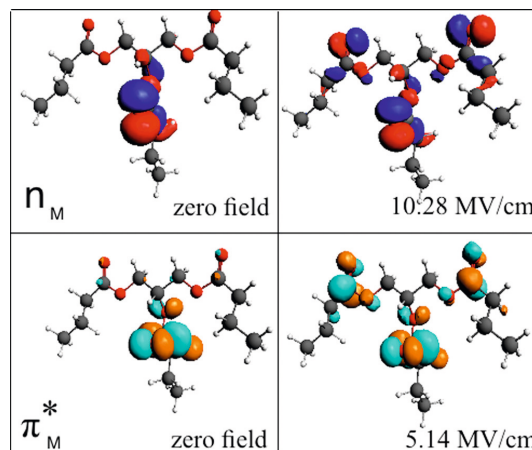


FIG. 9. The molecular orbitals that are involved in the second excitation in y direction for GTB (M refers to the middle chain).

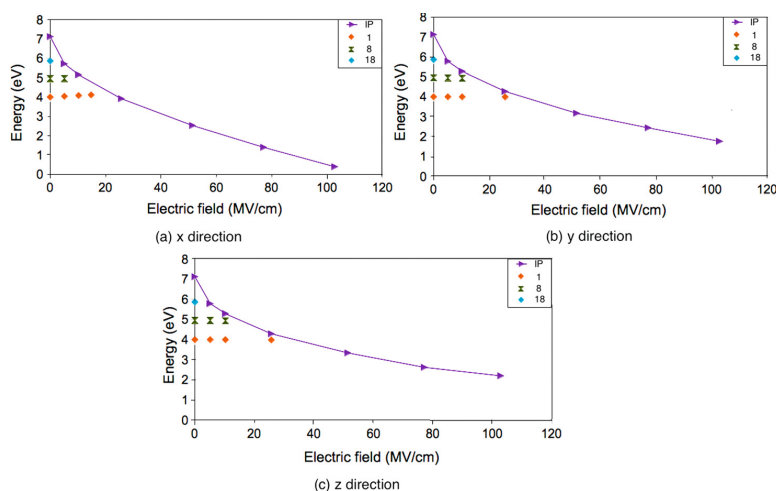


FIG. 10. The ionization potential and the excitation energies (eV) in different directions of the electric field for DMA. The solid line shows the IP and the dots are the excitation energies.

second excitation are shown in Figure 9. The lone pairs and carbonyl π^* orbitals are delocalized over the three chains. At $E_y > 31.0$ MV/cm, the excitation energies are quite similar to the IP, again indicating that this may be a result of using different approaches for the IP and the excitation energies. Ideally, these excitations should have been above the IP.

In the field perpendicular to the molecule, the excitation energies remain constant. At $E_z = 41.1$ MV/cm, the excitation energies are almost equal to the IP and should be regarded as an ionization.

C. N,N-dimethylaniline

The nitrogen atom in DMA is the origin of the coordinate system and the x and y directions are the in-plane and z is the out-of-plane electric field, respectively (see Figure 5). The molecular structure is in good agreement with the structure obtained from the gas-phase electron diffraction experiment.⁴⁶ Figure 10 shows the reduction of the IP and the two excitation energies in the field. The calculated and experimental IP are both 7.12 eV at zero electric field.⁴⁷ The first excitation around 4.0 eV, compared to the experimental lowest excitation energy of 4.08 eV,⁴⁸ is from the lone pair of nitrogen atom (n) to the first π_{b1}^* orbital of benzene ring. The second excitation with the energy about 5.0 eV is from n to the second π_{b2}^* orbital of benzene ring. The excitation energies are high in comparison to TAB, but with a similar IP. Therefore, there are fewer excited states with energy

between first excitation and the IP. The first excitation disappears at the fields higher than 26 MV/cm in y and z directions, whereas the threshold field in x direction is 15.4 MV/cm. The π_{b1}^* orbital changes into an ionized state at fields higher than the threshold field (Figure 11).

D. Tetrakis-(dimethylamino)ethylene

The results obtained for TDAE do not correspond to the experimental structure,⁵⁰ since with our computational approach we obtain a planar geometry apart from the methyl groups (see Figure 5). There is a dihedral angle of 28.2° around the central ethylene bond in the experimental structure.⁵⁰ Table I summarizes the structural parameters obtained in this work (first column) in comparison to literature values.^{49,50} The experimental vertical IP in zero field is about 6.11 eV,³⁹ while for the planar geometry it is 7.49 eV. This molecule therefore seems to be a difficult model to handle with DFT functionals, but we still include a brief comparison in our study and we will return to it in a more detailed study.

Figure 5 shows that a carbon in the ethylene bond is chosen as the origin of the coordinate system. In Figure 12, the IP shows a reduction in the field similar to the other molecules. There are four MOs of the lone pairs of the nitrogen atoms that are involved in the 20 lowest excitations. Four excited states remain up to 25.7 MV/cm in all directions of the field. The first excitation is from the lone pairs of nitrogen 3 and 6 (n_1) (see Figure 5 for the labels) to the π^* orbital of ethylene bond. This orbital becomes unbound at E_x and

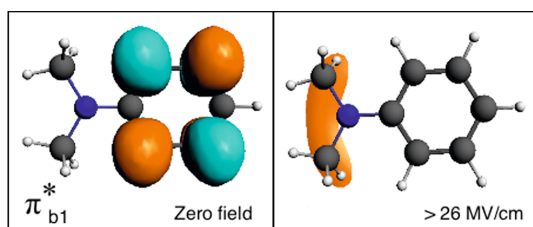


FIG. 11. LUMO at $E_z = 0$ and >26 MV/cm for DMA.

TABLE I. Structural parameters for TDAE based on the labels shown in Figure 5 (bond lengths (Å) and angles ($^\circ$)).

	PBE/aug-TZP	B3LYP/cc-pVTZ ⁴⁹	Exp. ⁵⁰
1-2	1.35	1.36	1.36
1-4	1.44	1.45	1.40
4-10	1.47	1.44	1.45
6-2-5	116.0	112.8	118.4
4-1-2-6	0.0	31.1	28.2

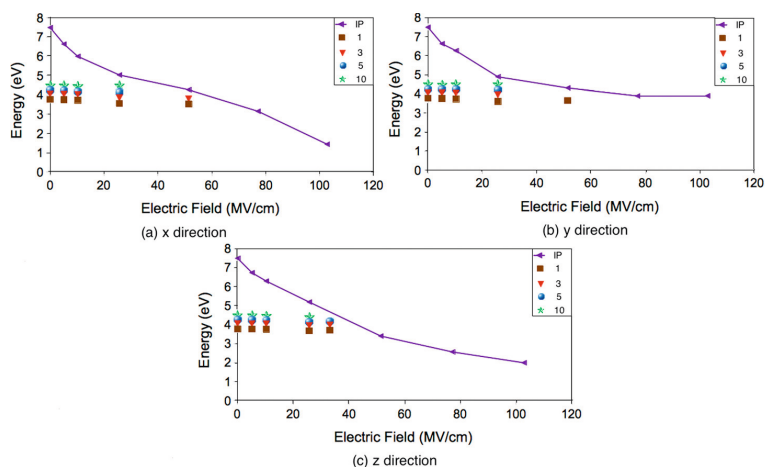


FIG. 12. The variation of the ionization potential and excitation energies (eV) in different directions of the electric field for TDAE. The solid line shows the IP and the dots are the excitation energies.

$E_y > 51.7$ MV/cm. The second excitation is from the lone pairs of nitrogen 3 and 5 in combination with nitrogen 4 and 6 (n_2) to the ethylene π^* orbital. The third and fourth excitations are n_3 and n_4 to π^* , respectively. n_3 is the lone pairs of nitrogen 4 and 5 and n_4 is the lone pairs of nitrogen 3 and 4 in combination with 5 and 6. The threshold field is 51.7 MV/cm in the x and y directions and 36.0 MV/cm in the z direction, respectively.

E. Trichloroethylene

One of the ethylene carbon atoms in TCE is chosen as the origin (see Figure 5). The obtained structure is in good agreement with the experimental structure⁵¹ and the calculated IP is 9.17 eV compared to the experimental value of 9.68 eV.⁵² Figure 13 shows that the IP decreases with the field as seen for the other molecules. TCE has a large number of excitations at $E < 25.7$ MV/cm. The excitation energies remain almost constant in the different directions of the field. The first two excitations around 5 eV remain in the higher fields. The electron transfers in these two excitations are between ethylene π orbital to carbon-chlorine σ^* orbitals.

There are two σ^* orbitals, σ_1^* which is corresponding to the bond between carbon and chlorine 1 and σ_2^* which is related to chlorine 2 and 3 (see Figure 5). The experimental value of this transition energy is 5.34 eV.⁵³ In addition to the first two excitations, at 25.7 MV/cm there are two more excitations that are from the ethylene π orbital and lone pairs of chlorine atoms to the ethylene π^* orbital.

F. 9,10-dimethyloctadecane

The chosen origin for DMOD is shown in Figure 5. E_x is along the molecular chain and E_y and E_z are perpendicular to the chain, respectively. Figure 14 shows that E_x reduces the IP significantly so that at about 60 MV/cm, the IP is around 2 eV. The same behavior was found for n -tridecane.⁷ This molecule is sensitive to the direction of the field similar to GTB and n -tridecane. The excited states change into ionized states in the fields higher than 1.0 MV/cm. At $E_x = 1.0$ MV/cm there are five excited states, where the electron is transferred from carbon-hydrogen and carbon-carbon σ orbitals to the σ^* orbitals.

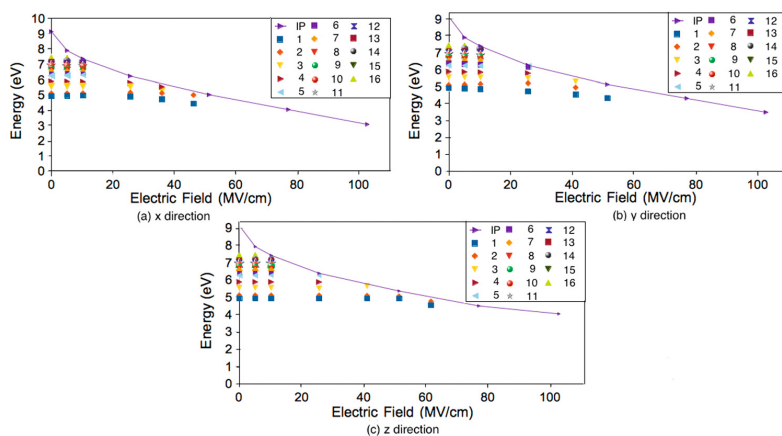


FIG. 13. The variation of the ionization potential and excitation energies (eV) in different directions of the electric field for TCE. The solid line shows the IP and the dots are the excitation energies.

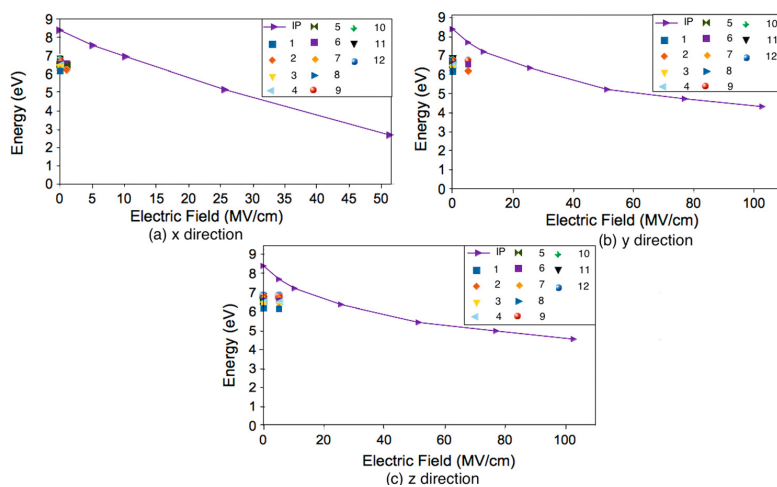


FIG. 14. The variation of the ionization potential and the excitation energies (eV) in different directions of the electric field for DMOD. The solid line shows the IP and the dots are the excitation energies.

For E_y , four excitations remain up to 5.1 MV/cm and the electron transfer is between carbon-hydrogen and carbon-carbon σ orbitals to σ^* orbitals. For E_z , there are three carbon-carbon and carbon-hydrogen σ^* orbitals. Therefore, there are 11 excitations at $E_z = 5.1$ MV/cm.

By comparing DMOD with *n*-tridecane in Ref. 7, we can conclude that the number of carbon atoms has a small effect on the IP of alkanes. Moreover, the first excitation energy is almost the same for both molecules.

V. DISCUSSION

In the lower fields, the deduction of IP is more significant than in the higher fields. The excitation energies of most of the molecules are almost constant in the field as compared to the field-dependence of the IP. In some cases, there is a smooth decrease in the excitation energies that can be explained by that some of the excited states tend to become more delocalized as the field increases. The number of excited states decreases by increasing the field for all the studied molecules. Figure 15 shows the maximum number of excited states for each molecule in the in-plane (or along the chain) and the out-of-plane (or perpendicular to the chain) electric field, respectively. At high fields, the number of excited states might be less than what is shown in Figure 15 since the excitation energies that are close to the IP should be regarded as ionizations.

TAB and TCE have the largest number of excited states at low electric fields but for DMOD all the excited states vanish at a relatively low electric field. TCE has a higher number of excited states than TAB, but its excited states vanish at fields lower than for TAB. In an electric field, an electron has sufficient energy to excite a molecule and lose most of its energy before ionizing the molecule. As the field increases, the number of excited states decreases and ionization is more likely to take place since also the IP is decreasing with the field. Furthermore, that excited states important for the insulation process vanish may be one of the reasons to the transition to fast mode streamers.

VI. CONCLUSION

The behavior of different types of molecules is different in the field. For the studied molecules, the IP decreases in the electric field, whereas the excitation energies remain almost constant as compared to the IP. At a threshold field, all the excited states vanish and the value of the threshold field depends on the type of the molecule. For example, the first excited state in TAB remains at $E = 102.8$ MV/cm,

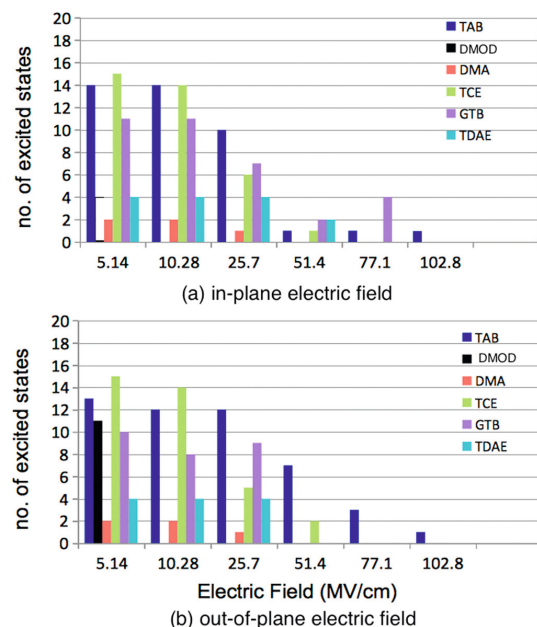


FIG. 15. The maximum number of excited states in the in-plane and out-of-plane electric field (for GTB and DMOD) (a) electric field along the chain, (b) perpendicular to the chain).

because of its low excitation energy compare to the IP, while, in DMOD the first excited state disappears at $E = 5$ MV/cm. The effect of the direction of the field on IP is significant in GTB and DMOD, but it has a little effect on the excitation energy. It is indicated that excitation energies are important factors for electrically insulating materials and its role will be investigated in more detail both experimentally and theoretically in future studies.

ACKNOWLEDGMENTS

We would like to acknowledge a research grant "Modeling of electrical pre-breakdown and breakdown phenomena in insulating liquids" (200631/560) from the Norwegian Research Council, ABB and Statnett and a grant of computer time (account nn2920k) from the NOTUR project.

- ¹R. A. Lipshtein and M. Shakhovich, *Transformer Oil* (IPST Press, Moskva, 1970).
- ²A. C. M. Wilson, *Insulating Liquids, Their Uses, Manufacture and Properties* (The Institution of Electrical Engineers, London, 1980).
- ³R. Bartnikas, *Electrical Insulating Liquids. Engineering Dielectrics* (ASTM International, 1994), Vol. 3.
- ⁴N. Berger, M. Randoux, G. Ottmann, and P. Vuarchex, "Review on insulating liquids," *Electra* **171**, 33 (1997).
- ⁵A. Denat, "High field conduction and prebreakdown phenomena in dielectric liquids," *IEEE Trans. Dielectr. Electr. Insul.* **13**, 518 (2006).
- ⁶A. Denat, "Conduction and breakdown initiation in dielectric liquids," in *International Conference on Dielectric Liquids* (Trondheim, Norway, 2011).
- ⁷H. S. Smalø, Ø. Hestad, S. Ingebrigtsen, and P.-O. Åstrand, "Field dependence on the molecular ionization potential and excitation energies compared to conductivity models for insulation materials at high electrical fields," *J. Appl. Phys.* **109**, 073306 (2011).
- ⁸A. A. Zaky and R. Hawley, *Conduction and Breakdown in Mineral Oil* (Peter Peregrinus, London, UK, 1973).
- ⁹R. E. Hebner, *Measurements of Electrical Breakdown in Liquids, The Liquid State and its Electrical Properties* (Plenum, New York, 1989).
- ¹⁰A. Beroual, M. Zahn, A. Badent, K. Kist, A. J. Schwabe, H. Yamashita, K. Yamazawa, M. Danikas, W. G. Chadband, and Y. Torshin, "Propagation and structure of streamers in liquid dielectrics," *IEEE Electr. Insul. Mag. (USA)* **14**, 6 (1998).
- ¹¹V. Y. Ushakov, V. Klimkin, and S. Korobeynikov, *Impulse Breakdown of Liquids, Power Systems* (Springer, 2007).
- ¹²L. Angerer, "Effect of organic additives on electrical breakdown in transformer oil and liquid paraffin," *Proc. IEE* **112**, 1025 (1965).
- ¹³S. Sakamoto and H. Yamada, "Optical study of conduction and breakdown in dielectric liquids," *IEEE Trans. Electr. Insul.* **EI-15**, 171 (1980).
- ¹⁴J. C. Devins, S. J. Rząd, and R. J. Schwabe, "Breakdown and prebreakdown phenomena in liquids," *J. Appl. Phys.* **52**, 4531 (1981).
- ¹⁵R. E. Hebner, E. F. Kelley, E. O. Forster, and G. J. Fitzpatrick, "Observation of prebreakdown and breakdown phenomena in liquid hydrocarbons-II. Non-uniform field conditions," *IEEE Trans. Electr. Insul.* **EI-20**, 281 (1985).
- ¹⁶W. G. Chadband and T. Sufian, "Experimental support for a model of positive streamer propagation in liquid insulation," *IEEE Trans. Electr. Insul.* **EI-20**, 239 (1985).
- ¹⁷Y. Nakao, H. Itoh, S. Hoshino, Y. Sakai, and T. Hagashira, "Effects of additives on prebreakdown phenomena in n-hexane," *IEEE Trans. Dielectr. Electr. Insul.* **1**, 383 (1994).
- ¹⁸O. Lesaint and M. Jung, "On the relationship between streamer branching and propagation in liquids: Influence of pyrene in cyclohexane," *J. Phys. D: Appl. Phys.* **33**, 1360 (2000).
- ¹⁹Y. Nakao, T. Yamazaki, K. Miyagi, Y. Sakai, and H. Tagashira, "The effect of molecular structure on prebreakdown phenomena in dielectric liquids under a nonuniform field," *Electr. Eng. Jpn.* **139**, 1 (2002).
- ²⁰S. Ingebrigtsen, H. S. Smalø, P.-O. Åstrand, and L. E. Lundgaard, "Effects of electron-attaching and electron-releasing additives on streamers in liquid cyclohexane," *IEEE Trans. Dielectr. Electr. Insul.* **16**, 1524 (2009).
- ²¹S. Ingebrigtsen, L. E. Lundgaard, and P.-O. Åstrand, "Effects of additives on prebreakdown phenomena in liquid cyclohexane: II. Streamer propagation," *J. Phys. D: Appl. Phys.* **40**, 5624 (2007).
- ²²Ø. Hestad, H. S. Smalø, P.-O. Åstrand, S. Ingebrigtsen, and L. E. Lundgaard, "Effects of N,N-dimethylaniline and trichloroethene on prebreakdown phenomena in liquid and solid n-tridecane," *IEEE Trans. Dielectr. Electr. Insul.* **18**, 1886 (2011).
- ²³O. Lesaint and G. Massala, "Positive streamer propagation in large oil gaps. Experimental characterization of propagation modes," *IEEE Trans. Dielectr. Electr. Insul.* **5**, 360 (1998).
- ²⁴L. Lundgaard, D. Linhjell, G. Berg, and S. Sigmond, "Propagation of positive and negative streamers in oil with and without pressboard interfaces," *IEEE Trans. Dielectr. Electr. Insul.* **5**, 388 (1998).
- ²⁵L. A. Dissado and J. C. Fothergill, *Electrical Degradation and Breakdown in Polymers*, IEE Material and Devices Series, Vol. 9 (Peter Peregrinus Ltd., London, United Kingdom, 1992).
- ²⁶N. Erdmann, M. Nunnemann, K. Eberhardt, G. Herrmann, G. Huber, S. Köhler, J. V. Kratz, G. Passler, J. R. Peterson, N. Trautmann, and A. Waldek, "Determination of the first ionization potential of nine actinide elements by resonance ionization mass spectroscopy (RIMS)," *J. Alloys Compd.* **271-273**, 837 (1998).
- ²⁷S. Douin, P. Parneix, and P. Brechignac, "Solvent shift of the ionization potential of the aniline-argon system," *Z. Phys. D* **21**, 343 (1991).
- ²⁸G. Zhang and C. B. Musgrave, "Comparison of DFT methods for molecular orbital eigenvalue calculations," *J. Phys. Chem. A* **111**, 1554 (2007).
- ²⁹K. Burke, J. Werschnik, and E. K. Gross, "Time-dependent density functional theory: Past, present, and future," *J. Chem. Phys.* **123**, 062206 (2005).
- ³⁰A. Dreuw and M. H. Gordon, "Failure of time-dependent density functional theory for long-range charge-transfer excited states: The zincbacteriochlorin-bacteriochlorin and bacteriochlorophyll-spheroidene complexes," *J. Am. Chem. Soc.* **126**, 4007 (2004).
- ³¹I. Ciofini and C. Adamo, "Accurate evaluation of valence and low-lying rydberg states with standard time-dependent density functional theory," *J. Phys. Chem. A* **111**, 5549 (2007).
- ³²M. E. Casida and D. R. Salahub, "Asymptotic correction approach to improving approximate exchange correlation potentials: Time-dependent density-functional theory calculations of molecular excitation spectra," *J. Chem. Phys.* **113**, 8918 (2000).
- ³³G. te Velde, F. M. Bickelhaupt, E. J. Baerends, C. F. Guerra, S. J. A. van Gisbergen, J. G. Snijders, and T. Ziegler, "Chemistry with ADF," *J. Comput. Chem.* **22**, 931 (2001).
- ³⁴C. F. Guerra, J. G. Snijders, G. te Velde, and E. J. Baerends, "Towards an order-*N* DFT method," *Theor. Chem. Acc.* **99**, 391 (1998).
- ³⁵J. P. Perdew, K. Burke, and M. Ernzerhof, "Generalized gradient approximation made simple," *Phys. Rev. Lett.* **77**, 3865 (1996).
- ³⁶E. van Lenthe, E. J. Baerends, C. F. Guerra, S. J. A. van Gisbergen, J. G. Snijders, and T. Ziegler, "Optimized Slater-type basis sets for the elements 1-118," *J. Comput. Chem.* **24**, 1142 (2003).
- ³⁷D. P. Chong, "Augmenting basis set for time-dependent density functional theory calculation of excitation energies: Slater-type orbitals for hydrogen to krypton," *Mol. Phys.* **103**, 749 (2005).
- ³⁸S. Ingebrigtsen, L. E. Lundgaard, and P.-O. Åstrand, "Effects of additives on prebreakdown phenomena in liquid cyclohexane: I. Streamer initiation," *J. Phys. D: Appl. Phys.* **40**, 5161 (2007).
- ³⁹Y. Nakato, M. Ozaki, E. Egawa, and H. Tsubomura, "Organic amino compounds with very low ionization potentials," *Chem. Phys. Lett.* **9**, 615 (1971).
- ⁴⁰P.-O. Åstrand, P. S. Ramanujam, S. Hvilsted, K. L. Bak, and S. P. A. Sauer, "Ab initio calculation of the electronic spectrum of azobenzene dyes and its impact on the design of optical data storage materials," *J. Am. Chem. Soc.* **122**, 3482 (2000).
- ⁴¹S. S. Scheuermann, S. Eibl, and P. Bartl, "Detailed characterisation of isomers present in polyalpaolefin dimer and the effect of isomeric distribution on bulk properties," *Lubr. Sci.* **23**, 221 (2011).
- ⁴²T. V. Oomen, "Vegetable oils for liquid-filled transformers," *IEEE Electr. Insul. Mag. (USA)* **18**, 6 (2002).
- ⁴³L. Rongsheng, C. Törnkvist, V. Chandramouli, O. Girlanda, and L. A. A. Pettersson, "Ester fluids as alternative for mineral oil: The difference in streamer velocity and LI breakdown voltage," in *IEEE Conference on Electrical Insulation and Dielectric Phenomena* (2009), pp. 543-548.
- ⁴⁴C. J. Brown, "A refinement of the crystal structure of azobenzene," *Acta Crystallogr.* **21**, 146 (1966).


- ⁴⁵J. F. Rabek, *Photochemistry and Photophysics* (CRC Press, Boca Raton, USA, 1990), Vol. 2.
- ⁴⁶V. P. Novikov, S. Samdal, and L. V. Vilkov, "Molecular structure and conformation of n,n-dimethylaniline by gas-phase electron diffraction and quantum-chemical calculations," *Russ. J. Gen. Chem.* **74**, 1247 (2004).
- ⁴⁷D. R. Lide, *Handbook of Chemistry and Physics*, 84th ed. (CRC Press, Boca Raton, 2004).
- ⁴⁸R. A. Weersink, S. C. Wallace, and R. D. Gordon, "A reexamination of the S₀ → S₁ excitation spectrum of dimethylaniline," *J. Chem. Phys.* **103**, 9530 (1995).
- ⁴⁹J. Böhlín, M. Unge, and S. Stafström, "TDAE chemisorbed on gold," *J. Phys.: Condens. Matter* **20**, 315008 (2008).
- ⁵⁰H. Bock, H. Borrmann, Z. Havlas, H. Oberhammer, K. Ruppert, and A. Simon, "Tetrakis(dimethylamino)ethene: An extremely electron-rich molecule with unusual structure both in the crystal and in the gas phase," *Angew. Chem., Int. Ed.* **30**, 1678 (1991).
- ⁵¹Z. Kisiel and L. Pszczółkowski, "Assignment and analysis of the mm-wave rotational spectrum of trichloroethylene: Observation of a new, extended R-Band and an overview of High-J_r-Type bands," *J. Mol. Struct.* **178**, 125 (1996).
- ⁵²K. Kimura, S. Katsumata, Y. Achiba, T. Yamazaki, and S. Iwata, *Handbook of HeI Photoelectron Spectra of Fundamental Organic Compounds: Ionization Energies, Ab Initio Assignments, and Valence Electronic Structure for 200 Molecules* (Japan Scientific Societies Press, 1981).
- ⁵³Z. G. Min, C. Z. Xing, X. Min, and Q. X. Qing, "Study on the gas-phase photolytic and photocatalytic oxidation of trichloroethylene," *J. Photochem. Photobiol. A: Chem.* **161**, 51 (2003).

Paper 2

Field-dependent ionisation potential by constrained
density functional theory

Nazanin Davari, Per-Olof Åstrand and Troy Van Voorhis

Molecular Physics, 111, 1456-1461 (2013)



Is not included due to copyright

Paper 3

Field-dependent molecular ionization and excitation energies: Implications for electrically insulating liquids

Nazanin Davari, Per-Olof Åstrand, Mikael Unge, Lars E. Lundgaard and Dag Linhjell

AIP Advances, 4, 037117 (2014)





Field-dependent molecular ionization and excitation energies: Implications for electrically insulating liquids

N. Davari,¹ P.-O. Åstrand,^{1,a} M. Unge,² L. E. Lundgaard,³ and D. Linhjell³

¹Department of Chemistry, Norwegian University of Science and Technology (NTNU), NO 7491, Trondheim, Norway

²ABB Corporate Research, SE 72178 Västerås, Sweden

³Department of Electric Power Engineering, SINTEF Energy Research, NO 7491, Trondheim, Norway

(Received 6 January 2014; accepted 6 March 2014; published online 20 March 2014)

The molecular ionization potential has a relatively strong electric-field dependence as compared to the excitation energies which has implications for electrical insulation since the excited states work as an energy sink emitting light in the UV/VIS region. At some threshold field, all the excited states of the molecule have vanished and the molecule is a two-state system with the ground state and the ionized state, which has been hypothesized as a possible origin of different streamer propagation modes. Constrained density-functional theory is used to calculate the field-dependent ionization potential of different types of molecules relevant for electrically insulating liquids. The low singlet-singlet excitation energies of each molecule have also been calculated using time-dependent density functional theory. It is shown that low-energy singlet-singlet excitation of the type $n \rightarrow \pi^*$ (lone pair to unoccupied π^* orbital) has the ability to survive at higher fields. This type of excitation can for example be found in esters, diketones and many color dyes. For alkanes (as for example *n*-tridecane and cyclohexane) on the other hand, all the excited states, in particular the $\sigma \rightarrow \sigma^*$ excitations vanish in electric fields higher than 10 MV/cm. Further implications for the design of electrically insulating dielectric liquids based on the molecular ionization potential and excitation energies are discussed. © 2014 Author(s). All article content, except where otherwise noted, is licensed under a Creative Commons Attribution 3.0 Unported License. [<http://dx.doi.org/10.1063/1.4869311>]

I. INTRODUCTION

The molecular ionization potential (IP) in high electric fields is an important parameter in pre-breakdown and breakdown phenomena in electrically insulating liquids.^{1,2} In addition to the applied electric field, a molecule is influenced by the electric moments of its neighboring molecules. Therefore, the local field at a liquid molecule becomes larger than the applied field that may result in a considerable effect on the ionization in models describing streamer dynamics.³⁻⁵ It has also been discussed that the molecular excitation energies may affect streamer propagation.^{1,2} It has been suggested that since the number of available excited states decrease with increasing electric field, it may be the molecular origin of different streamer modes.² For molecules with many low excitation energies, some excited states survive at higher fields as compared to molecules with only a few relatively high excitation energies. In an applied voltage, an insulating liquid may lose the continuously added energy by emitting heat or light. It may therefore be anticipated that additives with low excitation energies will improve the insulating properties of a liquid.² We may have excitations by electron impact or by photon absorption. If the excited states have long life-times compared to the frequency of either electron impact or photon absorption, a two-step ionization

^aElectronic mail: per-olof.astrand@ntnu.no



process may take place where the excited molecule can be ionized,^{1,2} meaning that the excited states of additives should have relatively short life times to improve the insulating properties of a liquid. The strong field-dependence of the molecular IP also implies that photoionization should be regarded as a local effect since high-energy photons generated in regions with a low field may give ionization in high-field regions of the insulating liquid.² The strong field-dependent IP therefore gives rise to multitude of possible processes on the molecular scale, where the importance of each process will depend on the chemical composition.

Experimental studies on the effect of additives on streamer behavior demonstrate that the chemical composition and electronic properties of the base liquids and additives are important in describing the changes of the streamer characteristics.⁶⁻¹² It has been demonstrated that additives with electron-scavenging capabilities increase the velocity of negative streamers, while additives with low IP speed up positive streamers.¹³ In a recent work, the effect of a low-IP additive (N,N-dimethylaniline) on white oil (Exxsol-D140 and Marcol-52) has been studied in a long point-to-plane gap.¹⁴ It was found that N,N-dimethylaniline increases the streamer branching and velocity at low voltages. The branching becomes widespread and dense with increasing the voltage and reduces the field in front of the streamer channels as a result of the shielding effect. Therefore, the streamer speed decreases at specific voltage. In another recent work, azobenzene and N,N-dimethylaniline were added to an ester liquid and it was shown that azobenzene with lower excitation energies than N,N-dimethylaniline causes a significant increase in the acceleration voltage.¹⁵

Quantum chemistry provides methods to calculate molecular parameters that are comparable with experiments in terms of accuracy. Among the different quantum-chemical methods, density-functional theory (DFT) calculations are accurate and computationally efficient based on the choice of exchange-correlation functionals.¹⁶ Methods for calculating the field-dependent IP has been developed recently.^{1,17} In the first studies, a point-charge model is used^{1,2} that is a quantum-classical method based on the electrostatic interactions between a negative point-charge and a cation to find the transition state for the dissociation of an electron in an electric field. A more recent method is based on constrained DFT (CDFT),¹⁷ which is a full quantum-chemical approach that includes both the electrostatic interactions and the exchange effects between the electron and the cation. In CDFT, a constraint is placed on the electron density by a potential that is optimized to minimize the total energy of the system.^{18,19} For example, in long-range charge-transfer systems, the charges on molecular fragments are constrained to +1 or -1^{20,21} and also the spin on molecular fragments can be constrained to a desired value.²² The CDFT method has been used successfully for numerous chemical phenomena.²³⁻²⁶ In our approach, the electron is represented with a ghost atom, i.e. basis functions are added to an expansion center without a nuclear charge, and the charge of this ghost atom is constrained to -1. If the total system is electrically neutral, we thus have a DFT model for the interaction between an electron and a cation.¹⁷

For the field-dependent IP, the CDFT method was applied on a few small molecules in a model study.¹⁷ In this work, the CDFT method is used for different types of molecules relevant for insulation in dielectric liquids. The type of insulating liquids used in high-voltage applications are mainly mineral oils composed of paraffinic, naphthenic and aromatic contributions.^{27,28} Ester liquids have recently become an alternative to mineral oil.²⁹ Different liquids have different dielectric performances because of different electrochemical properties of the molecules in the liquids. Here, the IP and excitation energies of different types of molecules in the electric field are studied and compared to each other, as well as with our previous work.^{1,2,17}

II. THEORY

The IP is here calculated from the dissociation energy barrier of the interaction between an electron and a molecular cation. In the point-charge model,^{1,2} the interaction between a negative point charge, as a model for the electron, and a molecular cation is calculated by varying the distance between the point charge and the molecular cation in the electric field. The IP is calculated as the difference between the energy of a neutral molecule and the dissociation energy barrier in the field.¹

In this work, the CDFT method is used in which the electron is considered as a ghost atom, i.e. an atom without a nuclear charge.¹⁷ The charge on the ghost atom is constrained to -1 as a model

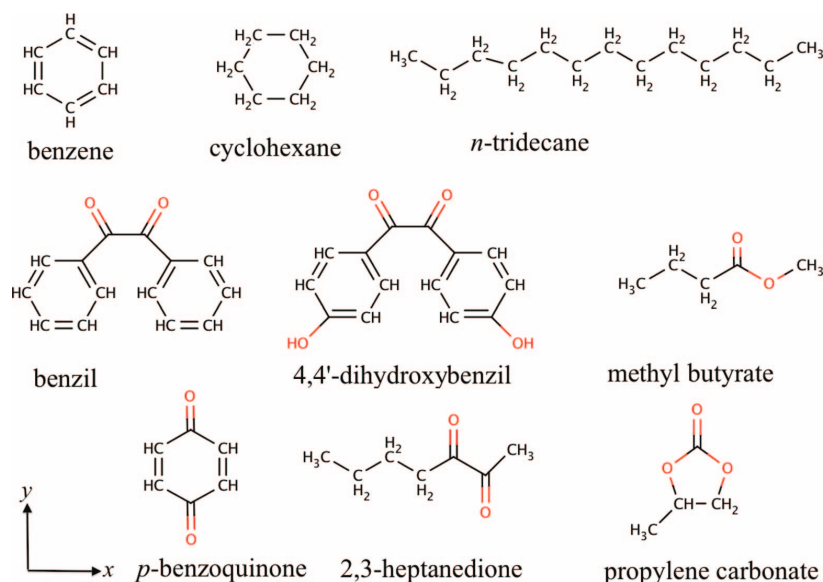


FIG. 1. The molecules included in this study with the coordinate system specified.

for the electron, and the spin of the electron is constrained to a doublet state while the entire system is kept electrically neutral with a singlet spin state. The distance between the ghost atom and the molecular cation is changed to obtain the dissociation barrier in an electric field.

The basis set on the ghost atom, i.e. the electron, is a linear combination of 6 primitive Gaussian *s*-functions with the exponents 0.5, 0.1, 0.02, 0.004, 0.008 and 0.00016. The number of basis functions is obtained to converge the IP to the order of 0.01 eV.¹⁷ Spherically symmetric *s*-functions are used so that the centre-of-charge of the electron remains at the expansion point of the basis functions, leading to that the position of the electron can be defined. There are some limitations in the calculation of the dissociation barrier since the dissociation barrier becomes closer to the molecule at higher fields.¹⁷ In these cases, the orbital of the electron becomes a linear combination of the basis functions of the electron and the basis functions of the cation and it therefore becomes difficult to control the position of the electron.

The geometry optimizations of all the molecules in zero field are done using the B3LYP functional^{30,31} with the cc-pVTZ basis set.³² This molecular geometry is used in subsequent calculations on the molecule and the cation at all electric fields. The Löwdin population scheme³³ is applied in the CDFT calculations for partitioning the electron distribution. The unrestricted open-shell DFT method is used for the cation calculations. More details about the approach is found in Ref. 17. The time-dependent DFT (TDDFT)³⁴ method is used to calculate the 20 lowest singlet-singlet excitation energies. For the excitation energies the aug-cc-pVTZ basis set³⁵ is applied since the excited states become more diffuse in the electric field. All the DFT calculations are performed using the NWChem software.³⁶ The electric field in NWChem is simulated by point charges that in this work are located at 50 and -50 Å whereas the molecule is located at the origin. The electric field is in the range 0 to 30 MV/cm.

III. RESULTS AND DISCUSSION

Figure 1 shows the structure of the included molecules, and in this figure also the coordinate system is defined. Different types of molecules are investigated related to electrically insulating

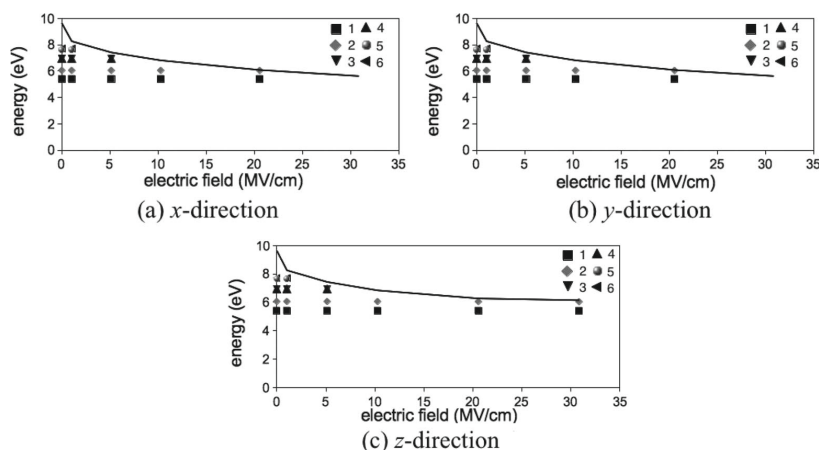


FIG. 2. The IP and excitation energies (eV) in the (a) x , (b) y , and (c) z direction of the electric field for benzene. The solid line is the IP and the dots are excitation energies.

liquids either as base liquids or as additives. The IP and excitation energies in different directions of the electric field are studied for benzene (aromatic), cyclohexane and n -tridecane (alkanes), propylene carbonate and methyl butyrate (esters), benzil, 4,4'-dihydroxybenzil, 2,3-heptanedione and p -benzoquinone (diketones). The excitations that remain at higher fields are investigated in more detail. The reported experimental IPs are adiabatic, whereas the calculated IPs are vertical.

A. Benzene

The presence of polyaromatics in transformer oil affects the streamer behavior. For example, 2-methyl naphthalene can speed up both negative and positive streamers in Marcol-70, even at very low concentrations.¹³ Benzene is included as the simplest aromatic molecule. The calculated zero-field vertical IP for benzene is 9.63 eV compared to the adiabatic experimental IP of 9.24 eV.³⁷ The result is in good agreement with a focal point analysis giving a vertical IP around 9.45 eV.³⁸ In the focal point analysis, the Hartree-Fock (HF) energy is converged with respect to the completeness of the basis set (cc-pV ∞ Z) and a correlation correction to the HF energy (coupled-cluster with single and double and perturbative triple excitations CCSD(T)) at the basis set limit.³⁸ The lowest excitation energy is from the π to π^* orbital with the energy 5.41 eV, which is in good agreement with results from the HCTH functional,³⁹ using various augmented basis sets (5.32–5.44 eV).⁴⁰ Figure 2 shows the IP and excitation energies in different directions of the field. The x - and y -directions are the in-plane and z is the out-of-plane electric field, respectively (Figure 1). The center of benzene ring is the origin of the coordinate system. The field-dependent IP calculated here is in good agreement with the point-charge model.¹ While the IP is decreasing with increasing electric field, the π to π^* excitation energies remain almost constant in the field. A few excitations have energies at or above the IP. Since we use different methods for calculating the IP and the excitation energies, it could be that some of the excitations just below the IP should instead be interpreted as ionized states just above the IP.

B. Alkanes: Cyclohexane and n -tridecane

Alkanes are the major components of mineral oils.²⁷ Cyclohexane and n -tridecane are chosen because of earlier experimental studies of liquid cyclohexane^{9,10,41–43} and n -tridecane^{44,45} with different additives, and also to find out whether the CDF method can be applied on longer chains. The electric field in x - and y -directions are through the ring of the chair conformation of cyclohexane

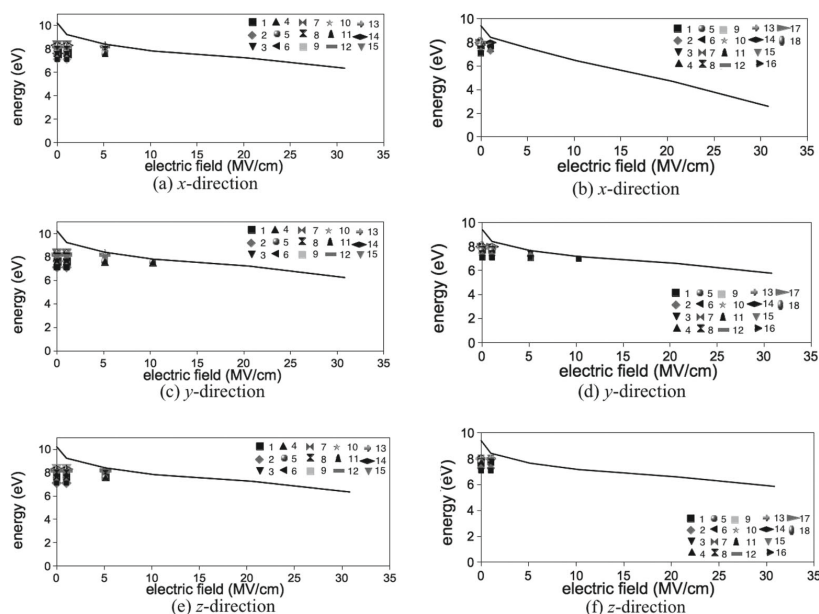


FIG. 3. The IP and excitation energies (eV) in the (a) and (b) x, (c) and (d) y, (e) and (f) z direction of the electric field for cyclohexane (left) and *n*-tridecane (right). The solid line is the IP and the dots are excitation energies.

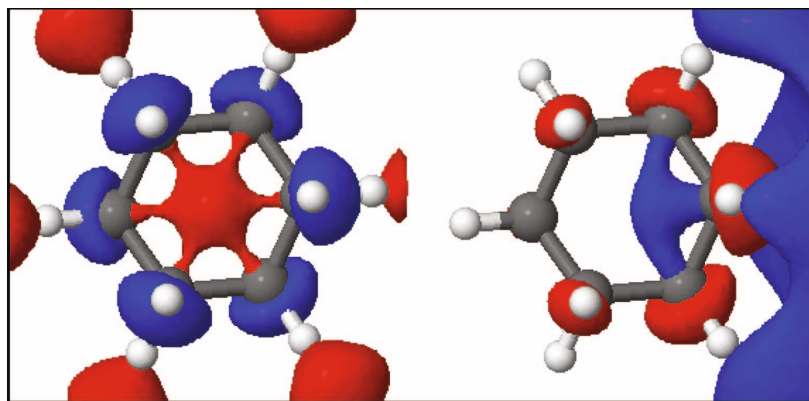


FIG. 4. The σ^* orbital of carbon-carbon bonds (LUMO) in zero-field (left) and 10 MV/cm (right) in *x*-direction of the electric field for cyclohexane.

and *z* is perpendicular to the ring (see Figure 1). The center of the ring is the origin of the coordinate system. The experimental IP is around 9.8 eV^{37,46} and the calculated zero-field IP is 10.22 eV, which is in good agreement with the result of the B3P86 functional of 10.0 eV.⁴⁶ The lowest excitation energy of cyclohexane is 7.11 eV, in good accordance to the experimental value around 7.0 eV.⁴⁷ Figure 3 (left) shows that the excited states vanish at fields higher than 5 MV/cm except in the *y*-direction where excitation energies remain close to the IP and should possibly be interpreted as ionized states. Figure 4 shows the lowest unoccupied molecular orbital (LUMO) in zero-field and

the corresponding ionized orbital in 10 MV/cm in the x -direction, which clearly demonstrates the general effect of increasing the field, that an unoccupied orbital changes from a bound to an ionized state. The two lowest excitations in cyclohexane are from carbon σ orbitals to σ^* orbitals.

The calculated zero-field IP for n -tridecane is 9.41 eV, in good agreement with the B3P86 functional, 9.42 eV⁴⁶ and the experimental value of 9.72 eV.⁴⁶ The lowest excitation energy is 7.08 eV. In the field calculations of the IP, the origin of the coordinate system is located on the middle of the carbon chain. The x -direction of the field is along the chain and the y - and z -directions are perpendicular to the chain, respectively (see Figure 1). The excited states become ionized already at fields close to 1 MV/cm except in the y -direction (perpendicular to the chain) where the first excited state remains up to 10 MV/cm (see Figure 3(d)). This excited state should probably be regarded as an ionized state, since its energy is very close to the IP at 10 MV/cm.

n -tridecane and cyclohexane are alkanes with higher IPs and excitation energies as compared to molecules with π -systems, as for example benzene discussed in the previous section, since their excitations are from low-lying σ orbitals to high-lying σ^* orbitals. All the excited states vanish at a relatively low electric field for both molecules. The difference between the two molecules is that n -tridecane is more influenced by the direction of the electric field along the alkane chain. Figure 3(b) shows that the decrease in the IP is around 70% in the field along the chain comparing zero field with 30 MV/cm, whereas it is around 40% in the field perpendicular to the chain as shown in Figure 3 (right). Consequently, the direction of the field is important for relatively long linear alkanes, such as n -tridecane and also 9,10-dimethyl octadecane as in our previous study.² The field-dependent IPs of cyclohexane and n -tridecane calculated by CDFT method are in good agreement with the earlier study using the point-charge model.¹

In general, the excited states of alkanes vanish at lower fields as compared to other molecules in the study, and for the linear alkanes the direction of the electric field becomes important. Alkanes have fewer number of excited states in the field compared to esters, diketones and quinones as will be discussed here. Therefore, alkanes have a reduced ability to be excited at a high electric field. The light emission from the streamers in cyclohexane is experimentally difficult to detect,⁴⁸⁻⁵⁰ which maybe explained by that the excited states of cyclohexane vanish already at an electric field around 5 MV/cm.

C. Esters: Propylene carbonate and methyl butyrate

Propylene carbonate and methyl butyrate are chosen as model compound for ester molecules. Ester-based oils are more biodegradable and have lower volatility and higher flash points than mineral oils,^{29,51} and are investigated intensively as a replacement for mineral oils in electrically insulating devices. Propylene carbonate is a carbonate ester that is mainly used as a polar solvent with a high dielectric constant of 66 at 293 K.³⁷ The ionic conduction of chloride ions in propylene carbonate has been studied to understand conduction mechanisms in dielectric liquids.⁵²

The optimized geometry of propylene carbonate is in good agreement with the obtained geometry using BLYP/DNP method.⁵³ The calculated zero-field IP for propylene carbonate is 10.81 eV compared to the experimental adiabatic IP of 10.52 eV and the vertical IP of 10.71 eV,⁵⁴ respectively. Figure 5 (left) shows the IP and excitation energies in a field. The center of the ring is the origin of the coordinate system. The x - and y -directions are through the ring, with the y -direction parallel to the carbonyl bond, and z -direction is perpendicular to the ring, respectively (see Figure 1). The decrease in the IP with increasing field is not dependent on the direction of the field. The lowest excitation energy for propylene carbonate is 6.97 eV and it is the only excitation that survives at 30 MV/cm. The three lowest excitations are from oxygen lone pairs, n orbitals, to $\pi_{C=O}^*$ orbitals.

The calculated zero-field IP for methyl butyrate is 10.13 eV and the experimental IP is 10.07 eV.³⁷ The origin of the coordinate system is located on the center of the carbon-carbon bond adjacent to the carboxylate group. The x -direction is along the carbon-carbon bonds, y -direction is parallel to the carbonyl bond and z -direction is perpendicular to the central carbon-carbon bond, respectively (see Figure 1). For methyl butyrate the IP is also independent of the direction of the field (Figure 5 (right)). As shown in Figure 5 (right), the lowest excitation energy is 5.88 eV and it

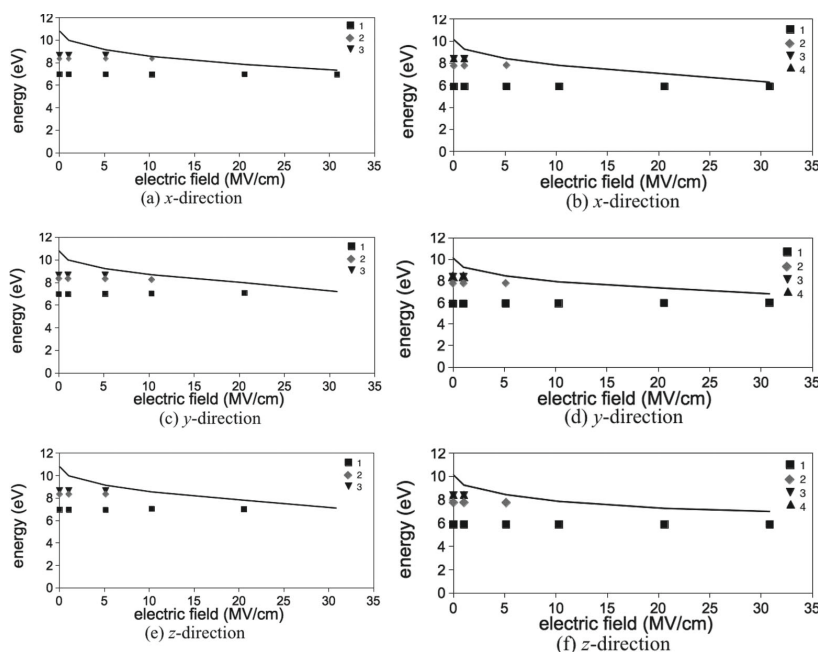


FIG. 5. The IP and excitation energies (eV) in the (a) and (b) x, (c) and (d) y, (e) and (f) z direction of the electric field for propylene carbonate (left) and methyl butyrate (right). The solid line is the IP and the dots are excitation energies.

survives at 30 MV/cm. The excitations are from n orbitals of oxygen atoms to π_{CO}^* orbital similar to propylene carbonate.

For the ester molecules included in this study, there are few excited states in the field, but the lowest excited state survives at 30 MV/cm. The results do not depend on the direction of the electric field. For larger ester molecules such as glyceryltributyrate,² there are a larger number of excited states in the field but they have all vanished at fields higher than 30 MV/cm. Also the IP is more influenced by the electric field than for the small ester molecules studied here. Glyceryltributyrate is sensitive to the direction of the field and the molecular orbitals involved in some of the excitations change in the field which results in an increase or decrease in their energies with increasing field.²

D. Diketones: Benzil, 4,4'-dihydroxybenzil, 2,3-heptanedione and *p*-benzoquinone

Benzil is a typical aromatic α -diketone molecule that has been the subject of many spectroscopic investigations.⁵⁵⁻⁵⁸ Benzil and 4,4'-dihydroxybenzil have been evaluated as voltage stabilizer to resist electrical treeing in polymer dielectrics used for high-voltage cable applications.⁵⁹ The most stable gas phase structure of benzil is *cis*-skew with the calculated torsion angle of 125°, in good agreement with the RHF (121°) method and the BLYP (123°) functional.⁶⁰ The experimental torsion angle is 108° for the crystal phase⁶¹ and 117° for the gas phase,⁶² respectively. The bond lengths and angles are in good agreement with the X-ray data⁶¹ and calculated data.⁶⁰ The long central carbon-carbon bond is 1.54 Å resulting in a non-conjugated structure which gives the molecule some specific features.

Figure 6 (left) shows the IP and excitation energies for the *cis*-skew configuration of benzil in different directions of the electric field. The center of the central carbon-carbon bond is the origin of the coordinate system. The x -direction is through one of the phenyl rings, the y -direction is along one of the central carbonyl bonds and the z -direction is perpendicular to the central carbon-carbon bond,

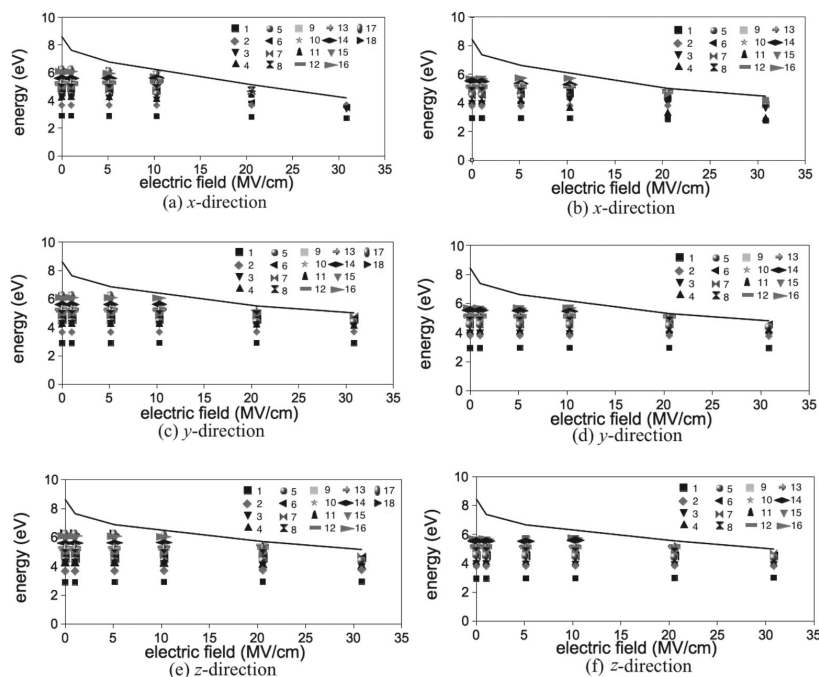


FIG. 6. The IP and excitation energies (eV) in the (a) and (b) x, (c) and (d) y, (e) and (f) z direction of the electric field for the *cis*-skew configuration of benzil (left) and the *cis*-skew configuration of 4,4'-dihydroxybenzil (right). The solid line is the IP and the dots are excitation energies.

respectively. The calculated zero-field IP is 8.62 eV and the experimental IP is 8.68 eV.⁶³ The lowest excitation energy is 2.89 eV and it is from the lone pairs of oxygen atoms, n , to π^* orbital of benzoyl groups, π_{CO+CC}^* . The experimental value is around 3.34 eV.⁶⁴ The deviation from the experimental value is because of the photoisomerization of benzil molecule. After absorption of light, the excited molecule rearranges from *cis*-skew into a *trans*-planar configuration,^{65,66} and by computations it has been found that the first singlet and triplet excited states of benzil are *trans*-planar,⁶⁷ while in this work, the calculated vertical excitation energy is for the same configuration as the ground state (*cis*-skew).

The *trans*-planar configuration of benzil has also been investigated and according to our calculations, the *cis*-skew configuration is 0.20 eV more stable than the *trans*-planar configuration. The calculated IP of the *trans*-planar configuration is around 8.49 eV and the excitation energy is around 2.38 eV. The field-dependent IP is similar for the two configurations.

The calculated zero-field IP for the *cis*-skew configuration of 4,4'-dihydroxybenzil is 8.43 eV and the lowest excitation energy is 2.93 eV. The ground state configuration of this molecule is *cis*-skew. The IP and excitation energy of the *trans*-planar configuration are 8.15 and 2.46 eV, respectively. Comparing benzil and 4,4'-dihydroxybenzil shows that the two hydroxyl groups cause blue shifts of around 0.04 and 0.13 eV, respectively, for the two lowest excitations, which both are n to π_{CO+CC}^* excitations. Figure 6 (right) shows the IP and excitation energies in different directions of the field for *cis*-skew 4,4'-dihydroxybenzil. The directions of the field are the same as in benzil. A few of the excitations decrease substantially with increasing field. For example, the fourth excitation in 4,4'-dihydroxybenzil which is similar to the sixth excitation in benzil decreases with increasing field. This excitation energy in zero-field is 4.11 eV for 4,4'-dihydroxybenzil and 4.53 eV for benzil, respectively, and decreases to 2.96 eV for 4,4'-dihydroxybenzil and 3.50 eV for benzil at 30 MV/cm,

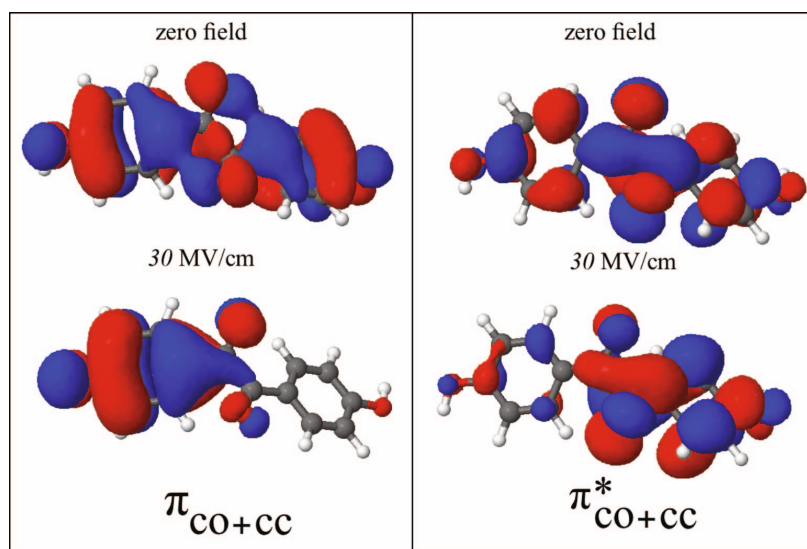


FIG. 7. The molecular orbitals (π_{CO+CC} to the left and π_{CO+CC}^* to the right) that are involved in the fourth excitation for 4,4'-dihydroxybenzil in zero-field (top) and 30 MV/cm (bottom) in the x -direction of the electric field.

respectively. The excitation is from π_{CO+CC} to π_{CO+CC}^* of benzoyl groups as shown in Figure 7. The molecular orbitals in zero-field and 30 MV/cm are shown in Figure 7. In zero-field, the molecular orbital is localized on the two benzoyl groups. As the field increases, the molecular orbital of one of the benzoyl groups gradually disappears until at 30 MV/cm is localized on one of the benzoyl groups. The excitations that remain in the higher fields have the same characteristics as in benzil and are from n to π_{CO+CC}^* , phenyl π orbitals, π_{CC} , to π_{CO+CC}^* and π_{CO+CC} to π_{CO+CC}^* , respectively.

Another diketone, 2,3-heptanedione, is included in this study to be compared with benzil since it has alkyl chains in its structure instead of the two phenyl rings as in benzil. The calculated IP is 9.03 eV, larger than for benzil (8.62 eV) and 4,4'-dihydroxybenzil (8.43 eV). The reason is that the ion is more stabilized in benzil and 4,4'-dihydroxybenzil due to the π systems of the two phenyl rings as compared to 2,3-heptanedione. The lowest excitation energy is 2.69 eV, lower than for benzil (2.89 eV) and 4,4'-dihydroxybenzil (2.93 eV). Figure 8 shows the IP and excitation energies in the field for this molecule. The origin of the coordinate system is on the carbon of the carbonyl bond connected to the butyl chain. The x -direction is along the carbon chain, the y -direction is along one of the carbonyl bonds and the z -direction is perpendicular to the carbonyl bond, respectively (Figure 1). The first two excitations are from n orbitals to π_{CO}^* which remains up to 30 MV/cm. The other excitations are from σ_{CH} , σ_{CC} and π_{CO} to π_{CO}^* , respectively. There are fewer excited states in the field for 2,3-heptanedione compared to benzil and 4,4'-dihydroxybenzil since the π to π^* excitations contribute to many excited states for the benzil molecules.

Quinone derivatives are conjugated diketone cyclic structures that are widely used as color pigments,^{68,69} and are well-known as electron acceptors in many charge-transfer type organic conductors.⁷⁰ Among the quinones, *p*-benzoquinone is selected as a reference molecule in studying the IP and excitation energies since it has been used as an electron-attaching additive to study its effect on the propagation of streamer in liquid cyclohexane.⁹ The calculated molecular structure is close to the structure obtained from X-ray diffraction.⁷¹ The calculated zero-field IP is 9.84 eV compared to the experimental IP of 9.99 eV.⁷² The calculated energies of the four lowest excitations are 2.51, 2.74, 3.88 and 4.95 eV compared to the experimental values of 2.49, 2.52, 4.07 and 5.12 eV, respectively.^{71,73} Figure 9 shows the IP and excitation energies in different directions of

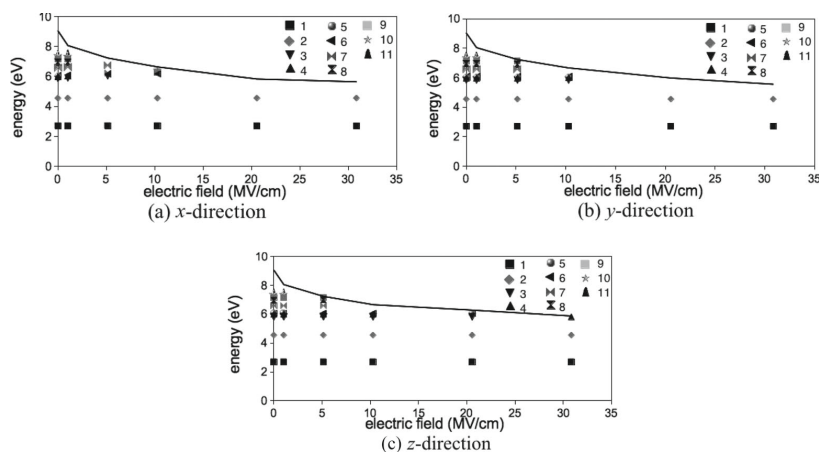


FIG. 8. The IP and excitation energies (eV) in the (a) *x*, (b) *y*, and (c) *z* direction of the electric field for 2,3-heptanedione. The solid line is the IP and the dots are excitation energies.

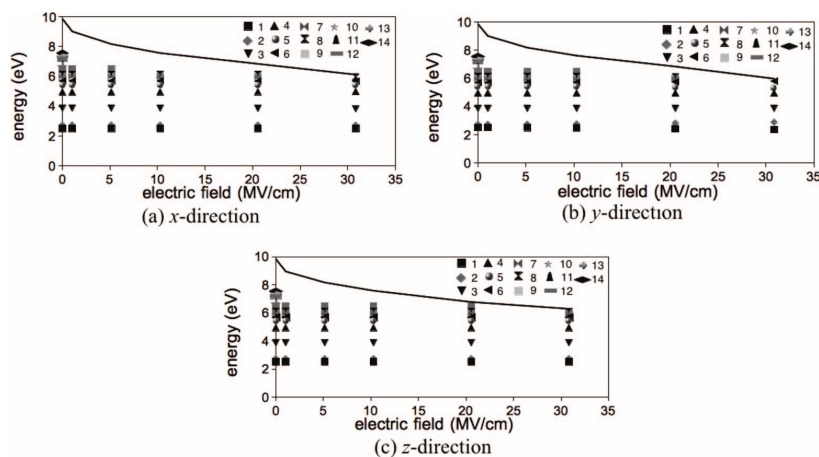


FIG. 9. The IP and excitation energies (eV) in the (a) *x*, (b) *y*, and (c) *z* direction of the electric field for *p*-benzoquinone. The solid line is the IP and the dots are excitation energies.

the field. The *x*- and *y*-directions are through the ring, with the *y*-direction along the carbonyl bonds and the *z*-direction is perpendicular to the ring, respectively (see Figure 1). The center of the ring is the origin of the coordinate system. The lowest two singlet-singlet excitations are from *n* orbitals to the delocalized π_{CO+CC}^* orbital, the third and fourth excitations are from π_{CC} and π_{CO+CC} orbitals to π_{CO+CC}^* orbital, respectively. Several semiempirical^{74–76} and ab-initio^{77–79} studies on the excited states of *p*-benzoquinone show that the first two excitations have $n \rightarrow \pi^*$ character followed by two $\pi \rightarrow \pi^*$ excitations. These excitations survive in the field up to 30 MV/cm. The two additional excitations at 30 MV/cm are from oxygen *n* orbitals to π_{CC}^* orbital.

In general, for diketones there is a large gap between the IP and the lowest excitation energy which results in a larger number of excited states at higher fields. This behavior was also found for *trans*-azobenzene.² The lowest excitation which is from the lone pairs of nitrogen atoms to the π^* orbital of azo bond can survive in the field up to 100 MV/cm.² In addition to the ester and

diketone molecules included in this study, the excitation of the type n to π^* in N,N-dimethylaniline, tetrakis-(dimethylamino)ethylene, glyceryltributyrate in our previous work² can remain in the field of 30 MV/cm. Consequently, n to π^* excitations have the ability to survive at higher fields.

IV. CONCLUSION

The constrained DFT method is demonstrated as an efficient method for calculating the field-dependent IP of different types of molecules. The strong decrease of the IP with increasing electric field causes a reduction in the number of available excited states at high electric fields. At a threshold field, different for each molecule, all the excited states have vanished. The threshold field value is much lower for alkanes compared to esters and diketones, i.e. the excitations of the alkanes vanish at lower fields as compared to the other types of molecules included in our studies. The direction of the electric field is important for linear alkanes. The ester molecules included in this work have fewer excited states in high fields compared to the color dyes, but the lowest excitation which is from n to π^* survives at 30 MV/cm. Diketones have a higher number of excited states in the field since the n to π^* excitation has a relatively low energy compared to the field-dependent IP. Therefore, diketones are more likely to become excited, whereas alkanes become ionized with increasing field. A general conclusion is that n to π^* excitations can survive at higher fields, while σ to σ^* excitations vanish at relatively low fields.

ACKNOWLEDGMENTS

We would like to acknowledge a research grant "Modeling of electrical pre-breakdown and breakdown phenomena in insulating liquids" (200631/560) from the Norwegian Research Council, ABB and Statnett and a grant of computer time (account nn2920k) from the NOTUR project.

- ¹H. S. Smalø, Ø. Hestad, S. Ingebrigtsen, and P.-O. Åstrand, "Field dependence on the molecular ionization potential and excitation energies compared to conductivity models for insulation materials at high electrical fields," *J. Appl. Phys.* **109**, 073306 (2011).
- ²N. Davari, P.-O. Åstrand, S. Ingebrigtsen, and M. Unge, "Excitation energies and ionization potentials at high electric fields for molecules relevant for electrically insulating liquids," *J. Appl. Phys.* **113**, 143707 (2013).
- ³J. Jadidian, M. Zahn, N. Lavesson, O. Widlund, and K. Borg, "Effect of impulse voltage polarity, peak amplitude, and rise time on streamers initiated from a needle electrode in transformer oil," *IEEE Trans. Plasma Sci.* **40**, 909 (2012).
- ⁴J. Jadidian, M. Zahn, N. Lavesson, O. Widlund, and K. Borg, "Stochastic and deterministic causes of streamer branching in liquid dielectrics," *J. Appl. Phys.* **114**, 063301 (2013).
- ⁵J. Jadidian and M. Zahn, "Charge transport analysis in two-phase composite dielectric systems," *IEEE Trans. Plasma Sci.* **41**, 2464 (2013).
- ⁶Y. Nakao, H. Itoh, S. Hoshino, Y. Sakai, and T. Hagashira, "Effects of additives on prebreakdown phenomena in n -hexane," *IEEE Trans. Dielect. Elect. Insul.* **1**, 383 (1994).
- ⁷L. Angerer, "Effect of organic additives on electrical breakdown in transformer oil and liquid paraffin," *Proc. IEE* **112**, 1025 (1965).
- ⁸N. V. Dung, H. K. Høidalen, D. Linhjell, L. E. Lundgaard, and M. Unge, "Influence of impurities and additives on positive streamers in paraffinic model oil," *IEEE Trans. Dielect. Elect. Insul.* **19**, 1593 (2012).
- ⁹S. Ingebrigtsen, H. S. Smalø, P.-O. Åstrand, and L. E. Lundgaard, "Effects of electron-attaching and electron-releasing additives on streamers in liquid cyclohexane," *IEEE Trans. Dielect. Elect. Insul.* **16**, 1524 (2009).
- ¹⁰O. Lesaint and M. Jung, "On the relationship between streamer branching and propagation in liquids: influence of pyrene in cyclohexane," *J. Phys. D: Appl. Phys.* **33**, 1360 (2000).
- ¹¹A. Beroual and R. Tobazeon, "Prebreakdown phenomena in liquid dielectrics," *IEEE Trans. Dielect. Elect. Insul.* **21**, 613 (1986).
- ¹²W. G. Chadband and T. Sufian, "Experimental support for a model of positive streamer propagation in liquid insulation," *IEEE Trans. Elect. Insul.* **20**, 239 (1985).
- ¹³J. C. Devins, S. J. Rząd, and R. J. Schwabe, "Breakdown and prebreakdown phenomena in liquids," *J. Appl. Phys.* **52**, 4531 (1981).
- ¹⁴N. V. Dung, H. K. Høidalen, D. Linhjell, L. E. Lundgaard, and M. Unge, "Effects of reduced pressure and additives on streamers in white oil in long point-plane gap," *J. Phys. D: Appl. Phys.* **46**, 255501 (2013).
- ¹⁵M. Unge, S. Singha, N. V. Dung, D. Linhjell, S. Ingebrigtsen, and L. E. Lundgaard, "Enhancements in the lightning impulse breakdown characteristics of natural ester dielectric liquids," *Appl. Phys. Lett.* **102**, 172905 (2013).
- ¹⁶K. Burke, "Perspective on density functional theory," *J. Chem. Phys.* **136**, 150901 (2012).
- ¹⁷N. Davari, P.-O. Åstrand, and T. Van Voorhis, "Field-dependent ionisation potential by constrained density functional theory," *Mol. Phys.* **111**, 1456 (2013).

- ¹⁸ Q. Wu and T. Van Voorhis, "Direct optimization method to study constrained systems within density-functional theory," *Phys. Rev. A* **72**, 024502 (2005).
- ¹⁹ B. Kaduk, T. Kowalczyk, and T. Van Voorhis, "Constrained density functional theory," *Chem. Rev.* **112**, 321 (2012).
- ²⁰ Q. Wu and T. Van Voorhis, "Constrained density functional theory and its application in long-range electron transfer," *J. Chem. Theory Comput.* **2**, 765 (2006).
- ²¹ T. Kowalczyk, Z. Lin, and T. Van Voorhis, "Fluorescence quenching by photoinduced electron transfer in the Zn²⁺ sensor Zinpyr-1: A computational investigation," *J. Phys. Chem. A* **114**, 10427 (2010).
- ²² I. Rudra, Q. Wu, and T. Van Voorhis, "Predicting exchange coupling constants in frustrated molecular magnets using density functional theory," *Inorg. Chem.* **46**, 10539 (2007).
- ²³ Q. Wu, B. Kaduk, and T. Van Voorhis, "Constrained density functional theory based configuration interaction improves the prediction of reaction barrier heights," *J. Chem. Phys.* **130**, 034109 (2009).
- ²⁴ H. Oberhofer and J. Blumberger, "Charge constrained density functional molecular dynamics for simulation of condensed phase electron transfer reactions," *J. Chem. Phys.* **131**, 064101 (2009).
- ²⁵ Y. Lu, R. Quardokus, C. S. Lent, F. Justaud, C. Lapinte, and S. A. Kande, "Charge localization in isolated mixed-valence complexes: An STM and theoretical study," *J. Am. Chem. Soc.* **132**, 13519 (2010).
- ²⁶ T. Van Voorhis, T. Kowalczyk, B. Kaduk, L.-P. Wang, C.-L. Cheng, and Q. Wu, "The diabatic picture of electron transfer, reaction barriers, and molecular dynamics," *Ann. Rev. Phys. Chem.* **61**, 149 (2010).
- ²⁷ M. Nishimatsu, T. Miyamoto, and T. Suzuki, *Liquid Insulation* (Wiley Encyclopedia of Electrical and Electronics Engineering, 1999) John Wiley & Sons.
- ²⁸ N. Berger, M. Randoux, G. Ottmann, and P. Vuarchex, "Review on insulating liquids," *Electra* **171**, 33 (1997).
- ²⁹ L. Rongsheng, C. Törnkqvist, V. Chandramouli, O. Girlanda, and L. A. A. Pettersson, "Ester fluids as alternative for mineral oil: The difference in streamer velocity and LI breakdown voltage," in *IEEE Conf. Elect. Insul. Dielect. Phenomena* (2009) pp. 543–548.
- ³⁰ A. D. Becke, "Density-functional thermochemistry. III. The role of exact exchange," *J. Chem. Phys.* **98**, 5648 (1993).
- ³¹ C. Lee, W. Yang, and R. G. Parr, "Development of the Colle-Salvetti correlation-energy formula into a functional of the electron density," *Phys. Rev. B* **37**, 785 (1988).
- ³² T. H. Dunning, Jr., "Gaussian basis sets for use in correlated molecular calculations. I. The atoms boron through neon and hydrogen," *J. Chem. Phys.* **90**, 1007 (1989).
- ³³ P.-O. Löwdin, "On the nonorthogonality problem connected with the use of atomic wave functions in the theory of molecules and crystals," *J. Chem. Phys.* **18**, 365 (1950).
- ³⁴ G. Zhang and C. B. Musgrave, "Comparison of DFT methods for molecular orbital eigenvalue calculations," *J. Phys. Chem. A* **111**, 1554 (2007).
- ³⁵ R. A. Kendall, T. H. Dunning, and R. J. Harrison, "Electron affinities of the first-row atoms revisited. Systematic basis sets and wave functions," *J. Chem. Phys.* **96**, 6796 (1992).
- ³⁶ M. Valiev, E. J. Bylaska, N. Govind, K. Kowalski, T. P. Straatsma, H. J. J. van Dam, D. Wang, J. Nieplocha, E. Apra, T. L. Windus, and W. A. de Jong, "NWChem: a comprehensive and scalable open-source solution for large scale molecular simulations," *Comput. Phys. Commun.* **181**, 1477 (2010).
- ³⁷ D. R. Lide, *Handbook of Chemistry and Physics*, 84th ed. (FL: CRC Press, Boca Raton, 2004).
- ³⁸ M. S. Deleuze, L. Claes, E. S. Kryachko, and J.-P. François, "Benchmark theoretical study of the ionization threshold of benzene and oligoacenes," *J. Chem. Phys.* **119**, 3106 (2003).
- ³⁹ F. A. Hamprecht, A. J. Cohen, D. J. Tozer, and N. C. Handy, "Development and assessment of new exchange-correlation functionals," *J. Chem. Phys.* **109**, 6264 (1998).
- ⁴⁰ N. C. Handy and D. J. Tozer, "Excitation energies of benzene from Kohn-Sham theory," *J. Comput. Chem.* **20**, 106 (1999).
- ⁴¹ A. Denat, J. P. Gosse, and B. Gosse, "Electrical conduction of purified cyclohexane in a divergent electric field," *IEEE Trans. Elect. Insul.* **23**, 545 (1988).
- ⁴² S. Ingebrigtsen, L. E. Lundgaard, and P.-O. Åstrand, "Effects of additives on prebreakdown phenomena in liquid cyclohexane: II. streamer propagation," *J. Phys. D: Appl. Phys.* **40**, 5624 (2007).
- ⁴³ S. Ingebrigtsen, L. E. Lundgaard, and P.-O. Åstrand, "Effects of additives on prebreakdown phenomena in liquid cyclohexane: I. streamer initiation," *J. Phys. D: Appl. Phys.* **40**, 5161 (2007).
- ⁴⁴ Ø. Hestad, H. S. Smalø, P.-O. Åstrand, S. Ingebrigtsen, and L. E. Lundgaard, "Effects of N,N-dimethylaniline and trichloroethene on prebreakdown phenomena in liquid and solid *n*-tridecane," *IEEE Trans. Dielect. Elect. Insul.* **18**, 1886 (2011).
- ⁴⁵ Ø. L. Hestad, P.-O. Åstrand, and L. E. Lundgaard, "*n*-tridecane as a model system for polyethylene: Comparison of pre-breakdown phenomena in liquid and solid phase stressed by fast transient," *IEEE Trans. Dielect. Elect. Insul.* **18**, 1929 (2011).
- ⁴⁶ Z. Zhou, L. Zhang, M. Xie, Z. Wang, D. Chen, and F. Qi, "Determination of absolute photoionization cross-sections of alkanes and cyclo-alkanes," *Rapid Commun. Mass Spectrom.* **24**, 1335 (2010).
- ⁴⁷ L. W. Pickett, M. Muntz, and E. M. McPherson, "Vacuum ultraviolet absorption spectra of cyclic compounds. I. cyclohexane, cyclohexene, cyclopentane, cyclopentene and benzene," *J. Am. Chem. Soc.* **73**, 4862 (1951).
- ⁴⁸ N. Bonifaci and A. Denat, "Spectral analysis of light emitted by prebreakdown phenomena in non-polar liquids and gases," *IEEE Trans. Elect. Insul.* **26**, 610 (1991).
- ⁴⁹ S. Ingebrigtsen, N. Bonifaci, A. Denat, and O. Lesaint, "Spectral analysis of the light emitted from streamers in chlorinated alkane and alkene liquids," *J. Phys. D: Appl. Phys.* **41**, 235204 (2008).
- ⁵⁰ D. Linhjell, S. Ingebrigtsen, L. E. Lundgaard, and M. Unge, "Streamers in long point-plane gaps in cyclohexane with and without additives under step voltage," in *IEEE International Conference on Dielectric Liquids (ICDL)* (Trondheim, Norway, 2011).
- ⁵¹ T. V. Oomen, "Vegetable oils for liquid-filled transformers," *IEEE Electric. Insul. Mag.* **18**, 6 (2002).
- ⁵² J. P. Gosse, "Electric conduction in dielectric liquids," *NATO ASI Series* **193**, 503 (1989).

- ⁵³ R. Chen, F. Wu, L. Li, Y. Guan, X. Qiu, S. Chen, Y. Li, and S. Wu, "Butylene sulfite as a film-forming additive to propylene carbonate-based electrolytes for lithium ion batteries," *J. Electrochem. Soc.* **172**, 395 (2007).
- ⁵⁴ Y. Yokoyama and M. Jinno, "Identification of accidentally degenerate bands in UV and propylene photoelectron spectra of propylene carbonate," *J. Electron Spectrosc. Rel. Phen.* **5**, 1095 (1974).
- ⁵⁵ S. C. Bera, R. Mukherjee, and M. Chowdhury, "Spectra of benzil," *J. Chem. Phys.* **51**, 754 (1969).
- ⁵⁶ J. Arnett and S. P. McGlynn, "Photomerism of aromatic α -dicarbonyls," *J. Phys. Chem.* **79**, 626 (1975).
- ⁵⁷ S. Lopes, A. Gómez-Zavaglia, L. Lapinski, N. Chattopadhyay, and R. Fausto, "Matrix-isolation FTIR spectroscopy of benzil: Probing the flexibility of the C-C torsional coordinate," *J. Phys. Chem. A* **108**, 8256 (2004).
- ⁵⁸ A. Singh, D. K. Palit, and J. P. Mittal, "Conformational relaxation dynamics in the excited electronic states of benzil in solution," *Chem. Phys. Lett.* **360**, 443 (2002).
- ⁵⁹ M. Jarvid, A. Johansson, V. Englund, S. Gubanski, and M. R. Andersson, "Electrical tree inhibition by voltage stabilizers," in *IEEE Conference on Electrical Insulation and Dielectric Phenomena (CEIDP)* (Montreal, Canada, 2012) pp. 605–608.
- ⁶⁰ T. M. Kolev and B. A. Stamboliyska, "Vibrational spectra and structure of benzil and its 18O and d10-labelled derivatives: a quantum chemical and experimental study," *Spectrochim. Acta A* **58**, 3127 (2002).
- ⁶¹ C. Brown and R. Sadanaga, "The crystal structure of benzil," *Acta Cryst.* **18**, 158 (1965).
- ⁶² Q. Shen and K. Hagen, "Gas-phase molecular structure and conformation of benzil as determined by electron diffraction," *J. Phys. Chem.* **91**, 1357 (1987).
- ⁶³ A. V. Polevoi, V. M. Matyuk, G. A. Grigoréva, and V. K. Potapov, "Formation of intermediate products during the resonance stepwise polarization of dibenzil ketone and benzil molecules," *J. Phys. Chem.* **21**, 12 (1987).
- ⁶⁴ W. G. Herkstroeter, A. A. Lamola, and G. S. Hammond, "Mechanisms of photochemical reactions in solution. XXVIII. Values of triplet excitation energies of selected sensitizers," *J. Am. Chem. Soc.* **86**, 4537 (1964).
- ⁶⁵ D. J. Morantz and A. J. C. Wright, "Structures of the excited states of benzil and related dicarbonyl molecules," *J. Chem. Phys.* **54**, 692 (1971).
- ⁶⁶ A. Chakrabarty, P. Purkayastha, and N. Chattopadhyay, "Laser induced optacoustic spectroscopy of benzil: Evaluation of structural volume change upon photoisomerization," *J. Photochem. Photobiol. A: Chem.* **198**, 256 (2008).
- ⁶⁷ K. K. Das and D. Majumdar, "Ground and excited states of benzil: A theoretical study," *J. Mol. Struct. (THEOCHEM)* **288**, 55 (1993).
- ⁶⁸ K. Venkataraman, ed., *The Chemistry of Synthetic Dyes* (Academic press, New York, 1971).
- ⁶⁹ M. Matsuoka, *Infrared Absorbing Dyes* (Plenum Press, New York, USA, 1990).
- ⁷⁰ V. Khodorkovsky and J. Y. Becker, *In Organic Conductors: Fundamentals and Applications*. (Matcel Dekker, New York, 1994).
- ⁷¹ H. P. Trommsdorff, "Electronic states and spectra of *p*-benzoquinone," *J. Chem. Phys.* **56**, 5358 (1972).
- ⁷² L. Åsbrink, G. Bieri, C. Fridh, E. Lindholm, and D. P. Chong, "Spectra of *p*-benzoquinone, studied with HAM/3," *Chem. Phys.* **43**, 189 (1979).
- ⁷³ H. Yasushi, H. Masahiko, E. Masahiro, and N. Hiroshi, "Excited and ionized states of *p*-benzoquinone and its anion radical: SAC-CI theoretical study," *J. Phys. Chem. A* **106**, 3838 (2002).
- ⁷⁴ P. Jacques, J. Faure, O. Chalvet, and H. H. Jaffe, "A reexamination of the oxygen parameters in the CNDO/S method. Application to UV and photoelectron spectra of *p*-benzoquinone," *J. Phys. Chem.* **85**, 473 (1981).
- ⁷⁵ A. Kuboyama, Y. Kozima, and J. Maeda, "The CNDO/S-CI calculations of the singlet $n\pi^*$ and $\pi\pi^*$ levels of quinones," *Bull. Chem. Soc (Jpn)* **55**, 3635 (1982).
- ⁷⁶ A. A. Meier and G. H. Wagnière, "The long-wavelength MCD of some quinones and its interpretation by semi-empirical MO methods," *Chem. Phys.* **113**, 287 (1987).
- ⁷⁷ S. Coriani, P. Jørgensen, A. Rizzo, K. Ruud, and J. Olsen, "Ab initio determinations of magnetic circular dichroism," *Chem. Phys. Lett.* **300**, 61 (1999).
- ⁷⁸ R. Broer and W. Nieuwpoort, "Hole localization and symmetry breaking," *J. Mol. Struct. (THEOCHEM)* **458**, 19 (1999).
- ⁷⁹ J. Weber, K. Malsch, and G. Hohlneicher, "Excited electronic states of *p*-benzoquinone," *Chem. Phys.* **264**, 275 (2001).

Paper 4

Density-functional calculations of field-dependent
ionization potentials and excitation energies of
aromatic molecules

Nazanin Davari, Per-Olof Åstrand and Mikael Unge

Chemical Physics, 447, 22-29 (2015)





Contents lists available at ScienceDirect

Chemical Physics

journal homepage: www.elsevier.com/locate/chemphys

Density-functional calculations of field-dependent ionization potentials and excitation energies of aromatic molecules



Nazanin Davari^a, Per-Olof Åstrand^{a,*}, Mikael Unge^b

^a Department of Chemistry, Norwegian University of Science and Technology (NTNU), NO-7491 Trondheim, Norway

^b ABB Corporate Research, SE-72178 Västerås, Sweden

ARTICLE INFO

Article history:

Received 9 October 2014
In final form 27 November 2014
Available online 5 December 2014

Keywords:

Ionization potential
Electric field
Polyaromatic molecules
Excitation energy
Insulating liquids

ABSTRACT

A recent method based on constrained density functional theory (CDFT) has been used to calculate the field-dependent ionization potential by determining the dissociation barrier for the interaction between a cation and an electron in an electric field. In the CDFT model, we rely on that the barrier is located somewhere outside the cation, which has limited the applicability for polyaromatic molecules where the barrier is located closer to the cation than for other molecules. Different density functionals, basis sets and choices of constraints in the CDFT calculations are tested for benzene as a case study. The field-dependent ionization potential calculated by constraining the charge with the B3LYP functional and the cc-pVDZ basis set shows a good agreement with our previous work and has a low computational cost for the larger aromatic molecules included here. In addition, field-dependent excitation energies are investigated using time-dependent DFT.

© 2014 Elsevier B.V. All rights reserved.

1. Introduction

In an electric field, the ionization potential (IP) of a molecule can be calculated from the dissociation barrier of the interaction between a molecular cation and an electron [1–4]. An electric field decreases the dissociation barrier required to ionize a molecule, and accelerates the charged particles. The field-dependent IP has been calculated in a numerical approach for the hydrogen molecule and the molecular hydrogen cation based on a classical theory for ionized atoms [5]. The critical fields for the ionization were obtained as a function of the distance between the nuclei of the molecule or the cation and the electron parallel to the external electric field.

Recently, a method has been developed to calculate the field-dependent IP, first based on the interaction between a point charge and a cation [1,2] and subsequently based on constrained density functional theory (CDFT) [3,4]. In the point-charge model, the electron is modeled as a point-charge [1,2] and the field-dependent IP is determined by finding the maximum of the energy barrier of the interaction between the point-charge and the molecular cation. In the CDFT method the electron is considered as a ghost atom (an atom without a nuclear charge, but with basis functions at the position of the atom) and the charge of the electron is constrained

to -1 and/or the spin of the electron is constrained to a doublet state [3,4]. The CDFT method in general has provided insight in different chemical phenomena such as the prediction of transition state energies of chemical reactions or the lowest energy states of long-range charge-transfer systems [6–9]. A viable alternative approach that should be explored to calculate the field-dependent IP is via continuum wavefunction approaches developed for studying photoionization spectra [10–12].

It has been shown by DFT calculations that the decrease of the IP is proportional to the square root of the electric field [1], in agreement with the classical Poole–Frenkel effect describing the excitation of an electron to the conduction band at high electric fields [13]. The distance between the electron and the molecular cation at the energy barrier decreases as the electric field increases. In the CDFT method, we rely on that the electron orbital is sufficiently far away from the molecule so that we can control the position of the electron, i.e. the center of charge of the electron orbital is at the position of basis functions of the electron. At high electric fields and thereby at shorter distances between the electron and the cation, the CDFT method has a limitation since the orbital of the escaping electron becomes a linear combination of the basis functions of the electron with significant contributions from the basis functions of the cation. Consequently, the center-of-charge of the resulting orbital moves towards the molecule away from the position of the electron basis functions [3]. For molecules with diffuse π -systems such as polyaromatic molecules, the dissociation

* Corresponding author.

E-mail address: per-olof.astrand@ntnu.no (P.-O. Åstrand).

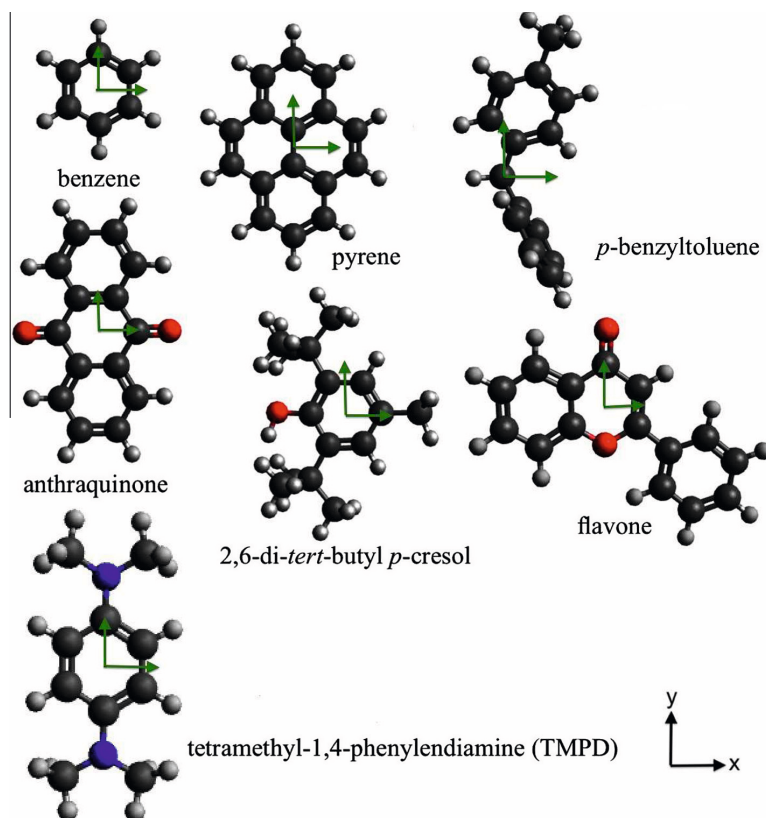


Fig. 1. The molecules included in this study with the coordinate system specified.

Table 1
IP (eV) in zero field.

Molecule	Vertical						Adiabatic	
	B3LYP		BNL		CAM-B3LYP		B3LYP	Exp.
	cc-pVDZ	cc-pVTZ	cc-pVDZ	cc-pVTZ	cc-pVDZ	cc-pVTZ	cc-pVDZ	
Benzene	9.54	9.63	10.47	10.57	10.20	10.27	9.53	9.24 [48]
Pyrene	7.09	7.16	7.03	7.14	7.20	7.28	7.00	7.42 [48]
Anthraquinone	9.00	9.30	8.98	9.16	9.43	9.55	8.90	9.30 [49]
<i>p</i> -Benzyltoluene	7.89	7.99	8.02	8.11	8.19	8.25	7.72	
2,6-Di- <i>tert</i> -butyl- <i>p</i> -cresol	7.42	7.51	7.18	7.31	7.51	7.59	7.20	
Flavone	8.40	8.19	8.09	8.28	8.32	8.44	8.27	
TMPD	6.30	6.20	5.87	6.03	6.23	6.35	5.97	6.25 [39]

barrier is located at shorter distances even at relatively low electric fields which has hampered studies of polyaromatic molecules in our previous work.

The field-dependent IP is an important parameter in ionization mechanisms in dielectric liquids at high electric fields, and recently, it has been used as a parameter in models describing streamer dynamics [14,15]. A streamer is a conductive plasma channel created in high-field regions of the dielectric liquid and propagates through the liquid and bridges the gap between two electrodes at a breakdown voltage [16,17]. Thus, the breakdown voltage is a measure of the dielectric strength of a liquid. It has been found that in dielectric liquids, polyaromatic additives with lower IPs than paraffinic and naphthenic molecules may increase the inception voltage of fast streamers with positive polarity

[18]. It has been shown experimentally that a low-IP additive increases the streamer branching at relatively low voltages [18]. The branching becomes dense with increasing voltage leading to a lower electric field in front of the streamer. Thus, the speed of the streamer propagation decreases at a specific voltage [19].

In addition to the IP, excitation energies may influence the ionization processes [1,2]. The excitation energies has a relatively weak electric field dependence as compared to the IP [1,2,4]. In other words, the number of available excited states decreases with increasing electric field and at a specific field, different for different types of molecules, all the excited states of the molecule disappear [2]. For example, for alkanes this field is lower than for esters, diketones and azo dyes [2,4]. In an applied voltage, energy is continuously added to the liquid and the means of the liquid to release

energy and maintain a steady-state condition is by emitting heat in the infrared region or light in the UV/VIS region. We can have excitation by impact of accelerated electrons in an electric field or photoexcitation in a dielectric liquid. If the frequency of the electron impact is shorter than the life-times of the excited states, a two-step ionization may take place where the excited molecule is ionized [1,2]. Thus, that excited states disappear with increasing electric field can have large effects on the insulating properties of a dielectric liquid [1,2]. The influence of additives with low excitation energies has been investigated experimentally [20].

In this work, the IP and the 20 lowest singlet–singlet excitation energies of aromatic molecules including polyaromatic molecules, which are one of the constituents of mineral oil used as insulating oils in high-voltage applications [21], are calculated and the results are compared to our previous work [2,4]. Experimental investigations are performed presently to study new synthetic insulating liquids and vegetable-based oils [20,22–24]. This work and our previous studies represent molecules that could be used in the design of electrically insulating liquids with appropriate properties with respect to the molecular ionization potential and excitation energies.

2. Computational methods

The IP of molecules in an electric field is calculated by the CDFT method [3,4]. In this method a constraint is placed on the charge and/or spin density of a given group of atoms and the minimum energy state consistent with the constraint is obtained by optimizing the constraint potential [6,9]. In the CDFT approach, it is recommended to constrain charge and spin together when possible [9]. For unrestricted calculations, however, constraining only the charge or the charge and spin give nearly identical energy states [9]. In our model for the IP, the electron is considered as a ghost atom, i.e. an atom without a nuclear charge. The charge on the ghost atom is constrained to -1 while the total system is kept neutral, and the spin of the electron is constrained to a doublet state, while the total system has a singlet spin state. The distance between the electron and the cation is varied to obtain the dissociation energy barrier, and the IP is calculated as the difference between the energy of the molecule in the field and the dissociation energy barrier. A detailed example in determining the dissociation barrier by the CDFT approach is given in Ref. [3]. The basis set on the ghost atom is a linear combination of 6 primitive Gaussian s -functions with the exponents of 0.5, 0.1, 0.02, 0.004, 0.008 and 0.00016 and the electron basis set was established so the IP of a molecule is converged to the order of 0.01 eV [3]. The choice of

spherically symmetric basis functions leads to that the center-of-charge of the electron orbital is at the position of the basis functions as long as the electron orbital does not have substantial contributions from the basis set of the cation. The chosen molecular basis sets are cc-pVDZ and cc-pVTZ [25] in the IP calculations and the aug-cc-pVTZ [26] in the calculation of excitation energies, respectively. The zero-field IP is investigated using the Becke, three-parameter, Lee–Yang–Parr (B3LYP) functional [27,28], and two long-ranged corrected (LC) functionals, Baer–Neuhauser–Livshits (BNL) [29,30] and the B3LYP functional modified with a Coulomb-attenuation term (CAM-B3LYP) [31]. In a previous work [3], the field-dependent IP has been calculated by the CDFT model using both the B3LYP and CAM-B3LYP functionals and the results of the two functionals were close to each other. Thus, only the B3LYP functional is used to calculate the field-dependence of the IP. The Löwdin population scheme is used for partitioning the electron density [32] in the CDFT method. The unrestricted open-shell DFT method is used in the IP calculations. Time-dependent density functional theory (TDDFT) [33,34] is used to calculate the 20 lowest singlet–singlet excitation energies with the B3LYP functional. All the geometries are optimized in zero field using the B3LYP functional and the cc-pVDZ basis set. These geometries are used in all subsequent calculations and we therefore report vertical IPs. The electric field is simulated by point charges located at 50 and -50 Å whereas the molecule is placed at the origin and the electric field is between 0 and 30.84 MV/cm. The calculations are done using the NWChem software, version 6.3 [35].

3. Results and discussion

The structures of the studied molecules are shown in Fig. 1. Benzene is a suitable model for investigating different methods of calculating the field-dependent IP for aromatic systems. Pyrene with a relatively low IP and *p*-benzyltoluene have been used as a part of a dielectric barrier between two conductors in high-field streamer experiments [18,36]. In our previous study, *p*-benzoquinone was chosen [4] and here, anthraquinone is investigated which is a conjugated diketone with three fused aromatic rings and is used mainly as a color pigment. 2,6-di-*tert*-butyl-*p*-cresol is an antioxidant that exists in mineral oil in transformers and affects the dielectric properties of the oil [37]. Flavone is a plant pigment [38], and could be regarded as an environmentally friendly additive in dielectric liquids applications. *N,N,N',N'*-tetramethyl-1,4-phenylenediamine (TMPD) has a very low IP compared to the other molecules [39] (see Table 1) and is comparable with tetrakis-(dimethylamino)-ethene (TDAE) studied previously [2].

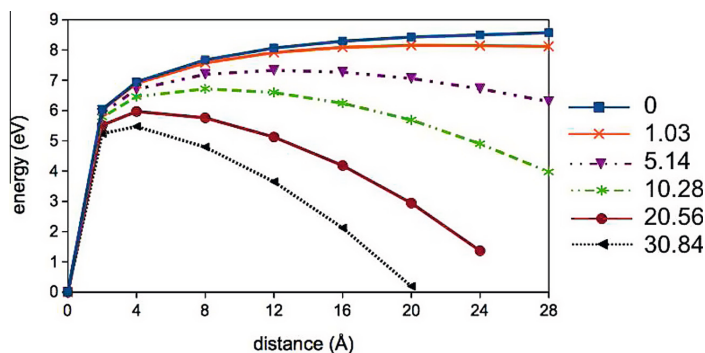


Fig. 2. The interaction energy between the benzene cation and the electron as a function of distance in the z -direction of the electric field (MV/cm) calculated by CDFT/B3LYP with the cc-pVDZ basis set.

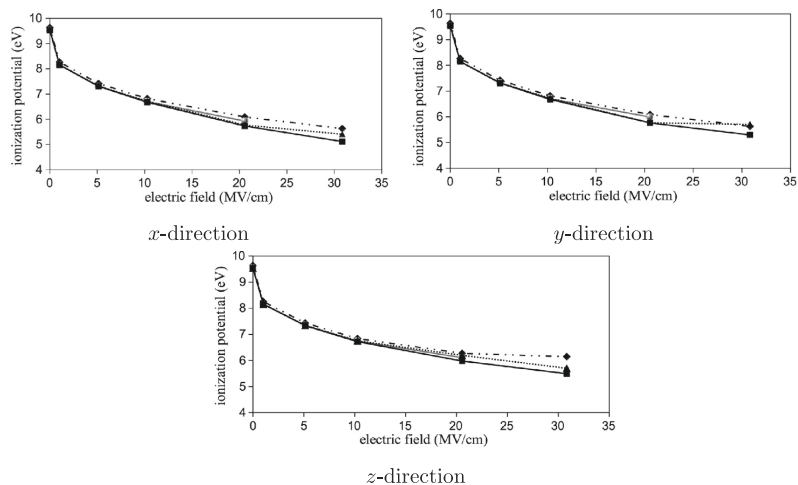


Fig. 3. The IP (eV) in the x , y , and z direction of the electric field for benzene. The solid square line shows the charge/cc-pVDZ method, the dashed triangular line shows the charge&spin/cc-pVDZ method, the solid circle line shows the spin/cc-pVDZ method and the dashed diamond line shows charge&spin/cc-pVTZ method, respectively.

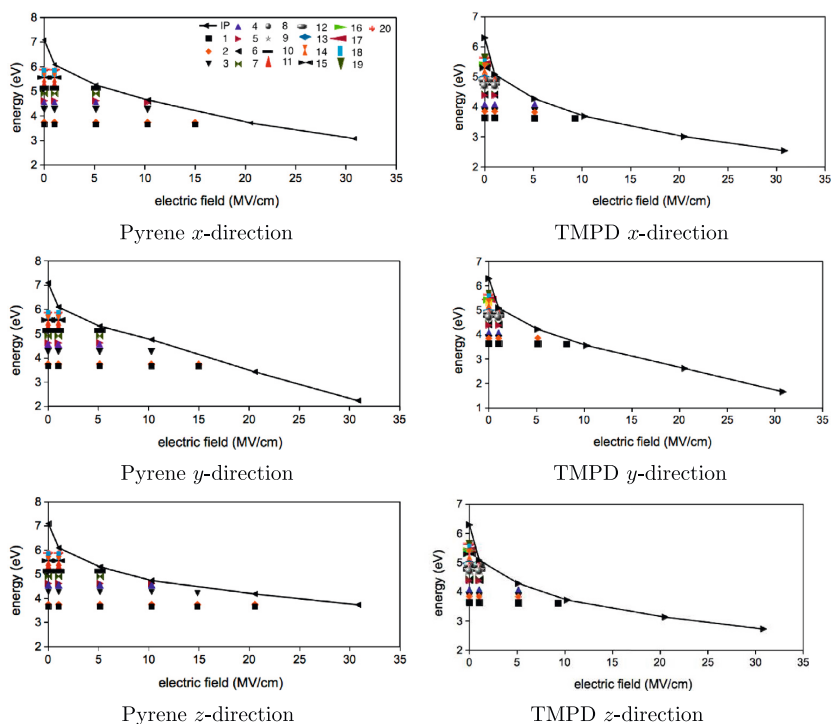


Fig. 4. The IP and excitation energies (eV) in the different directions of the electric field for pyrene and TMPD. The solid line is the IP and the dots are excitation energies.

3.1. Zero-field IP

The gas-phase IP of the molecules are listed in Table 1. The experimental IPs are adiabatic and the adiabatic IPs are calculated with the B3LYP functional and the cc-pVDZ basis set to compare with the experimental values. The adiabatic IPs are in general a few tenths of eV lower than the vertical with the largest difference

of 0.33 eV for TMPD in reasonable agreement with experiments and in line with our previous work [40]. The vertical IPs are calculated with three functionals, B3LYP and two LC functionals, CAM-B3LYP and BNL, where the LC functionals have been reported to be successful for predicting IPs and excitation energies [41–44]. The LC functionals are based on the separation of the Coulomb part into a short-range and a long-range part, and a range-separation or

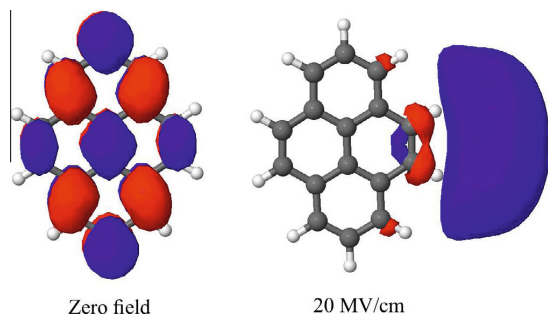


Fig. 5. The LUMO + 1 orbital for pyrene at zero and 20 MV/cm in the x-direction of the electric field.

attenuation parameter is introduced. The choice of this parameter is important and it has been shown that the results can be improved if this parameter is optimized for a molecular training set [30]. For example, one of the optimization approaches in the BNL functional is to obey the ionization potential theorem, i.e. the negative of the energy of the highest occupied molecular orbital is equal to ΔSCF , where ΔSCF is obtained as the difference between SCF energies of the molecule and the cation. This is the reason for our interest in the BNL functional since we are interested in calculating many excitation energies below the ionization threshold and density functionals in general do not fulfill the ionization potential theorem which may lead to unphysical excited states [45]. We have chosen the default parameter $0.33 a_0^{-1}$ for the BNL functional [42] and $0.3 a_0^{-1}$ for the CAM-B3LYP functional [31], respectively. Table 1 shows that all the functionals are in good agreement for all the molecules except benzene. The LC functionals overestimate the IP of benzene, which shows that these functionals, and especially the BNL functional, are system-dependent and the parameter should be optimized for each molecule separately [46,47]. We have therefore chosen to use the B3LYP functional in line with our previous work [3,4] for the field-dependent IP also in this work, and will return to the IP of benzene using LC functionals in a separate study.

3.2. Field-dependent IP of benzene

Fig. 2 shows the interaction energy between the benzene cation and the electron as a function of the distance from the z-direction of the electric fields between 0 and 30.84 MV/cm (the coordinate system and the origin of benzene is defined in Fig. 1). The interaction barrier is located around 20 Å at 1.03 MV/cm, while it is at a shorter distance of around 4 Å at 30.84 MV/cm, respectively.

Fig. 3 shows the IP of benzene in an electric field in the x, y and z-directions, respectively. Four different methods are used to investigate the CDFT model at high electric fields, which are combinations of constraining charge and/or spin and two basis sets, cc-pVDZ and cc-pVTZ. In the CDFT method used previously [3,4], both the charge and spin were constrained with the cc-pVTZ basis set (denoted by charge & spin/cc-pVTZ). As shown in Fig. 3, the four methods, charge & spin/cc-pVTZ or cc-pVDZ, charge/cc-pVDZ and spin/cc-pVDZ, are in good agreement with each other. It is noted that by constraining spin disregarding the charge constraint, the dissociation barrier cannot be obtained for fields higher than 20 MV/cm due to convergence problems. In some cases, constraining both charge and spin also lead to convergence problems. In these cases, we first constrained only spin or charge and then restarted the calculation with both the spin and charge constraints. Constraining only the charge therefore results in a smaller amount of computations (less computations with convergence problems),

but with results of similar accuracy as the other methods. Thus, the field-dependent IP calculated by constraining charge with the cc-pVDZ basis set (charge/cc-pVDZ) is selected because of its good agreement with our previous selection (charge & spin/cc-pVTZ) and also its low computational cost for the molecules studied here.

For the aromatic molecules included in this study, the energy barrier distance is closer to the cation than for other molecules we studied. As an example, the barrier distance between the electron and the pyrene cation in the z-direction (out-of-plane) of the electric field, decreases from around 20 Å at 1.03 MV/cm to around 2 Å at 30.84 MV/cm, respectively. In this case, using a smaller basis set, cc-pVDZ, on the cation gives a more compact description of the cation electron density and extends the applicability of the method to higher electric fields.

Figs. 4, 6 and 7 show the IP and excitation energies of the molecules in Fig. 1 in the different directions of the electric field. The solid line shows the IP and the dots are singlet excitation energies. At some electric fields, the excitation energies are very close to the IP. These excitations should in these cases be regarded as ionized states just above the IP, and the differences originate from using different methodologies for the calculation of the IP and excitation energies, respectively. Therefore, the excitations very close to the IP and above the IP are disregarded in this work. The possibility of bound states in the continuum exists [50–52], but that has not been investigated further here.

3.3. Field-dependent IP of pyrene and TMPD

Fig. 4 (left) shows the field-dependent IP and excitation energies of pyrene in the x, y and z-directions of the field, respectively. The optimized geometry is in good agreement with another theoretical study, for example, the calculated central bond length in pyrene is 1.42 Å, in good agreement with the calculated value of 1.43 Å in Ref. [53]. The lowest excitation energy of pyrene, a $\pi \rightarrow \pi^*$ excitation, is 3.66 eV at zero field compared to the experimental value of 3.69 eV [54]. The two lowest excited states survive up to 20 MV/cm in the z-direction, while they become unbound at fields higher than 15 MV/cm in the x and y-directions. Therefore, at fields higher than approximately 20 MV/cm we have a two-state system for pyrene containing the ground state and the ionized state. Fig. 5 illustrates that the π^* excited state (LUMO + 1) changes into an unbound state at fields higher than 20 MV/cm and in this way the orbitals have to be inspected at each field strength. This is consistent with our previous results [2,4], in which the number of available excited states decreases with increasing field since the excitation energies are almost constant in the electric field as compared to the IP.

The TMPD structure is in good agreement with experiment, for example, the calculated carbon–nitrogen bond lengths are around 1.40 Å close to the experimental value of 1.42 Å [55]. The two lowest excitations with approximately the same excitation energies, 3.64 eV, are $n \rightarrow \sigma^*$ excitations. The third excitation is an $n \rightarrow \pi^*$ excitation at 3.86 eV as compared to the experimental value at 3.90 eV [56]. TMPD and TDAE [2,57] with low IPs of 6.30 and 6.11 eV, respectively, are interesting to study since low-IP additives have strong effects on streamer speed and branching in pre-breakdown and breakdown phenomena in dielectric liquids [19]. The field-dependent IP of TMPD is shown in Fig. 4 (right). The excited states for TMPD vanish at 10 MV/cm, while for TDAE, the lowest $n \rightarrow \pi^*$ excitation survive until higher fields of around 50 MV/cm [2]. There are fewer excitations in TDAE compared to TMPD due to the larger number of $\pi \rightarrow \pi^*$ excitations in TMPD. Thus, at relatively low electric fields, TMPD is a better choice to be used as an additive in streamer experiments as compared to TDAE, since molecules with a large number of excited states in the field are expected to be good candidates to be used as additives in insulating liquids in high-voltage devices [1,2,20]. The reason is

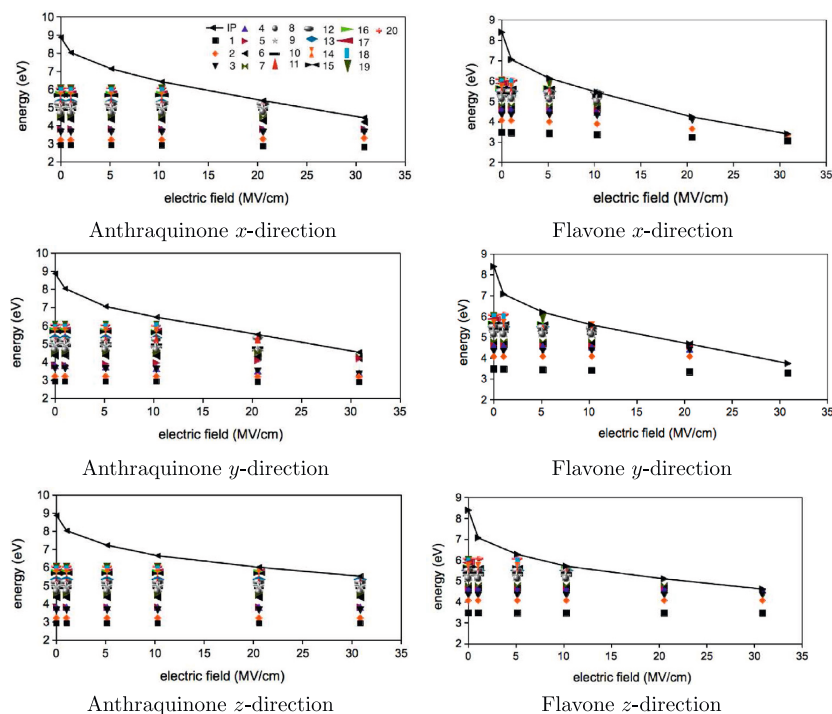


Fig. 6. The IP and excitation energies (eV) in the different directions of the electric field for anthraquinone and flavone. The solid line is the IP and the dots are excitation energies.

that electronic excitations and thus emission of UV/VIS light, together with emitting heat, is a way for the liquid to release energy.

The zero-field IP of *N,N*-dimethylaniline (DMA) is 7.12 eV [2], showing that adding a dimethylamino group to the *para*-position of DMA (giving TMPD) causes a reduction of around 1 eV in the IP. The lowest $n \rightarrow \pi^*$ excitation of DMA at 4.0 eV disappears at around 25 MV/cm. Although TMPD has a larger number of excited states, they vanish at lower fields as compared to TDAE and DMA. Thus, at relatively high electric fields, TMPD is a good candidate to study as only a low-IP additive in breakdown processes. Streamer initiation in dielectric liquids requires an electric field of around 1 MV/cm and greater [15,58,59]. However, the external electric field results in a larger local field especially at absorption frequencies of the liquids, i.e. the electric field of 1 MV/cm and greater is smaller than the local electric field. The response of the local field to the external field is different in the different liquids [60].

The decrease of the IP is most significant in the *y*-direction for both pyrene and TMPD. The central bond in pyrene is along the *y*-direction of the field (Fig. 1) which is the reason for that the decrease of the IP in the *y*-direction is around 70%, while they are around 57 and 50% in the *x* and *z*-directions comparing zero field and 30.84 MV/cm. In TMPD, the *y*-direction is along the two carbon–nitrogen bonds attached to the phenyl ring. A similar direction dependence of the field-dependent IP has also been found for linear alkanes when the field is along or perpendicular to the linear chain such as in *n*-tridecane and 9,10-dimethyloctadecane (DMOD) [2,4].

3.4. Field-dependent IP of anthraquinone and flavone

Fig. 6 shows the field-dependent IP and excitation energies of anthraquinone (left) and flavone (right). The optimized structure

of anthraquinone is in good agreement with experiment [61]. The lowest excitation energy which is an $n \rightarrow \pi^*$ excitation is 2.93 eV compared to its experimental value of 3.1 eV [62]. The second lowest excitation energy at 3.21 eV is also an $n \rightarrow \pi^*$ excitation, while the third and fourth are $\pi \rightarrow \pi^*$ excitations at 3.64 and 3.81 eV, respectively.

The geometry of flavone is in good agreement with a reported computed geometry [63]. The first and second excitations are $n \rightarrow \pi^*$ with the energies 3.48 and 4.07 eV, respectively. The third and fourth excitation energies are 4.32 and 4.57 eV, respectively and are $\pi \rightarrow \pi^*$ excitations.

The field-dependent IPs of anthraquinone and flavone are only slightly dependent on the direction of the field, where the IP decreases more significantly in the *x* and *y* directions as compared to the *z*-direction (out-of-plane direction). There is a larger number of excited states also at relatively high fields for anthraquinone and flavone compared to the other molecules studied here, in line with diketones such as *p*-benzoquinone, benzil and 4–4-dihydroxybenzil as well as azo dyes such as *trans*-azobenzene [2,4]. The emission of UV/VIS radiation can be extended to higher electric fields by adding molecules absorbing in the visual region, i.e. both anthraquinone and flavone are good choices to be used as additives with low excitation energies in dielectric liquids even at relatively high electric fields.

3.5. Field-dependent IP of *p*-benzyltoluene and 2,6-di-*tert*-butyl *p*-cresol

Fig. 7 shows the field-dependent IP of *p*-benzyltoluene (left) and 2,6-di-*tert*-butyl *p*-cresol (right). The two lowest excitation energies of *p*-benzyltoluene are 5.0 and 5.17 eV, respectively, and are $\pi \rightarrow \pi^*$ excitations which survive up to 10 MV/cm in an electric

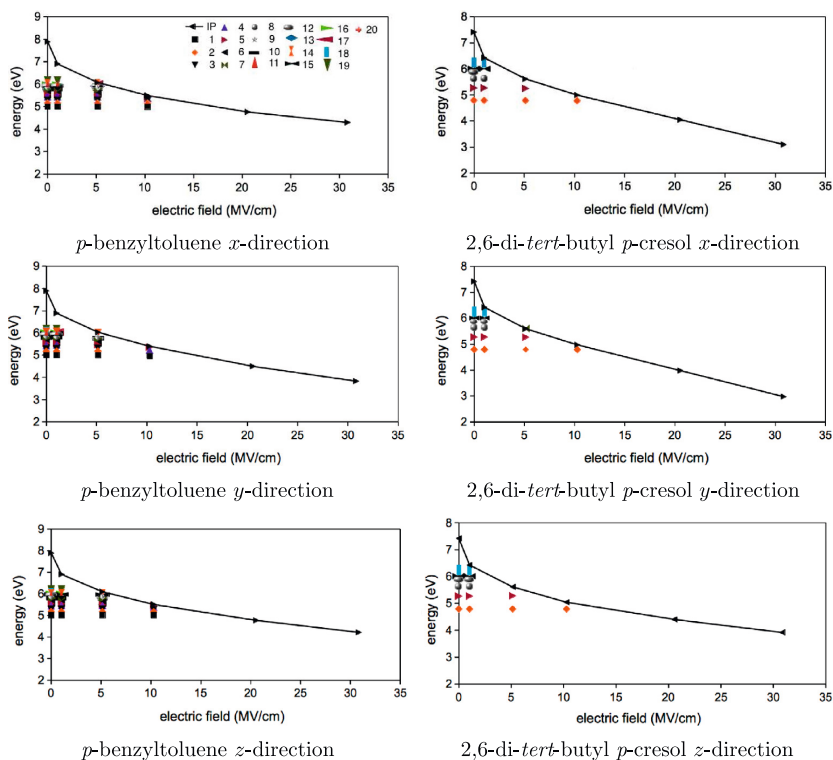


Fig. 7. The IP and excitation energies (eV) in the different directions of the electric field for *p*-benzyltoluene and 2,6-di-*tert*-butyl *p*-cresol. The solid line is the IP and the dots are excitation energies.

field. The field-dependent IP is independent of the direction of the field for this molecule.

For 2,6-di-*tert*-butyl *p*-cresol, the IP decreases more significantly in the *x* and *y*-directions as compared to the *z*-direction. The two lowest excitation energies are $n \rightarrow \pi^*$ excitations at 4.79 eV and 5.23 eV, respectively. The excited states vanish at around 10 MV/cm for all directions of the field due to the strong decrease of the IP and there are a fewer number of excited states in the field compared to anthraquinone and flavone for which the excitation energies remain at higher fields because of their higher IP compared to 2,6-di-*tert*-butyl *p*-cresol. Thus, the IP and excitation energies need to be considered together rather than separately when investigating their potential as additives in insulating liquids.

4. Conclusions

A limitation of the CDFT model for calculating the field-dependent ionization potential at high electric fields is investigated in this work for aromatic and polyaromatic molecules which was resolved by using a slightly smaller basis set, cc-pVDZ, than before [3,4] and constraining only the charge in the CDFT calculations. The results show, in line with previous work [1–4], that the IP decreases strongly in an electric field while the excitation energies remain relatively constant which results in the decrease of the number of available excited states with increasing field. The decrease of the IP is around 4–5 eV for all the molecules comparing zero field and 30.84 MV/cm. The effect of the field on the IP is for some molecules more significant in the direction along a specific bond in the molecule, e.g. along the *y*-direction in pyrene and

TMPD, which is consistent with the stronger field-dependence of the IP along alkane chains [2,4]. Anthraquinone and flavone have a larger number of excited states in the field even at 30 MV/cm, where flavone may be regarded as a more environmentally friendly additive as compared to azo dyes and quinones which have a similar behavior [2,4]. The survival of $n \rightarrow \pi^*$ excitations depends on the field-dependence of the IP, for example in 2,6-di-*tert*-butyl *p*-cresol it vanishes at 10 MV/cm due to its lower IP compared to anthraquinone and flavone.

Conflict of interest

There is no conflict of interest.

Acknowledgment

We would like to acknowledge a research Grant “Modeling of electrical pre-breakdown and breakdown phenomena in insulating liquids” (200631/560) from the Norwegian Research Council, ABB and Statnett and a Grant of computer time (account nn2920k) from the NOTUR project.

References

- [1] H.S. Smalø, Ø. Hestad, S. Ingebrigtsen, P.-O. Åstrand, *J. Appl. Phys.* 109 (2011) 073306.
- [2] N. Davari, P.-O. Åstrand, S. Ingebrigtsen, M. Unge, *J. Appl. Phys.* 113 (2013) 143707.
- [3] N. Davari, P.-O. Åstrand, T. Van Voorhis, *Mol. Phys.* 111 (2013) 1456.
- [4] N. Davari, P.-O. Åstrand, M. Unge, L.E. Lundgaard, D. Linhjell, *AIP Adv.* 4 (2014) 037117.
- [5] M.B. Smirnov, V.P. Krainov, *J. Exp. Theor. Phys.* 85 (1997) 447.

- [6] Q. Wu, T. Van Voorhis, *Phys. Rev. A* 72 (2005) 024502.
- [7] Q. Wu, B. Kaduk, T. Van Voorhis, *J. Chem. Phys.* 130 (2009) 034109.
- [8] T. Van Voorhis, T. Kowalczyk, B. Kaduk, L.-P. Wang, C.-L. Cheng, Q. Wu, *Ann. Rev. Phys. Chem.* 61 (2010) 149.
- [9] B. Kaduk, T. Kowalczyk, T. Van Voorhis, *Chem. Rev.* 112 (2012) 321.
- [10] H. Bachau, E. Cormier, P. Decleva, J.E. Hansen, F. Martín, *Rep. Prog. Phys.* 64 (2001) 1815.
- [11] D. Toffoli, M. Stener, G. Fronzoni, P. Decleva, *Chem. Phys.* 276 (2002) 25.
- [12] A. Ponzi, C. Angeli, R. Cimraglia, S. Coriani, P. Decleva, *J. Chem. Phys.* 140 (2014) 204304.
- [13] L.A. Dissado, J.C. Fothergill, in: *Electrical Degradation and Breakdown in Polymers*, IEE Material and Devices series, vol. 9, Peter Peregrinus Ltd., London, United Kingdom, 1992.
- [14] J. Jadidian, M. Zahn, *IEEE Trans. Plasma Sci.* 41 (2013) 2464.
- [15] J. Jadidian, M. Zahn, N. Lavesson, O. Widlund, K. Borg, *J. Appl. Phys.* 115 (2014) 143304.
- [16] J.C. Devins, S.J. Rząd, R.J. Schwabe, *J. Appl. Phys.* 52 (1981) 4531.
- [17] A. Denat, *IEEE Trans. Dielect. Elect. Insul.* 13 (2006) 518.
- [18] O. Lesaint, M. Jung, *J. Phys. D: Appl. Phys.* 33 (2000) 1360.
- [19] N.V. Dung, H.K. Hoidalén, D. Linhjell, L.E. Lundgaard, M. Unge, *J. Phys. D: Appl. Phys.* 46 (2013) 255501.
- [20] M. Unge, S. Singha, N.V. Dung, D. Linhjell, S. Ingebrigtsen, L.E. Lundgaard, *Appl. Phys. Lett.* 102 (2013) 172905.
- [21] N. Berger, M. Randoux, G. Ottmann, P. Vuarchex, *Electra* 171 (1997) 33.
- [22] C.T. Duy, O. Lesaint, A. Denat, N. Bonifaci, *IEEE Trans. Dielect. Elect. Insul.* 16 (2009) 1582.
- [23] Q. Liu, Z.D. Wang, *IEEE Trans. Dielect. Elect. Insul.* 18 (2011) 285.
- [24] X. Wang, Z.D. Wang, *IEEE Trans. Dielect. Elect. Insul.* 19 (2012) 1916.
- [25] T.H. Dunning Jr., *J. Chem. Phys.* 90 (1989) 1007.
- [26] R.A. Kendall, T.H. Dunning Jr., R.J. Harrison, *J. Chem. Phys.* 96 (1992) 6796.
- [27] C. Lee, W. Yang, R.G. Parr, *Phys. Rev. B* 37 (1988) 785.
- [28] A.D. Becke, *J. Chem. Phys.* 98 (1993) 5648.
- [29] R. Baer, D. Neuhauser, *Phys. Rev. Lett.* 94 (2005) 043002.
- [30] E. Livshits, R. Baer, *Phys. Chem. Chem. Phys.* 9 (2007) 2932.
- [31] T. Yanai, D.P. Tew, N.C. Handy, *Chem. Phys. Lett.* 393 (2004) 51.
- [32] P.-O. Löwdin, *J. Chem. Phys.* 18 (1950) 365.
- [33] G. Zhang, C.B. Musgrave, *J. Phys. Chem. A* 111 (2007) 1554.
- [34] S.J.A. van Gisbergen, J.G. Snijders, E.J. Baerends, *Comput. Phys. Commun.* 118 (1999) 119.
- [35] M. Valiev, E.J. Bylaska, N. Govind, K. Kowalski, T.P. Straatsma, H.J.J. van Dam, D. Wang, J. Nieplocha, E. Apra, T.L. Windus, W.A. de Jong, *Comput. Phys. Commun.* 181 (2010) 1477.
- [36] F.M.J. McCluskey, A. Denat, *IEEE Trans. Dielect. Elect. Insul.* 1 (1994) 672.
- [37] C. Lamarre, A. Gendron, *IEEE Trans. Dielect. Elect. Insul.* 2 (1995) 413.
- [38] A. Benthásáth, S. Ruzsnyák, A. Szent-Györgyi, *Nature* 139 (1937) 326–327.
- [39] M. Batley, L.E. Lyons, *Makromol. Chem.* 3 (1968) 357.
- [40] H.S. Smalø, P.-O. Åstrand, S. Ingebrigtsen, *IEEE Trans. Dielect. Elect. Insul.* 17 (2010) 733.
- [41] M.A. Rohrdanz, K.M. Martins, M. Herbert, *J. Chem. Phys.* 130 (2009) 054112.
- [42] L. Jensen, N. Govind, *J. Phys. Chem. A* 113 (2009) 9761.
- [43] T. Körzdöfer, J.S. Sears, C. Sutton, J.-L. Brédas, *J. Chem. Phys.* 135 (2011) 204107.
- [44] H. Phillips, Z. Zheng, E. Geva, B.D. Dunietz, *Org. Electr.* 15 (2014) 1509.
- [45] P.A. Pieniazek, S.A. Arnstein, S.E. Bradforth, A.I. Krylov, C.D. Sherrill, *J. Chem. Phys.* 127 (2007) 164110.
- [46] E. Livshits, R. Baer, *J. Phys. Chem. A* 112 (2008) 12789.
- [47] T. Stein, L. Kronik, R. Baer, *J. Am. Chem. Soc.* 131 (2009) 2818.
- [48] D.R. Lide, *Handbook of Chemistry and Physics*, eighty fourth ed., CRC Press, Boca Raton, FL, 2004.
- [49] S. Millefiori, A. Millefiori, *Spectrochim. Acta A* 44 (1988) 17.
- [50] J. von Neumann, E.P. Wigner, *Phys. Z* 30 (1929) 465.
- [51] H. Friedrich, D. Wintgen, *Phys. Rev. A* 31 (1985) 3964.
- [52] L.S. Cederbaum, R.S. Friedman, V.M. Ryaboy, N. Moiseyev, *Phys. Rev. Lett.* 90 (2003) 013001.
- [53] R.C. Peck, J.M. Schulman, R.L. Disch, *J. Phys. Chem.* 94 (1990) 6637.
- [54] G.B. Ray, I. Chakraborty, S.P. Moulik, *J. Colloid Interface Sci.* 294 (2006) 248.
- [55] I. Ikemoto, *Acta Cryst. B* 35 (1979) 2264.
- [56] A.C. Albrecht, W.T. Simpson, *J. Am. Chem. Soc.* 77 (1955) 4454.
- [57] Y. Nakato, M. Ozaki, E. Egawa, H. Tsubomura, *Chem. Phys. Lett.* 9 (1971) 615.
- [58] J. Jadidian, M. Zahn, N. Lavesson, O. Widlund, K. Borg, *IEEE Trans. Plasma Sci.* 40 (2012) 909.
- [59] J. Jadidian, M. Zahn, N. Lavesson, O. Widlund, K. Borg, *Appl. Phys. Lett.* 100 (2012) 172903.
- [60] N. Davari, S. Haghani, P.-O. Åstrand, G.C. Schatz, *Local field factors by a combined charge-transfer and point-dipole interaction model*, submitted for publication.
- [61] S.N. Ketker, M. Kelley, M. Fink, R.C. Ivey, *J. Mol. Struct.* 77 (1981) 127.
- [62] A.N. Diaz, *J. Photochem. Photobiol. A: Chem.* 53 (1990) 141.
- [63] S. Aparicio, *Int. J. Mol. Sci.* 11 (2010) 2017.

Paper 5

Local electric field factors by a combined
charge-transfer and point-dipole interaction model

Nazanin Davari, Shokouh Haghani, Per-Olof Åstrand and George C.
Schatz

RSC Advances, 5, 31594-31605, (2015)



Cite this: *RSC Adv.*, 2015, 5, 31594

Local electric field factors by a combined charge-transfer and point-dipole interaction model†

Nazanin Davari,^a Shokouh Haghdani,^a Per-Olof Åstrand^{*a} and George C. Schatz^b

A force-field model for the local electric field as a linear response to a frequency-dependent external electric field is presented based on a combined charge-transfer and point-dipole interaction (CT-PDI) force-field model for frequencies through the first absorption maximum. The local electric field provides a measure of the mutual interactions of the molecules with each other, as is important in problems ranging from dielectric breakdown to solvent polarization and energy transfer. It also indicates how resonant excitation of these molecules can perturb Raman scattering by a third molecule located nearby through an intensity borrowing mechanism. The CT-PDI model is a combination of a modified electronegativity equalization model including non-metallic behaviour and a point-dipole interaction model described by atomic polarizabilities which also includes the time-dependence of the atomic charges and atomic dipole moments. A parametrization of frequency-dependent polarizabilities through the first absorption maximum calculated by time-dependent density-functional theory has been extended for a set of hydrocarbon and azobenzene molecules to provide atom-type parameters for the CT-PDI model. As initial model systems, results are presented for the benzene and azobenzene dimers for the local electric field response at points between the molecules and at the atoms in the molecules. As expected, the response depends critically on the intermolecular distance between the monomers. The azobenzene dimer shows a larger local field response at the atoms in the phenyl rings compared to the benzene dimer and the response at the nitrogen atoms is larger than at the hydrogen and carbon atoms in the azobenzene dimer, which can be rationalized qualitatively by the charge and dipole contributions to the local field factor either adding up or to a large extent cancelling each other. At the absorption frequency, the largest local field factor of the benzene dimer is around 6 and for the azobenzene dimer it is around 12, respectively, at typical distances, indicating that the response may be significant.

Received 9th March 2015
Accepted 19th March 2015

DOI: 10.1039/c5ra04183j

www.rsc.org/advances

1 Introduction

In an external electric field, the molecules in a dielectric liquid are polarized resulting in a local electric field at the molecule which is different from the external electric field. The local electric field is a sum of the external electric field and the electric field of the permanent and induced multipole moments established in the presence of the external electric field.^{1–3} The Lorentz approach⁴ has been used frequently as an approximate method to determine the local electric field. In this approach, the local field at a certain point of a dielectric is the same as that inside a fictive sphere. However, the Lorentz model is limited to non-polar materials and it is assumed that the contribution of electric dipoles inside the sphere is zero. Polarization from an

atomistic point of view requires knowledge of the local field at the atoms of the dielectric as a response to an external electric field.

Quantum chemical response theory⁵ and time-dependent density-functional response theory (TDDFT)⁶ are standard methods to obtain response properties for small and medium-sized systems. Electric dipole shieldings and hypershieldings⁷ have been calculated at the Hartree-Fock level of theory^{8–10} which determine the linear and non-linear local field responses to the external field. In TDDFT calculations, the accuracy of the response properties depends critically on the choice of density functionals,^{11–15} because the exchange-correlation potential in approximate standard functionals shows incorrect asymptotic decay of the true electrostatic potential.^{16,17} Long-ranged corrected (LC) functionals with the correct asymptotic behaviour have been suggested as alternatives for this purpose.^{18–23}

Force-field models have been used as an alternative for the calculation of response properties of relatively large molecules. The point-dipole interaction (PDI) model,^{24–28} has been used for the calculation of the polarizabilities of carbon nanotubes and

^aDepartment of Chemistry, Norwegian University of Science and Technology (NTNU), NO-7491, Trondheim, Norway. E-mail: per-olof.astrand@ntnu.no

^bDepartment of Chemistry, Northwestern University, 2145 Sheridan Road, Evanston, IL 60208-3113, USA

† Electronic supplementary information (ESI) available. See DOI: 10.1039/c5ra04183j

fullerenes,^{29–34} boron nitride tubes³⁵ and proteins,³⁶ and it has also been extended to properties such as optical rotation^{37–40} and hyperpolarizabilities.^{30,31,33,41–45} In the PDI model, atomic polarizabilities couple with each other in an external electric field through the atomic induced dipole moments and the molecular polarizability is obtained by considering atomic polarizabilities as atom-type parameters.

To calculate atomic charges, the electronegativity equalization model (EEM)^{46–48} has been used where the charge-transfer between atoms is calculated using atomic electronegativities and chemical hardnesses as atom-type parameters. To resolve the limitation of the EEM regarding the charge transfer over large distances,^{49,50} the atom–atom charge-transfer (AACT) method⁴⁹ is adopted in a model that is transferable to both metallic and non-metallic systems.^{51–57} In a metallic model like EEM, charges are allowed to move without a significant resistance between the atoms such as in highly conjugated systems, while a non-metallic model describes molecules with much less charge-transfer, as for example in alkanes.

In the charge–dipole interaction model, *e.g.* a combined EEM and PDI model^{58–63} or a combined capacitance model and PDI model,^{50,64–67} each atom is associated with both a net electric charge and a dipole. In the capacitance model, the charge-transfer term is determined in terms of the atomic capacitance which is the inverse of the atomic chemical hardness. Frequency-dependent polarizabilities have been calculated using the charge–dipole interaction model, where the interaction with oscillating electric fields is considered by including the kinetic energy of the atomic charges and the atomic dipoles^{68–71} and it has been extended to the calculation of absorption spectra.^{72,73}

In this work, frequency-dependent polarizabilities have been parametrized by a combined charge-transfer and point–dipole interaction (CT-PDI) model,^{74,75} where the charge-transfer and dipole terms are obtained using the AACT and PDI models, respectively, and the charge–dipole interaction gives the coupling between the two models. An extra energy term is added to the charge-transfer term in our model to obtain polarizabilities that scale correctly with the size of the system. One set of atom-type parameters is used for each element, which can be determined assuming that the amount of charge-transfer in a bond is a function of the bond distance.⁵⁷

Solving the CT-PDI model, or any similar model, for the frequency-dependent polarizability gives direct information about the local electric fields as the response to an external electric field (both static and optical frequency). In the calculation of local electric fields, it is in most cases of interest to locate “hot spots”, *i.e.* points where the local field is very high which can initiate rare events in chemistry. As an example where static fields are important, in electrical breakdown in insulating liquids,⁷⁶ the probability of the production of free electrons increases at the location of high local electric fields. In this context, we have developed a model for calculating the field-dependent ionization potential,^{77–80} but the local field is needed to deduce the actual molecular ionization potential in an electrically insulating liquid.

Local electric fields at optical frequencies play a role in many other phenomena. For aggregates of molecules they determine the interactions between molecules that lead to exciton transport and shifts in excited state energies. For molecules in solvents they are responsible for the solvent-induced effects on optical spectra. In addition, they are important in surface-enhanced Raman scattering (SERS),^{81–84} where the local field near metal nanoparticles is enhanced by plasmon excitation. Indeed, previously there have been calculations of electric fields in the vicinity of silver clusters as models of SERS.^{85,86} However, metal clusters or particles are not required in order to generate observable effects. For example, solvent vibrational modes have been observed in the resonance Raman and resonance hyper-Raman spectra of small molecules.^{87,88} In addition, there is much current interest in the plasmonic states of aromatic molecules,^{89,90} where one expects to see enhanced fields and hot spots.

Previously, the CT-PDI model has been used to calculate frequency-dependent polarizability.^{74,75} In this work, the CT-PDI model is parametrized against TDDFT calculations and is applied to two molecular dimers, benzene and azobenzene, where the local field response to the frequency-dependent external electric field is calculated for frequencies through the first absorption maximum. Since the emphasis in this work is on method development and testing by comparisons with TDDFT, only simple dimer structures are considered. However the methods we are developing have the capability of being applied to much larger systems, including molecular aggregates and large graphene-like aromatic systems.

2 Theory

In this work, a force-field model for the response of the local electric field to the external field (local field factor) is presented. In our model, the local electric field at atom I , $E_{I,\beta}^{\text{loc}}$, is the sum of the external electric field, $E_{I,\beta}^{\text{ext}}$, and a field from the surrounding atoms, $E_{I,\beta}^{\text{pol}}$,

$$E_{I,\beta}^{\text{loc}} = E_{I,\beta}^{\text{ext}} + E_{I,\beta}^{\text{pol}} \quad (1)$$

where Greek subscripts denote the Cartesian coordinates, x , y , or z , respectively.

The polarization field at atom I arises from the charges and dipole moments of the surrounding atoms:

$$E_{I,\beta}^{\text{pol}} = \sum_{J \neq I}^N T_{IJ,\beta}^{(1)} q_J + T_{IJ,\beta\gamma}^{(2)} \mu_{J,\gamma} \quad (2)$$

where the Einstein summation convention is used for repeated subscripts. q_J is the atomic charge, $\mu_{J,\gamma}$ is the atomic dipole moment. Here, q_J and $\mu_{J,\gamma}$ include both permanent contributions (as the isolated molecule has a permanent dipole and/or quadrupole moment) and induced contributions from the electric field of the surroundings. In our model, Gaussian charge distributions for each atom are adopted instead of point-charges.^{49,91} The electrostatic energy between two Gaussian charge distributions is:

$$V_{IJ} = q_I q_J \frac{\text{erf}(\sqrt{a_{IJ}} R_{IJ})}{R_{IJ}} \quad (3)$$

where R_{IJ} is the distance between atoms I and J , and a_{IJ} is:

$$a_{IJ} = \frac{\phi_I \phi_J}{\phi_I + \phi_J} \quad (4)$$

where ϕ_I is an atom-type parameter describing the width of the Gaussian distribution. The relatively complex form of the error function can be approximated as:^{91,92}

$$V_{IJ} = \frac{q_I q_J}{\sqrt{R_{IJ}^2 + \frac{\pi}{4a_{IJ}}}} \quad (5)$$

where the limiting behaviour at $R_{IJ} \rightarrow 0$ and $R_{IJ} \rightarrow \infty$ in eqn (3) is retained.

In the same way, the electrostatic interaction between a point charge q_P and a Gaussian charge distribution of atom I is given as

$$V_{PI} = \frac{q_I q_P}{\sqrt{R_{PI}^2 + \frac{\pi}{4\phi_I}}} \quad (6)$$

Therefore, the local field factors at atoms are given with the electrostatic damping in eqn (5) and at other points in space eqn (6) is applied, respectively.

$T_{IJ,\beta}^{(1)}$ and $T_{IJ,\beta\gamma}^{(2)}$ in eqn (2) are the charge–dipole and dipole–dipole interaction tensors:

$$T_{IJ,\beta}^{(1)} = \nabla_{\beta} \frac{1}{\tilde{R}_{IJ}} = \frac{-R_{IJ,\beta}}{\tilde{R}_{IJ}^3} \quad (7)$$

and

$$T_{IJ,\beta\gamma}^{(2)} = \nabla_{\gamma} T_{IJ,\beta}^{(1)} = \frac{3R_{IJ,\beta} R_{IJ,\gamma} - \delta_{\beta\gamma} \tilde{R}_{IJ}^2}{\tilde{R}_{IJ}^5} \quad (8)$$

where $R_{IJ,\beta} = R_{I,\beta} - R_{J,\beta}$, $R_{I,\beta}$ is the coordinate of atom I and $\tilde{R}_{IJ} = \sqrt{R_{IJ}^2 + \frac{\pi}{4a_{IJ}}}$. In our model, the atomic charge is replaced by the charge-transfer term, q_{JM} ,^{49,57}

$$q_J = \sum_M q_{JM} \quad (9)$$

Inserting eqn (9) into eqn (2) gives the local field in terms of the charge-transfer variables instead of atomic charges,

$$E_{I,\beta}^{\text{pol}} = \sum_{J \neq I, M > J}^N \left(T_{IJ,\beta}^{(1)} - T_{IM,\beta}^{(1)} \right) q_{JM} + \sum_{J \neq I}^N T_{IJ,\beta\gamma}^{(2)} \mu_{J,\gamma} \quad (10)$$

where we have used $q_{MJ} = -q_{JM}$. In the CT-PDI model, the molecular polarizability for a homogenous external field, $E_{I,\alpha}^{\text{ext}} = E_{\alpha}^{\text{ext}}$, is given as:⁵⁷

$$\alpha_{\gamma\alpha} = \sum_{J, M > J}^N R_{JM,\gamma} \frac{\partial q_{JM}}{\partial E_{\alpha}^{\text{ext}}} + \sum_J^N \frac{\partial \mu_{J,\gamma}}{\partial E_{\alpha}^{\text{ext}}} \quad (11)$$

where $\partial q_{JM} / \partial E_{\alpha}^{\text{ext}}$ is the charge-transfer contribution to the polarizability and $\partial \mu_{J,\gamma} / \partial E_{\alpha}^{\text{ext}}$ is the dipole contribution to the polarizability. $\partial q_{JM} / \partial E_{\alpha}^{\text{ext}}$ and $\partial \mu_{J,\gamma} / \partial E_{\alpha}^{\text{ext}}$ are calculated by solving

a set of linear response equations for the frequency-dependent polarizability originating from minimizing a Lagrangian involving kinetic energies for the atomic charges and atomic dipole moments.^{69,74} A detailed presentation of the model for the calculation of the frequency-dependent polarizability can be found in ref. 74.

The response of the local field to the external field becomes:

$$\frac{\partial E_{I,\beta}^{\text{loc}}}{\partial E_{\alpha}^{\text{ext}}} = \delta_{\beta\alpha} + \sum_{J \neq I, M > J}^N \left(T_{IJ,\beta}^{(1)} - T_{IM,\beta}^{(1)} \right) \frac{\partial q_{JM}}{\partial E_{\alpha}^{\text{ext}}} + \sum_{J \neq I}^N T_{IJ,\beta\gamma}^{(2)} \frac{\partial \mu_{J,\gamma}}{\partial E_{\alpha}^{\text{ext}}} \quad (12)$$

i.e. it is given by the interaction tensors in eqn (7) and (8) as well as the solutions to the response problem for the polarizability.

3 Model parametrization

The static and frequency-dependent polarizabilities were calculated using the TDDFT method^{69,93,94} with the PBE functional⁹⁵ and the augmented TZP basis set.^{96,97} The optimized geometries were obtained using the PBE functional and the TZP basis set.⁹⁶ Since dissipation is included in the CT-PDI model, it was also included in the quantum chemical calculations of the frequency-dependent polarizability.^{98,99} The life-time of the excited states was chosen to be 0.004 a.u. in the TDDFT calculations. Thus, both the imaginary and the real parts of the polarizabilities were calculated. ADF software^{100,101} was applied in all the DFT calculations.

The TDDFT polarizabilities were used as reference data for the parametrization of the CT-PDI model. The first $\pi \rightarrow \pi^*$ excitation of azo dyes, aromatic molecules and polyenes as well as the first $\sigma \rightarrow \sigma^*$ excitation of alkanes were included in the parametrization, while higher excitations were ignored. The set of azobenzenes studied in our previous work⁷⁵ was here extended by a set of hydrocarbons. The parameters were optimized by a simplex algorithm to minimize the relative root mean square deviation (RMSD) between the polarizabilities calculated by the TDDFT method and the CT-PDI model. Both the real and the imaginary parts of the full polarizability tensor were parametrized.

Table 1 Atom-type parameters (a.u.) of the CT-PDI model with a brief description. The corresponding equations can be found in ref. 74

Description	C	H	N
α Isotropic atomic polarizability	8.2569	2.5564	4.8957
x Anisotropic atomic polarizability	0.2576	0.5021	0.2874
η Chemical hardness	2.7742	2.9595	3.1935
ϕ Width of a Gaussian distribution	1.2193	0.4599	2.6465
g_0 Charge-transfer in non-metallic systems	0.7765	0.2052	1.0624
g_1 Charge-transfer in metallic systems	0.9964	0.2236	1.2355
C Steepness of the charge-transfer	1.7372	2.1490	4.9503
R Atomic radius	1.3947	0.7516	1.1708
c_q Number of oscillating charges	3.1893	3.8734	1.1866
c_{μ} Number of oscillating dipoles	0.1222	2.3579	4.1181
γ_q Dissipation of charge	0.0121	0.0210	0.0033
γ_{μ} Dissipation of dipole	0.0127	0.0226	0.0018

The values of the parameters are presented in Table 1 with a brief description and Table 2 presents the molecules grouped as a training set for the parametrization and a validation set to evaluate the parameters. The equations including all parameters can be found in ref. 74 and are not repeated here. α and x are the isotropic and anisotropic atomic polarizability parameters, respectively, describing the atomic polarizability. η is the chemical hardness parameter in the regular EEM and the width of a Gaussian charge distribution is described by the ϕ parameter. To describe the non-metallic behaviour, a charge-transfer model was introduced that contains four atom-type parameters, g_0 , g_1 , C and R . Also four atom-type parameters, c_q , c_μ , γ_q and γ_μ were used to describe the frequency-dependence. More specifically, c_q and c_μ correspond to the inverse of the numbers of oscillating charges and dipoles, respectively, whereas γ_q and γ_μ describe the dissipation of the charge and dipole contributions, respectively.

The obtained values of the parameters are in some cases different from our previous work.⁷⁵ The largest change is in the c_q and c_μ parameters. The c_q parameter of the hydrogen atom decreases from 6.1514 a.u. (ref. 75) to 3.8734 a.u. in this work, while c_μ increases from 0.6823 to 2.3579 a.u., indicating that for

hydrogen the contribution from oscillating dipole moments decreases whereas the oscillating charge-transfer increases in importance. The reason for these discrepancies between the new and old parameters is that here we provide parameters for a wider set of molecules including a set of hydrocarbons in addition to the azo dyes in our previous work.⁷⁵ It is an ambitious goal to have a single set of atom-type parameters for carbon with the different properties of alkanes, aromatic systems, polyenes and polyynes, but we believe that the CT-PDI model^{74,75} is a step in the right direction. The instability of the parameter values is a common phenomenon especially in charge equilibration models, and there is no agreement on a generic set of optimal parameters.¹⁰² To provide a comprehensive model that can describe an extensive set of molecular systems, the parameters still need to be improved. The goal is to extend the set of molecules step by step but provide a single set of parameters for all included molecules rather than system-specific parameter sets. Also it is desirable to have atom-type parameters and not, for example, bond and three-body parameters, as well as to have only one set of parameters for each element. Further developments of the model should rather be in the direction of improving the physics of each term by

Table 2 The excitation energy (eV) and static polarizability (a.u.) calculated by the TDDFT and CT-PDI models

Molecule	Excitation energy				Static polarizability			
	TDDFT	CT-PDI	Error %	Exp.	TDDFT	CT-PDI	Error %	Exp.
Training set								
<i>trans</i> -Azobenzene	3.37	3.32	1.48	3.90 (ref. 103)	198.7	201.8	1.56	171.4 (ref. 104)
3-Methylazobenzene	3.40	3.27	3.82	3.85 (ref. 103)	215.5	226.7	5.20	
4-Methylazobenzene	3.27	3.18	2.75	3.72 (ref. 103)	220.8	224.7	1.77	
4-Aminoazobenzene	2.99	3.13	4.68	3.19 (ref. 105)	232.4	226.4	2.58	
4-Cyanoazobenzene	2.99	3.20	7.02	3.81 (ref. 105)	233.0	242.5	4.08	
4,4'-Di-diethylaminoazobenzene	2.53	2.88	13.80	2.91 (ref. 106)	432.6	377.3	12.78	
4-Methyl-4'-dimethylaminoazobenzene	2.76	3.02	9.42	3.05 (ref. 107)	297.6	290.0	2.55	
4,4'-Diaminoazobenzene	2.80	3.05	8.93		264.9	249.3	5.89	
Benzene	6.80	6.26	7.94	6.20 (ref. 108)	70.9	72.0	1.55	70.1 (ref. 109)
Toluene	6.53	5.28	19.14	5.76 (ref. 110)	85.5	92.1	7.72	82.7 (ref. 109)
1,3-Butadiene (C ₄ H ₆)	5.39	4.95	8.16	5.92 (ref. 111)	58.9	51.0	13.41	54.7 (ref. 112)
1,3,5,7,9,11,13-Tetradecaheptaene (C ₁₄ H ₁₆)	2.61	2.01	22.99		349.3	296.1	15.23	
Ethane	8.11	8.16	0.61	8.70 (ref. 113)	30.4	25.2	17.10	30.2 (ref. 109)
Propane	7.56	7.59	0.40	8.10 (ref. 113)	43.4	37.6	13.36	42.4 (ref. 109)
<i>n</i> -Tridecane	7.35	7.02	4.49		535.4	543.1	1.44	
Cyclohexane	7.40	7.51	1.49	7.00 (ref. 114)	75.3	72.6	3.59	74.2 (ref. 109)
Validation set								
2-Methylazobenzene	3.27	3.54	8.26		213.4	218.9	2.58	
4-Dimethylaminoazobenzene	2.79	2.99	7.17	3.07 (ref. 107)	274.5	265.7	3.21	
4-Diethylaminoazobenzene	2.75	3.05	10.91	2.99 (ref. 104)	312.6	290.4	7.10	
4-Cyano-4'-dimethylaminoazobenzene	2.67	2.90	8.61	2.75 (ref. 115)	328.9	306.6	6.78	
4,4'-Dimethylazobenzene	3.24	3.13	3.40		242.5	251.6	3.75	
4-Amino-4'-methylazobenzene	2.98	3.09	3.69		252.5	250.5	0.79	
4,4'-Di-dimethylaminoazobenzene	2.60	2.94	13.08	2.94 (ref. 116)	352.3	327.7	6.98	
4-Cyano-4'-diethylaminoazobenzene	2.58	2.86	10.85	2.66 (ref. 117)	362.9	331.1	8.78	
2,4,6-Tricyano-4'-diethylaminoazobenzene	2.48	2.86	15.32	2.21 (ref. 117)	401.4	395.9	1.37	
Aniline	4.35	4.24	2.53	4.40 (ref. 110)	84.5	88.3	4.50	78.1 (ref. 109)
1,3,5,7,9,11,13,15,17-Octadecanonaene (C ₁₈ H ₂₀)	2.18	1.80	17.43		539.5	413.0	23.45	
1,3,5,7,9,11,13,15,17,19,21-Docosaundecaene (C ₂₂ H ₂₄)	1.90	1.66	12.63		770.6	532.9	30.85	
Octane	6.80	7.07	3.97	7.50 (ref. 113)	110.0	107.0	2.73	104.2 (ref. 109)
Dodecane	7.35	7.02	4.49		164.7	166.1	0.85	153.5 (ref. 109)

including, for example, higher-order terms such as atomic quadrupole moments and atomic hyperpolarizabilities.

The excitation energies and the static polarizabilities calculated using the TDDFT and CT-PDI models are shown in Table 2 as well as experimental values. The $\pi \rightarrow \pi^*$ excitation energies of the azo dyes calculated using the CT-PDI model are in good agreement with those using the TDDFT method. The largest error is around 15% for 2,4,6-tricyano-4'-diethylaminoazobenzene in the validation set. Among the aromatic molecules, benzene, toluene and aniline, the largest error of the $\pi \rightarrow \pi^*$ excitation energy is 19% for toluene. The CT-PDI model overestimates the shift in the excitation energy when a methyl substituent is added to a phenyl ring of benzene (e.g. toluene) compared to the TDDFT method and the experimental value.

In the case of polyenes, the errors are larger for the longer chains, $C_{14}H_{16}$, $C_{18}H_{20}$ and $C_{22}H_{24}$, compared to the shorter one, C_4H_6 . For polyenes the shift in the excitation energy on increasing the chain length is in good agreement with results obtained using the TDDFT method. The $\sigma \rightarrow \sigma^*$ excitation energy of alkanes is in good agreement with the results using the TDDFT method and also the excitation energy shift is predicted well by the CT-PDI model. The CT-PDI excitation energies are in good agreement with the experimental values and the deviations arise from solvent effects in the experiments.

The errors in the static polarizability of azo dyes are comparable to those in our previous work⁷⁵ and in some cases are smaller. For example, 2,4,6-tricyano-4'-diethylaminoazobenzene has the largest error of the static polarizability, 23% in our previous work, while here it is 1%. For the alkanes, the static polarizability is in good agreement with the TDDFT results. The largest error is 17% in ethane, while in dodecane it is only 0.85%. The CT-PDI model also gives the static polarizability of aromatic molecules in good agreement with the TDDFT method. The static polarizability of polyenes shows the largest error of around 31% for $C_{22}H_{24}$.

Fig. 1 shows the carbon-carbon bond distance distribution of the molecules in the training set. As could be expected, the model works better for the bond distances with higher

probabilities which is due to the fact that our non-metallic correction to the charge-transfer model strongly depends on the bond distances. The highest peak around 1.40 Å shows the distribution of aromatic bonds, whereas the second highest peak at around 1.53 Å shows the bond distance distribution of single C-C bonds. The small peaks around 1.35 Å represent the bonds in polyenes and the small peak around 1.50 Å shows the carbon bond of a methyl group bound to a phenyl ring, as for example in toluene. In general, the molecules with the largest errors in Table 2 can be explained by their small contribution to the bond distance distribution in the training set. The charge-transfer model in CT-PDI has a strong bond-distance dependence and is based on the sum of the two distances between three connected atoms in a molecule ($R_{IJ} + R_{JK}$, $I \neq K$)⁵⁷ (the variation of the sum of the two distances is an order of magnitude smaller than the variation of the individual bond distances). In the molecules with methyl substituents, e.g. toluene, the sum of the two bond distances between the carbon atoms of the methyl group and phenyl ring is around 2.9 Å, and the charge-transfer through this bond is not well described, which leads to the relatively large error in the frequency-dependent polarizability. Since the $\pi \rightarrow \pi^*$ excitation in azo dyes is caused by the dipole term in the azo group and the adjacent carbon atoms,⁷⁵ the excitation energy in azobenzenes with methyl substituents is still well predicted because the charge-transfer in the phenyl-methyl bonds does not contribute substantially. The same problem appears for polyenes, with the sum of the two distances around being 2.7 Å in a π -conjugated chain of carbon atoms, which is not well represented in the parametrization.

Fig. 2 shows the frequency-dependent isotropic polarizability of some of the molecules in the training set (left) and in the validation set (right) as well as their charge and dipole contributions. The maximum of the imaginary part of the polarizability gives the absorption frequency. Although the absorption frequencies calculated by the CT-PDI model are in good agreement with those found using the TDDFT method, the polarizabilities at the absorption frequency are in some cases smaller than the TDDFT polarizabilities which affects the local field factor at the absorption frequency. The dipole term dominates the charge term for all the molecules but at the absorption frequency the charge and dipole terms become comparable, especially in the case of azo dyes and long polyenes.

4 Results and discussion

The local field response to the external field was calculated for two dimers, the benzene dimer and the *trans*-azobenzene dimer. The relative orientations of the dimers as well as the definitions of the coordinate systems are given in Fig. 3. Although the dimer structures are not optimized, the chosen structures give a good indication of the magnitude of the local field factors. It is important that the dimers are placed along one of the axes, here the *x*-axis, since, as discussed below, the response is larger for a field along a chain of molecules. The two molecules are in the training set and the CT-PDI model predicts

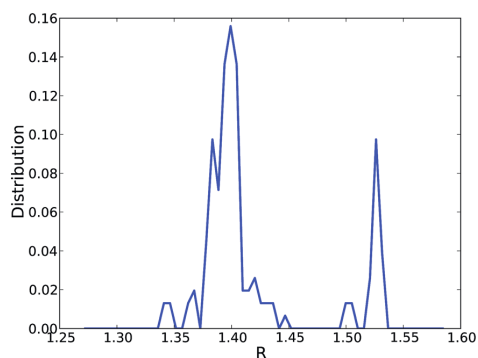


Fig. 1 The carbon-carbon bond distance (Å) distribution of the molecules in the training set.

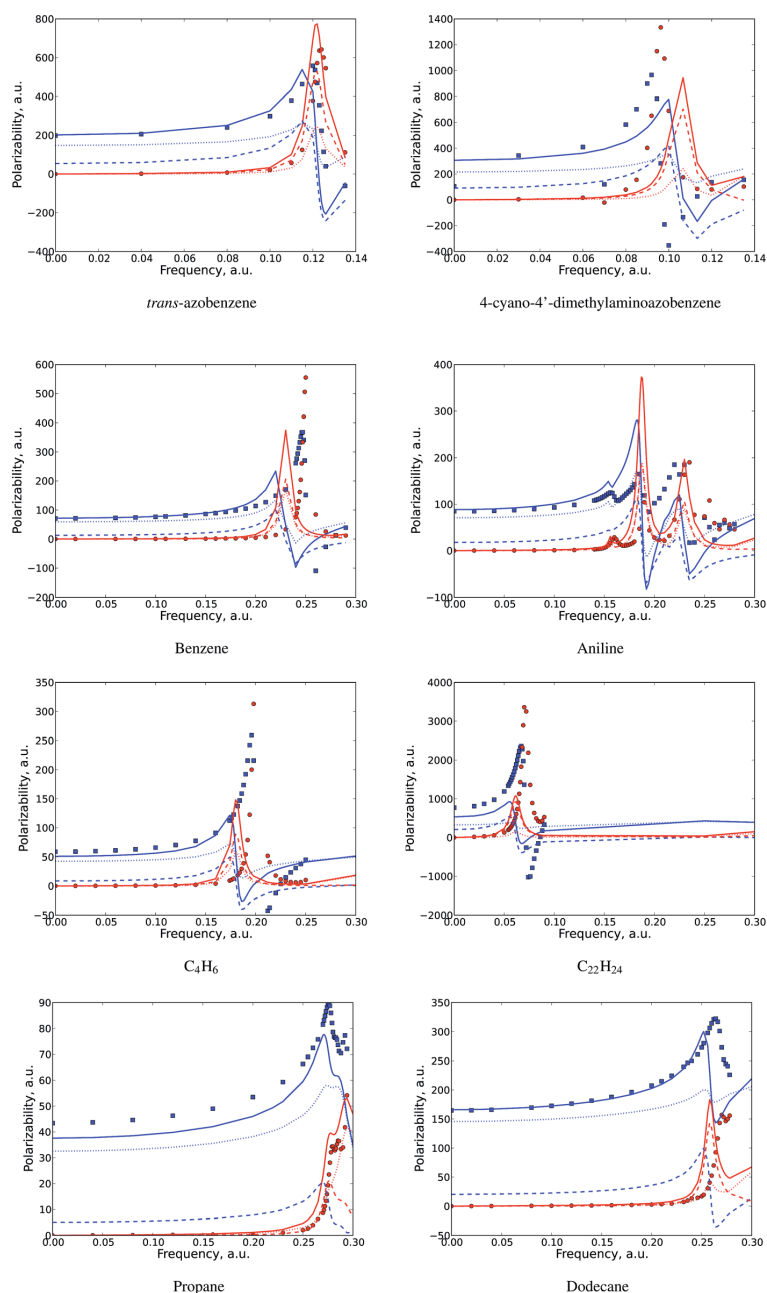


Fig. 2 The isotropic polarizability of the molecules in the training set (left) and validation set (right). The solid lines show the polarizability calculated using the CT-PDI model. The squares and circles show the results of TDDFT calculations. The dashed lines are the charge, and the dotted lines are the dipole contributions of the polarizability, respectively. The blue and red colors show the real and imaginary parts of the polarizability, respectively (1 a.u. = 27.21 eV).

their frequency-dependent polarizabilities in good agreement with TDDFT. At the absorption frequency, the CT-PDI polarizability of benzene is smaller than for TDDFT, leading to the

calculated local field factor of the benzene dimer at the absorption frequency being underestimated by the CT-PDI model as compared to TDDFT. The local field factor is

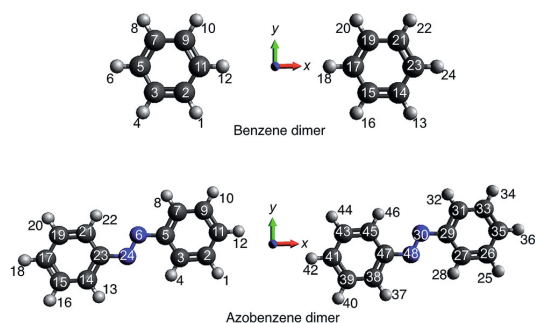


Fig. 3 The benzene and azobenzene dimers. The origin of the coordinate system for each dimer is shown at the point between the monomers.

calculated at a point between the monomers (at the origin of the coordinate system shown in Fig. 3) and at the atoms for different distances between the monomers. Results are presented for frequencies through the $\pi \rightarrow \pi^*$ absorption frequency for atoms with large responses and two intermolecular distances were chosen to study the distance dependence of the local field factor. The minimum distance was chosen to prevent van der Waals strain between the hydrogen atoms of monomers. Therefore, the distance between the hydrogen

atoms (with a van der Waals radius of 1.09 Å (ref. 118)) of the monomers is longer than twice the radius.

4.1 Benzene dimer

Fig. 4 shows the local field response of the benzene dimer at the point between the monomers (at the origin of the coordinate system) and at one of the hydrogen atoms (number 16 in Fig. 3) at two intermolecular distances, 8 and 10 Å (between the center of the benzene rings), in the x -direction of the external electric field. As expected, both the static and the frequency-dependent local field responses decrease with increasing distance. At 8 Å, the static local field response at the point, $\partial E_{p,x}^{\text{loc}}/\partial E_x^{\text{ext}}$, is around 2 and at the absorption frequency it increases to around 4.5, while at 10 Å it increases from around 1.5 to around 2.5 at the absorption frequency. The local field responses $\partial E_{p,y}^{\text{loc}}/\partial E_x^{\text{ext}}$ and $\partial E_{p,z}^{\text{loc}}/\partial E_x^{\text{ext}}$ are zero for symmetry reasons. At hydrogen atom 16 (see Fig. 3), $\partial E_{I,y}^{\text{loc}}/\partial E_x^{\text{ext}}$ is larger than $\partial E_{I,x}^{\text{loc}}/\partial E_x^{\text{ext}}$ and the responses are less dependent on the intermolecular distance compared to the local field factor at the point between the molecules. The response, $\partial E_{I,y}^{\text{loc}}/\partial E_x^{\text{ext}}$, is 0.9 at zero frequency and 3.5 at the absorption frequency, respectively, while $\partial E_{I,x}^{\text{loc}}/\partial E_x^{\text{ext}}$ is 0.6 at zero frequency and -0.5 at the absorption frequency, respectively. The dipole contribution dominates over the charge contribution at the frequencies below the absorption, while they are comparable at the absorption frequency.

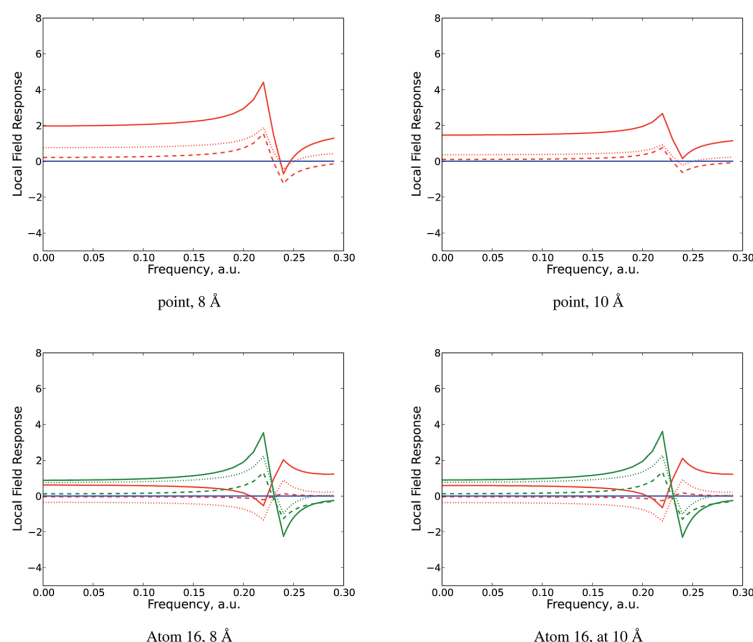


Fig. 4 The local field response of the benzene dimer at a point between the monomers and hydrogen atom 16 in the x -direction of the external electric field at the intermolecular distances of 8 and 10 Å. The red line is $\frac{\partial E_{I,x}^{\text{loc}}}{\partial E_x^{\text{ext}}}$, the green and blue lines are $\frac{\partial E_{I,y}^{\text{loc}}}{\partial E_x^{\text{ext}}}$ and $\frac{\partial E_{I,z}^{\text{loc}}}{\partial E_x^{\text{ext}}}$ respectively. The dashed lines are the charge contribution and the dotted lines are the dipole contribution, respectively (1 a.u. = 27.21 eV).

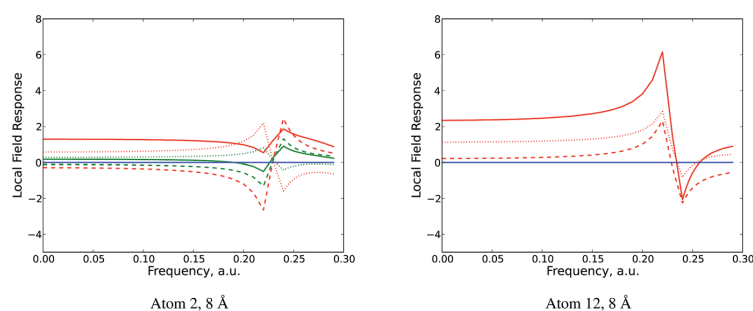


Fig. 5 The local field response of the benzene dimer at carbon atom 2 and hydrogen atom 12 in the x -direction of the external electric field at the intermolecular distance of 8 Å. The red line is $\frac{\partial E_{i,x}^{\text{loc}}}{\partial E_x^{\text{ext}}}$, the green and blue lines are $\frac{\partial E_{i,y}^{\text{loc}}}{\partial E_x^{\text{ext}}}$ and $\frac{\partial E_{i,z}^{\text{loc}}}{\partial E_x^{\text{ext}}}$, respectively. The dashed lines are the charge contribution and the dotted lines are the dipole contribution, respectively (1 a.u. = 27.21 eV).

Fig. 5 shows the local field response at carbon atom 2 and hydrogen atom 12 at 8 Å in the x -direction of the external electric field. The charge term at carbon atom 2 cancels to a large extent the dipole term at the absorption frequency leading to the small local field factor. At 8 Å, the largest local field factor is at hydrogen atoms 12 and 18 which is 2.3 at zero frequency and 6.2 at the absorption frequency. The results show that at these atoms, not only $\frac{\partial E_{i,x}^{\text{loc}}}{\partial E_x^{\text{ext}}}$ increases with frequency, but also $\frac{\partial E_{i,y}^{\text{loc}}}{\partial E_x^{\text{ext}}}$ increases from around 0 to 3.2 at the absorption frequency.

The local field responses at the atoms show that the response at the hydrogen atoms increases more significantly than at the carbon atoms due to a cancellation of the charge and dipole terms at the carbon atoms. $\frac{\partial E_{i,x}^{\text{loc}}}{\partial E_y^{\text{ext}}}$ and $\frac{\partial E_{i,y}^{\text{loc}}}{\partial E_x^{\text{ext}}}$ at the carbon and hydrogen atoms increase from 0.1 and 0.9 to 0.6 and 3.7, respectively, except for the atoms on the x -direction where these two responses are zero because of symmetry reasons. In general, the local field factor of the benzene dimer is large at the hydrogen atoms in the direction of the external electric field as well as at a point between the monomers as compared to at the carbon atoms which is explained if the charge and dipole terms add up or to a large extent cancel each other.

4.2 Azobenzene dimer

Fig. 6 shows the local field response of the azobenzene dimer at a point between the monomers (at the origin of the coordinate system shown in Fig. 3) and at carbon atom 11 in the x -direction of the external electric field at the intermolecular distances 13 and 15 Å (between the center of the azo bonds in the monomers). At the point between the dimers, the local field response at 13 Å, $\frac{\partial E_{p,x}^{\text{loc}}}{\partial E_x^{\text{ext}}}$, is 3.3 at zero frequency, while it is around 7 at the absorption frequency. At 15 Å, it only increases from around 2 at zero frequency to around 4 at the absorption frequency. At carbon atom 11, $\frac{\partial E_{i,x}^{\text{loc}}}{\partial E_x^{\text{ext}}}$ is 1.8 at zero frequency and it increases to 5.4 at the absorption frequency, while $\frac{\partial E_{i,y}^{\text{loc}}}{\partial E_x^{\text{ext}}}$ increases from around 0.1 at zero frequency to 2.3 at the absorption frequency. The charge term adds up to the dipole term giving rise to a larger local field factor as compared

to the carbon atoms in the benzene dimer where the charge and dipole terms to a large extent cancelled each other. The charge contribution increases more significantly at the absorption frequency compared to the dipole contribution as was the case also for the benzene dimer.

Fig. 7 (left) shows the largest local field response of the azobenzene dimer at 13 Å (on a scale different from the other figures). $\frac{\partial E_{i,x}^{\text{loc}}}{\partial E_x^{\text{ext}}}$ at the nitrogen atoms in the azo groups are around 4.5 at zero frequency and 12 at the absorption frequency. $\frac{\partial E_{i,y}^{\text{loc}}}{\partial E_x^{\text{ext}}}$ increases from 2 at zero frequency to around 10 at the absorption frequency. At the nitrogen atoms, the dipole term gives the major contribution to the local field factor whereas the contribution of the charge term is small. The second largest local field response is at hydrogen atoms 12 and 42 where $\frac{\partial E_{i,x}^{\text{loc}}}{\partial E_x^{\text{ext}}}$ at zero frequency is around 3.2 and at the absorption frequency is 7.7 (see Fig. 7 (right)).

The local field response, $\frac{\partial E_{i,y}^{\text{loc}}}{\partial E_x^{\text{ext}}}$, is also large but with an opposite sign at carbon atoms 3, 21, 27 and 45, around -1.4 at zero frequency and -8 at the absorption frequency, where both the charge and dipole terms have the same sign (negative). The local field response, $\frac{\partial E_{i,x}^{\text{loc}}}{\partial E_x^{\text{ext}}}$, at these atoms is smaller (around 1.8 and 3.5 at zero frequency and the absorption frequency, respectively) than $\frac{\partial E_{i,y}^{\text{loc}}}{\partial E_x^{\text{ext}}}$, again because of cancellation of the charge and dipole terms. Thus, in the azobenzene dimer the responses on the carbon and hydrogen atoms are comparable while at the nitrogen atoms they are significantly larger. A large degree of cancellation of charge and dipole terms is found in many of the remaining carbon and hydrogen atoms.

The azobenzene dimer shows in general larger static and frequency-dependent local field factors at the carbon and hydrogen atoms than the benzene dimer. An important feature of the CT-PDI model is the division into a charge and a dipole term which may add up to give a relatively large local field factor or the two terms may to a large extent cancel each other. The dependence on the distance between the dimers is significant, indicating for example that the molecular local field factors will vary substantially for a molecular liquid at normal and elevated temperatures and pressures. The model is presently used for

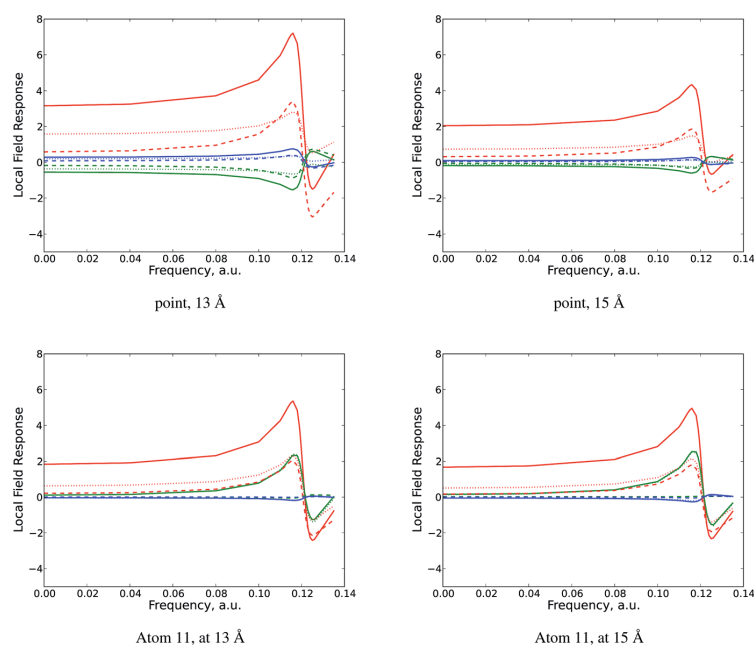


Fig. 6 The local field response of the azobenzene dimer at a point between monomers and carbon atom 11 in the x -direction of the external electric field at the intermolecular distances of 13 and 15 Å. The red line is $\frac{\partial E_{l,x}^{\text{loc}}}{\partial E_x^{\text{ext}}}$, the green and blue lines are $\frac{\partial E_{l,y}^{\text{loc}}}{\partial E_x^{\text{ext}}}$ and $\frac{\partial E_{l,z}^{\text{loc}}}{\partial E_x^{\text{ext}}}$ respectively. The dashed lines are the charge contribution and the dotted lines are the dipole contribution, respectively (1 a.u. = 27.21 eV).

dielectric liquids to determine the local field factor as well as the macroscopic polarization and thereby also the optical part of the dielectric constant is obtained by combining molecular dynamic simulations and a modified Lorentz–Lorentz approach developed for the PDI model.³¹

The local field factors at all atoms of a monomer in the benzene and azobenzene dimers are given in the ESI.†

5 Conclusions

A method to calculate local field factors based on a classical polarization model is presented, and some initial results for the benzene and azobenzene dimers are presented. The response increases significantly at the absorption frequency compared to frequencies below absorption and the largest local field response at the absorption frequency is around 12 at the nitrogen atoms of the azobenzene dimer and around 6 at the

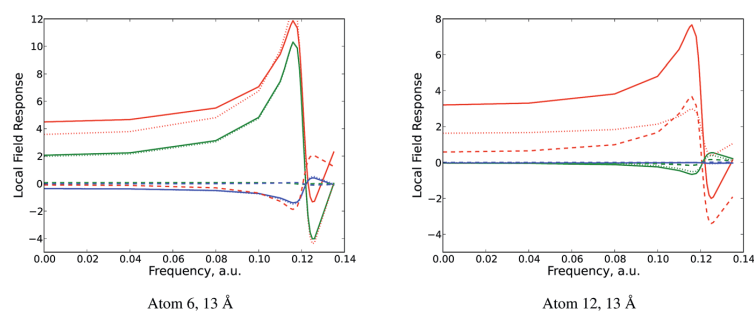


Fig. 7 The local field response of the azobenzene dimer at nitrogen atom 6 and hydrogen atom 12 in the x -direction of the external electric field at the intermolecular distance of 13 Å. The red line is $\frac{\partial E_{l,x}^{\text{loc}}}{\partial E_x^{\text{ext}}}$, the green and blue lines are $\frac{\partial E_{l,y}^{\text{loc}}}{\partial E_x^{\text{ext}}}$ and $\frac{\partial E_{l,z}^{\text{loc}}}{\partial E_x^{\text{ext}}}$ respectively. The dashed lines are the charge contribution and the dotted lines are the dipole contribution, respectively (1 a.u. = 27.21 eV).

hydrogen atoms of the benzene dimer. The presented method is a rapid alternative to quantum calculations for large systems and for a combination with molecular dynamics simulations where we need to average over many configurations.¹¹⁹ A major advantage of a force-field model is the division into different terms, each with a physical interpretation, in this case a charge and a dipole term. In addition to the local field factor, the present version of the CT-PDI model gives the first absorption maximum and the frequency-dependent polarizability. In the future this method will be useful for modeling the static and optical properties of much larger systems, including molecular aggregates sampled from molecular dynamics simulations.¹²⁰

Acknowledgements

ND and POÅ would like to acknowledge a research grant "Modeling of electrical pre-breakdown and breakdown phenomena in insulating liquids" (200631/560) from the Norwegian Research Council, ABB and Statnett and a grant of computer time (account nn2920k) from the NOTUR project. GCS acknowledges support from the Castl Center (Center for Chemistry at the Space-Time Limit). This is supported by the National Science Foundation, grant CHE-1414466. This project was initiated when POÅ was on a one-year sabbatical at Northwestern University, which is acknowledged.

References

- 1 C. J. F. Böttcher, *Theory of Electric Polarization*, Elsevier, Amsterdam, Netherlands, 2nd edn, 1973, vol. 1.
- 2 J. D. Jackson, *Classical Electrodynamics*, John Wiley and Sons, New York, 2nd edn, 1975.
- 3 R. Wortmann and D. M. Bishop, *J. Chem. Phys.*, 1998, **108**, 1001–1007.
- 4 C. Kittel, *Introduction to Solid State Physics*, Wiley, New York, 4th edn, 1971.
- 5 J. Olsen and P. Jørgensen, *J. Chem. Phys.*, 1985, **82**, 3235–3264.
- 6 E. Runge and E. K. U. Gross, *Phys. Rev. Lett.*, 1984, **52**, 997–1000.
- 7 P. Lazzeretti, *Adv. Chem. Phys.*, 1987, **75**, 507–549.
- 8 P. Lazzeretti and R. Zanasi, *Chem. Phys. Lett.*, 1980, **71**, 529–533.
- 9 P. Lazzeretti and R. Zanasi, *Phys. Rev. A*, 1981, **24**, 1696–1704.
- 10 A. Soncini, P. Lazzeretti, V. Bakken and T. Helgaker, *J. Chem. Phys.*, 2004, **120**, 3142–3151.
- 11 C. V. Caillie and R. D. Amos, *Chem. Phys. Lett.*, 1998, **291**, 71–77.
- 12 S. J. A. van Gisbergen, J. G. Snijders and E. J. Baerends, *J. Chem. Phys.*, 1998, **109**, 10657–10668.
- 13 S. J. A. van Gisbergen, F. Kootstra, P. R. T. Schipper, O. V. Gritsenko, J. G. Snijders and E. J. Baerends, *Phys. Rev. A*, 1998, **57**, 2556–2571.
- 14 D. Guillaumont and S. Nakamura, *Dyes Pigm.*, 2000, **46**, 85–92.
- 15 N. T. Maitra and M. van Faassen, *J. Chem. Phys.*, 2007, **126**, 191106.
- 16 M. E. Casida and D. R. Salahub, *J. Chem. Phys.*, 2000, **113**, 8918–8935.
- 17 K. Burke, J. Werschnik and E. K. Gross, *J. Chem. Phys.*, 2005, **123**, 062206.
- 18 L. Jensen and N. Govind, *J. Phys. Chem. A*, 2009, **113**, 9761–9765.
- 19 M. A. Rohrdanz, K. M. Martins and M. Herbert, *J. Chem. Phys.*, 2009, **130**, 054112.
- 20 B. M. Wong and T. H. Hsieh, *J. Chem. Theory Comput.*, 2010, **6**, 3704–3712.
- 21 T. Körzdöfer, J. S. Sears, C. Sutton and J.-L. Brédas, *J. Chem. Phys.*, 2011, **135**, 204107.
- 22 L. Kronik, T. Stein, S. Rafaely-Abramson and R. Baer, *J. Chem. Theory Comput.*, 2012, **8**, 1515–1531.
- 23 H. Phillips, Z. Zheng, E. Geva and B. D. Dunietz, *Org. Electron.*, 2014, **15**, 1509–1520.
- 24 L. Silberstein, *Philos. Mag.*, 1917, **33**, 92–128.
- 25 L. Silberstein, *Philos. Mag.*, 1917, **33**, 521–533.
- 26 J. Applequist, J. R. Carl and K.-F. Fung, *J. Am. Chem. Soc.*, 1972, **94**, 2952–2960.
- 27 J. Applequist, *Acc. Chem. Res.*, 1977, **10**, 79–85.
- 28 K. A. Bode and J. Applequist, *J. Phys. Chem.*, 1996, **100**, 17820–17824.
- 29 L. Jensen, O. H. Schmidt, K. V. Mikkelsen and P.-O. Åstrand, *J. Phys. Chem. B*, 2000, **104**, 10462–10466.
- 30 L. Jensen, P.-O. Åstrand and K. V. Mikkelsen, *Nano Lett.*, 2003, **3**, 661–665.
- 31 L. Jensen, P.-O. Åstrand and K. V. Mikkelsen, *J. Phys. Chem. B*, 2004, **108**, 8226–8233.
- 32 M. Swart, J. G. Snijders and P. T. van Duijnen, *J. Comput. Methods Sci. Eng.*, 2004, **4**, 419–425.
- 33 L. Jensen, P.-O. Åstrand and K. V. Mikkelsen, *J. Phys. Chem. A*, 2004, **108**, 8795–8800.
- 34 M. van Faassen, L. Jensen, J. A. Berger and P. L. de Boeij, *Chem. Phys. Lett.*, 2004, **395**, 274–278.
- 35 J. Kongsted, A. Osted, L. Jensen, P.-O. Åstrand and K. V. Mikkelsen, *J. Phys. Chem. B*, 2001, **105**, 10243–10248.
- 36 T. Hansen, L. Jensen, P.-O. Åstrand and K. V. Mikkelsen, *J. Chem. Theory Comput.*, 2005, **1**, 626–633.
- 37 J. Applequist, *J. Chem. Phys.*, 1973, **58**, 4251–4259.
- 38 J. Applequist, *J. Am. Chem. Soc.*, 1973, **95**, 8258–8262.
- 39 K. R. Sundberg, *J. Chem. Phys.*, 1978, **68**, 5271–5276.
- 40 J. Applequist, *J. Phys. Chem. A*, 1998, **102**, 7723–7724.
- 41 K. R. Sundberg, *J. Chem. Phys.*, 1977, **66**, 114–118.
- 42 A. D. Buckingham, E. P. Conannon and I. D. Hands, *J. Phys. Chem.*, 1994, **98**, 10455–10459.
- 43 L. Jensen, K. O. Sylvester-Hvid, K. V. Mikkelsen and P.-O. Åstrand, *J. Phys. Chem. A*, 2003, **107**, 2270–2276.
- 44 L. Jensen, A. L. Esbensen, P.-O. Åstrand and K. V. Mikkelsen, *J. Comput. Methods Sci. Eng.*, 2006, **6**, 353–364.
- 45 L. Jensen, P.-O. Åstrand and K. V. Mikkelsen, *J. Comput. Theor. Nanosci.*, 2009, **6**, 270–291.
- 46 W. J. Mortier, K. van Genechten and J. Gasteiger, *J. Am. Chem. Soc.*, 1985, **107**, 829–835.

- 47 A. K. Rappé and W. A. Goddard III, *J. Phys. Chem.*, 1991, **95**, 3358–3363.
- 48 H. A. Stern, G. A. Kaminski, J. L. Banks, R. Zhou, B. J. Berne and R. A. Friesner, *J. Phys. Chem. B*, 1999, **103**, 4730–4737.
- 49 R. Chelli, P. Procacci, R. Righini and S. Califano, *J. Chem. Phys.*, 1999, **111**, 8569–8575.
- 50 L. Jensen, P.-O. Åstrand and K. V. Mikkelsen, *Int. J. Quantum Chem.*, 2001, **84**, 513–522.
- 51 R. A. Nistor, J. G. Polihronov, M. H. Müser and N. J. Mosey, *J. Chem. Phys.*, 2006, **125**, 094108.
- 52 D. Mathieu, *J. Chem. Phys.*, 2007, **127**, 224103.
- 53 J. Chen and T. J. Martínez, *Chem. Phys. Lett.*, 2007, **438**, 315–320.
- 54 G. Lee Warren, J. E. Davis and S. Patel, *J. Chem. Phys.*, 2008, **128**, 144110.
- 55 J. Chen, D. Hundertmark and T. J. Martínez, *J. Chem. Phys.*, 2008, **129**, 214113.
- 56 R. A. Nistor and M. H. Müser, *Phys. Rev. B: Condens. Matter Mater. Phys.*, 2009, **79**, 104303.
- 57 H. S. Smalø, P.-O. Åstrand and L. Jensen, *J. Chem. Phys.*, 2009, **131**, 044101.
- 58 H. A. Stern, F. Rittner, B. J. Berne and R. A. Friesner, *J. Chem. Phys.*, 2001, **115**, 2237–2251.
- 59 A. Mayer, *Appl. Phys. Lett.*, 2005, **86**, 153110.
- 60 A. Mayer, *Phys. Rev. B: Condens. Matter Mater. Phys.*, 2005, **71**, 235333.
- 61 A. Mayer, P. Lambin and R. Langlet, *Appl. Phys. Lett.*, 2006, **89**, 063117.
- 62 A. Mayer, *Phys. Rev. B: Condens. Matter Mater. Phys.*, 2007, **75**, 045407.
- 63 A. Mayer and P.-O. Åstrand, *J. Phys. Chem. A*, 2008, **112**, 1277–1285.
- 64 M. L. Olson and K. R. Sundberg, *J. Chem. Phys.*, 1978, **69**, 5400–5404.
- 65 J. Applequist, *J. Phys. Chem.*, 1993, **97**, 6016–6023.
- 66 B. Shanker and J. Applequist, *J. Phys. Chem.*, 1994, **98**, 6486–6489.
- 67 L. L. Jensen and L. Jensen, *J. Phys. Chem. C*, 2008, **112**, 15697–15703.
- 68 L. Jensen, P.-O. Åstrand, K. O. Sylvester-Hvid and K. V. Mikkelsen, *J. Phys. Chem. A*, 2000, **104**, 1563–1569.
- 69 A. Mayer, P. Lambin and P.-O. Åstrand, *Nanotechnology*, 2008, **19**, 025203.
- 70 A. Mayer, A. L. González, C. M. Aikens and G. C. Schatz, *Nanotechnology*, 2009, **20**, 195204.
- 71 A. Mayer and G. C. Schatz, *J. Phys.: Condens. Matter*, 2009, **21**, 325301.
- 72 J. Applequist, K. R. Sundberg, M. L. Olson and L. C. Weiss, *J. Chem. Phys.*, 1979, **70**, 1240–1246.
- 73 B. Shanker and J. Applequist, *J. Chem. Phys.*, 1996, **104**, 6109–6116.
- 74 H. S. Smalø, P.-O. Åstrand and A. Mayer, *Mol. Phys.*, 2013, **111**, 1470.
- 75 Sh. Haghiani, N. Davari, R. Sandnes and P.-O. Åstrand, *J. Phys. Chem. A*, 2014, **118**, 11282–11292.
- 76 J. C. Devins, S. J. Rzad and R. J. Schwabe, *J. Appl. Phys.*, 1981, **52**, 4531–4545.
- 77 H. S. Smalø, Ø. Hestad, S. Ingebrigtsen and P.-O. Åstrand, *J. Appl. Phys.*, 2011, **109**, 073306.
- 78 N. Davari, P.-O. Åstrand, S. Ingebrigtsen and M. Unge, *J. Appl. Phys.*, 2013, **113**, 143707.
- 79 N. Davari, P.-O. Åstrand and T. Van Voorhis, *Mol. Phys.*, 2013, **111**, 1456–1461.
- 80 N. Davari, P.-O. Åstrand, M. Unge, L. E. Lundgaard and D. Linhjell, *AIP Adv.*, 2014, **4**, 037117.
- 81 H. Metiu and P. Das, *Annu. Rev. Phys. Chem.*, 1984, **35**, 507–536.
- 82 M. Moskovits, *Rev. Mod. Phys.*, 1985, **57**, 783–826.
- 83 G. S. Kedziora and G. C. Schatz, *Spectrochim. Acta, Part A*, 1999, **55**, 625–638.
- 84 M. Futamata, Y. Maruyama and M. Ishikawa, *J. Phys. Chem. B*, 2003, **107**, 7607–7617.
- 85 L. Zhao, L. Jensen and G. C. Schatz, *J. Am. Chem. Soc.*, 2006, **128**, 2911–2919.
- 86 L. Jensen, L. L. Zhao and G. C. Schatz, *J. Phys. Chem. C*, 2007, **111**, 4756–4764.
- 87 A. E. Johnson and A. B. Myers, *J. Phys. Chem.*, 1996, **100**, 7778–7788.
- 88 R. Shimada and H. Hamaguchi, *J. Chem. Phys.*, 2014, **140**, 204506.
- 89 E. B. Guidez and C. M. Aikens, *J. Phys. Chem. C*, 2013, **117**, 21466–21475.
- 90 A. Manjavacas, F. Marchesin, S. Thongrattanasiri, P. Koval, P. Nordlander, D. Sánchez-Portal and F. J. García de Abajo, *ACS Nano*, 2013, **7**, 3635–3643.
- 91 L. Jensen, P.-O. Åstrand, A. Osted, J. Kongsted and K. V. Mikkelsen, *J. Chem. Phys.*, 2002, **116**, 4001–4010.
- 92 G. A. van der Velde, *A Realistic Coulomb Potential, MD and MC on Water*, ed. H. J. C. Berendsen, CECAM, France, 1972.
- 93 E. K. U. Gross, J. F. Dobson and M. Petersilka, *Top. Curr. Chem.*, 1996, **181**, 81–172.
- 94 M. A. L. Marques and E. K. U. Gross, *Annu. Rev. Phys. Chem.*, 2004, **55**, 427–455.
- 95 J. P. Perdew, K. Burke and M. Ernzerhof, *Phys. Rev. Lett.*, 1996, **77**, 3865–3868.
- 96 E. van Lenthe, E. J. Baerends, C. F. Guerra, S. J. A. van Gisbergen, J. G. Snijders and T. Ziegler, *J. Comput. Chem.*, 2003, **24**, 1142–1156.
- 97 D. P. Chong, *Mol. Phys.*, 2005, **103**, 749–761.
- 98 P. Norman, D. M. Bishop, H. J. A. Jensen and J. Oddershede, *J. Chem. Phys.*, 2001, **115**, 10323–10334.
- 99 L. Jensen, J. Autschbach and G. C. Schatz, *J. Chem. Phys.*, 2005, **122**, 224115.
- 100 C. F. Guerra, J. G. Snijders, G. te Velde and E. J. Baerends, *Theor. Chem. Acc.*, 1998, **99**, 391–401.
- 101 G. te Velde, F. M. Bickelhaupt, E. J. Baerends, C. F. Guerra, S. J. A. van Gisbergen, J. G. Snijders and T. Ziegler, *J. Comput. Chem.*, 2001, **22**, 931–967.
- 102 T. Verstraelen, P. Bultinck, V. V. Speybroeck, P. W. Ayers, D. V. Neck and M. Waroquier, *J. Chem. Theory Comput.*, 2011, **7**, 1750–1764.
- 103 E. Sawicki, *J. Org. Chem.*, 1957, **22**, 915–919.
- 104 T. Halicioğlu and O. Sinanoğlu, *Ann. N. Y. Acad. Sci.*, 1969, **158**, 308–317.

Paper

- 105 H. H. Jaffé, S. J. Yeh and R. W. Gardner, *J. Mol. Struct.*, 1958, **2**, 120–136.
- 106 C. Haessner and H. Mustroph, *J. Prakt. Chem.*, 1987, **329**, 493–498.
- 107 L. M. Yagupol'skij and L. Z. Gandel'sman, *Zh. Obshch. Khim.*, 1965, **35**, 1252–1262.
- 108 J. Lorentzon, P.-Å. Malmqvist, M. Fülcher and B. O. Roos, *Theor. Chim. Acta*, 1995, **91**, 91–108.
- 109 K. J. Miller, *J. Am. Chem. Soc.*, 1990, **112**, 8533–8542.
- 110 K. Kimura and S. Nagakura, *Mol. Phys.*, 1965, **9**, 117–135.
- 111 R. McDiarmid, *J. Chem. Phys.*, 1976, **64**, 514–521.
- 112 C. Van Caillie and R. D. Amos, *Chem. Phys. Lett.*, 2000, **328**, 446.
- 113 J. W. Au, G. Cooper, G. R. Burton, T. N. Olney and C. E. Brion, *Chem. Phys.*, 1993, **173**, 209–239.
- 114 L. W. Pickett, M. Muntz and E. M. McPherson, *J. Am. Chem. Soc.*, 1951, **73**, 4862–4865.
- 115 F. Gerson and E. Heilbronner, *Helv. Chim. Acta*, 1962, **45**, 42–50.
- 116 F. Gerson and E. Heilbronner, *Helv. Chim. Acta*, 1962, **45**, 51–59.
- 117 J. Griffiths and B. Roozpeikar, *J. Chem. Soc., Perkin Trans. 1*, 1976, 42–45.
- 118 R. S. Rowland and R. Taylor, *J. Phys. Chem.*, 1996, **100**, 7384–7391.
- 119 A. Osted, J. Kongsted, K. V. Mikkelsen, P.-O. Åstrand and O. Christiansen, *J. Chem. Phys.*, 2006, **124**, 124503.
- 120 N. Davari, C. D. Daub, P.-O. Åstrand and M. Unge, submitted.

Paper 6

Local electric field factors and dielectric properties of
liquid benzene

Nazanin Davari, Christopher D. Daub, Per-Olof Åstrand and Mikael
Unge

Manuscript



Local field factors and dielectric properties of liquid benzene

Nazanin Davari,[†] Christopher D. Daub,[†] Per-Olof Åstrand,^{*,†} and Mikael Unge[‡]

Department of Chemistry, Norwegian University of Science and Technology (NTNU), NO-7491 Trondheim, Norway, and ABB Corporate Research, SE-72178 Västerås, Sweden

E-mail: per-olof.aastrand@ntnu.no

Abstract

Local electric field factors are calculated for liquid benzene by combining molecular dynamic simulations with a subsequent force-field model based on a combined charge-transfer and point-dipole interaction model for the local field factor. The local field factor is obtained as a linear response of the local field to an external electric field and the response is calculated at frequencies through the first absorption maximum. It is found that the largest static local field factor is around 2.4, while it is around 6.4 at the absorption frequency. The linear susceptibility, the dielectric constant and the first absorption maximum of liquid benzene are also studied. The dielectric constant is around 2.3 at zero frequency in good agreement with experimental data, while it increases to 6.3 at the absorption frequency. The $\pi \rightarrow \pi^*$ excitation energy is around 6.0 eV as compared to the gas phase value of around 6.3 eV.

In a molecular mechanics approach, the local electric field at an atom, $E_{I,\alpha}^{\text{loc}}$, is the sum of the external electric field, $E_{I,\alpha}^{\text{ext}}$, and the electric field of the permanent and induced multipole

*To whom correspondence should be addressed

[†]Department of Chemistry, Norwegian University of Science and Technology (NTNU), NO-7491 Trondheim, Norway

[‡]ABB Corporate Research, SE-72178 Västerås, Sweden

moments of the neighbouring atoms, here restricted to atomic charges and atomic dipole moments,

$$E_{I,\alpha}^{\text{loc}} = E_{I,\alpha}^{\text{ext}} + \sum_{J \neq I}^N \frac{-R_{IJ,\alpha}}{\tilde{R}_{IJ}^3} q_J + \frac{3R_{IJ,\alpha}R_{IJ,\beta} - \delta_{\alpha\beta}\tilde{R}_{IJ}^2}{\tilde{R}_{IJ}^5} \mu_{J,\beta} \quad (1)$$

where Greek subscripts α , β and γ denote the Cartesian coordinates and the Einstein summation convention is used for repeated subscripts. q_J is an atomic charge and $\mu_{J,\beta}$ is an atomic dipole moment. In our model, \tilde{R}_{IJ} is a scaled distance between atoms I and J ,

$$\tilde{R}_{IJ} = \sqrt{R_{IJ}^2 + \frac{\pi}{4} \frac{\phi_I \phi_J}{\phi_I + \phi_J}} \quad (2)$$

where ϕ_I is an atom-type parameter describing the width of a Gaussian charge distribution. $R_{IJ,\alpha} = R_{I,\alpha} - R_{J,\alpha}$, where $R_{I,\alpha}$ is a component of the coordinate of atom I .

The local field effects at zero and optical frequencies are important in many applications. In surface-enhanced Raman scattering (SERS),¹⁻⁴ local field enhancement is observed in plasmonic nanoparticles showing very strong scattering of light due to the localized surface plasmon resonances.⁵⁻⁷ In addition to metal nanoparticles, the plasmonic character of some aromatic molecules such as linear acenes also enhances the local field factor.⁸ In resonance Raman and resonance Hyper-Raman spectra,^{9,10} the intermolecular vibronic coupling between solute molecules and neighbouring solvent molecules causes enhanced local fields, a phenomenon called the molecular near-field effect.¹¹

The local field at a molecule is caused by polarization of the surroundings and it is a measure of the strength of the interaction between the solute and the solvent molecules and thus it is used to determine the solvent induced effects on molecular properties.¹²⁻¹⁴ It can also be used in calculating the dielectric constant and refractive index of different materials.¹⁵ In electrical breakdown of insulating liquids,¹⁶ finding points where the local field is very high, i.e. *hot-spots*, is useful. At hot-spots, an electron avalanche may be initiated that can lead to a conductive plasma channel and an electrical breakdown.

The response of the local field to the external electric field has been calculated at the Hartree-Fock level of theory in terms of the nuclear electric shielding factor, which is the effective field seen by the nucleus.¹⁷⁻¹⁹ In our recent work on force-field models, a combined charge-transfer and point-dipole interaction (CT-PDI) model is extended to calculate the local field factor and initial results were presented for the benzene and azobenzene dimers.²⁰ Here, we extend the study of local field factors to aggregates of molecules, in this case liquid benzene due to its application in breakdown experiments.^{21,22}

The CT-PDI model²³⁻²⁵ is basically a model to calculate the static and frequency-dependent polarizabilities, where the polarizability is partitioned into charge-transfer and dipole terms. In the CT-PDI model, these terms are obtained using the electronegativity equalization model (EEM)²⁶⁻²⁸ rephrased in terms of the atom-atom charge-transfer (AACT) model²⁹ in combination with the point-dipole interaction (PDI) model.³⁰⁻³⁴

The CT-PDI model has several important features: (i) Atomic charges are replaced by charge-transfer terms using the AACT model, $q_I = \sum_K^N q_{IK}$.²⁹ (ii) A Gaussian charge

distribution is used for each atom instead of point charges.³⁵ (iii) The model can be used for both metallic and non-metallic systems, i.e. polarizabilities scale correctly with the size of the system.²³ In a metallic model such as EEM, the charge-transfer between two atoms at infinite distance is not zero. In the CT-PDI model, an energy cost for charge-transfer between atoms is added such that the charge-transfer is zero between atoms at infinite separation.^{23,24} (iv) The partitioning of the polarizability into charge and dipole terms is advantageous since for different types of molecules the main contribution will vary. For example, in azo dyes, the contribution of the dipole term to the polarizability at the absorption frequency is more significant than the charge term.²⁵ Also the charge and the dipole term may add up to give a relatively large local field factor or the two terms may to a large extent cancel each other.²⁰

The linear response of the charge-transfer and the dipole terms to a homogenous frequency-dependent external electric field, $E_{I,\alpha}^{\text{ext}}(\omega) = E_{\alpha}^{\text{ext}}(\omega)$, is calculated by solving the Lagrangian involving potential energies and kinetic energies of the atomic charge-transfer terms and the atomic dipole moments oscillating with the same frequency as the external electric field.^{24,36} The details of the model can be found in Ref. 24.

The parameters of the CT-PDI model are optimized by fitting the full tensor of the complex frequency-dependent polarizabilities against time-dependent density functional theory (TDDFT)³⁷⁻³⁹ polarizabilities through the first absorption maximum adopting finite life times of the excited state.^{40,41} The parameters are not reoptimized in this work but the values reported previously for a series of hydrocarbon and azo molecules are adopted here.²⁰

The molecular-dynamics (MD) simulations are performed using the LAMMPS package, version June 28, 2014⁴² to generate sample configurations as shown in Figure 1. A system of 216 benzene molecules is generated in a cubic box with a length of 31.8 Å and periodic boundary conditions. The cut-off distance for van der Waals interactions is 15 Å and the force-field model used is OPLS-AA.⁴³⁻⁴⁵ The system is equilibrated for 500 ps and trajectories are generated in the canonical (NVT) ensemble at 300 K employing the Nosé-Hoover thermostat.^{46,47} The simulation results are in good agreement with Ref. 45. The radial distribution functions (RDFs) are collected over 1500 ps and the carbon RDF shows a small peak at around 4.3 Å and two large peaks at around 5.3 and 6.2 Å in good agreement with experimental data.⁴⁸ Snapshots of structures are taken every 2.5 ps and 50 benzene molecules are chosen such that a benzene molecule is located at the center of the box and the molecules are rotated to be aligned to the axes of the moment of inertia of the central molecule. 100 configurations are chosen and the local field factor is calculated at carbon atom 1 and hydrogen atom 2 of the central molecule marked in blue in Figure 1, giving 600 samples in total from the equivalence of carbon and hydrogen atoms in benzene.

Figure 2 shows the local field factor distribution of the carbon and hydrogen atoms in the static limit and at the absorption frequency around 0.22 a.u. (6.0 eV). Only four components, $\partial E_{I,x}^{\text{loc}}/\partial E_x^{\text{ext}}$, $\partial E_{I,y}^{\text{loc}}/\partial E_y^{\text{ext}}$, $\partial E_{I,x}^{\text{loc}}/\partial E_y^{\text{ext}}$ and $\partial E_{I,z}^{\text{loc}}/\partial E_z^{\text{ext}}$ are shown since the other components have distributions very similar to $\partial E_{I,x}^{\text{loc}}/\partial E_y^{\text{ext}}$. At zero frequency, the distributions are narrower than at the absorption frequency and the largest local field factors, $\partial E_{I,x}^{\text{loc}}/\partial E_x^{\text{ext}}$, $\partial E_{I,y}^{\text{loc}}/\partial E_y^{\text{ext}}$, $\partial E_{I,x}^{\text{loc}}/\partial E_y^{\text{ext}}$ and $\partial E_{I,z}^{\text{loc}}/\partial E_z^{\text{ext}}$ at the carbon atom are around 1.8, 1.2, 0.2 and 0.6, respectively, while at the hydrogen atom are around 0.3, 2.4, 0.2 and 0.9, respectively. At the absorption frequency, the largest local field factors, $\partial E_{I,x}^{\text{loc}}/\partial E_x^{\text{ext}}$, $\partial E_{I,y}^{\text{loc}}/\partial E_y^{\text{ext}}$, $\partial E_{I,x}^{\text{loc}}/\partial E_y^{\text{ext}}$ and $\partial E_{I,z}^{\text{loc}}/\partial E_z^{\text{ext}}$ at the carbon atom are around -1.3, 2.1, 1.0 and 1.5, respectively, while at the hydrogen atom they are around -4.8, 6.4, 1.1 and 1.9,

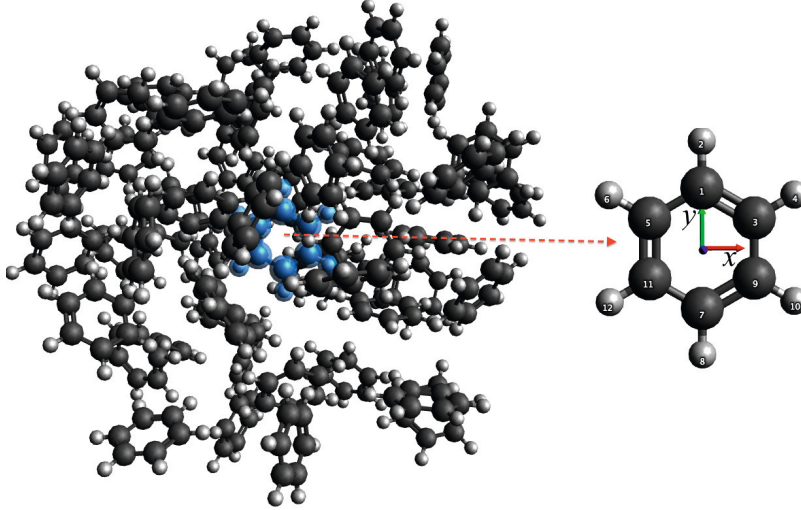


Figure 1: A typical sample with the central benzene molecule marked in blue.

respectively.

Since we are interested in large local field enhancements, atoms with high local field factors are studied in more detail. From the distribution plots, we found that the largest local field factor at the absorption frequency is 6.4 at the hydrogen atom. The local field factor at the hydrogen atom for this configuration is shown in Figure 3 as a function of frequency. The local field factor, $\partial E_{I,y}^{\text{loc}}/\partial E_y^{\text{ext}}$, increases from 2.4 at zero frequency to 6.4 at the absorption frequency. The dipole contribution to the local field factor is larger than the charge term at frequencies below the absorption, while they are comparable at the absorption frequency in line with our previous results.²⁰ The hydrogen RDF has three peaks located around 3.4, 4.6 and 6.7 Å, respectively. The intermolecular H-H distance in this configuration is around 2 Å which results in a large local field factor since the local field factor depends strongly on the intermolecular distances.²⁰

In Figure 4, the average of $\partial E_{I,y}^{\text{loc}}/\partial E_y^{\text{ext}}$ and its variance at the hydrogen atom are shown as a function of the number of samples. Both quantities achieve reasonable convergence after 100 samples, indicating that the chosen number of samples is sufficient for the local field factor calculations.

The linear susceptibility is calculated using the CT-PDI model by combining molecular dynamic simulations and a modified Clausius-Mossotti equation,¹⁵ where the PDI model is combined with the Clausius-Mossotti equation.⁴⁹ Here, the CT-PDI model is used instead of the PDI model which gives an improvement by including the charge-transfer terms and the complex frequency-dependence as compared to the PDI model including only the static dipole term. Assuming the polarization in z -direction of the external field, the macroscopic polarization, P_z , is given in terms of the molecular induced dipole moments,^{15,50,51}

$$P_z = N_d \langle \mu_\alpha \rangle_z = N_d \langle \alpha_{\alpha\beta}^{\text{mol}} \rangle E_z^{\text{loc}} \quad (3)$$

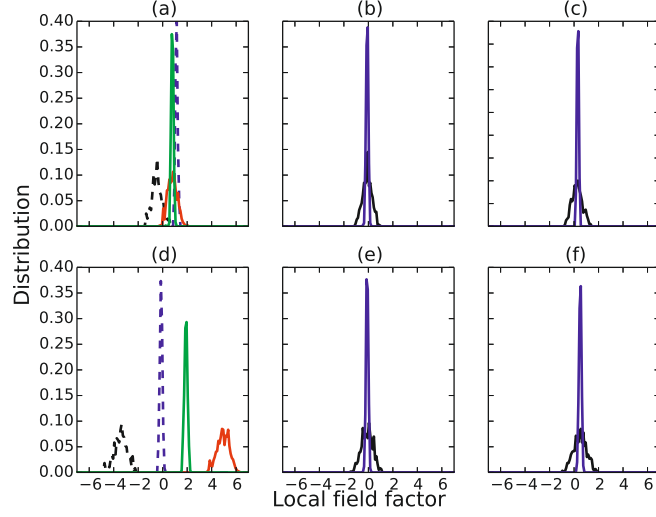


Figure 2: The local field factor distribution of the carbon (a,b,c), and hydrogen (d,e,f) atoms, respectively. The dashed line in (a) and (d) is $\frac{\partial E_{I,x}^{\text{loc}}}{\partial E_y^{\text{ext}}}$ and the solid line is $\frac{\partial E_{I,y}^{\text{loc}}}{\partial E_x^{\text{ext}}}$. (b) and (e) are $\frac{\partial E_{I,x}^{\text{loc}}}{\partial E_x^{\text{ext}}}$, and (c) and (f) are $\frac{\partial E_{I,z}^{\text{loc}}}{\partial E_z^{\text{ext}}}$. The blue and green lines are at zero frequency and the black and red lines are at the absorption frequency, respectively.

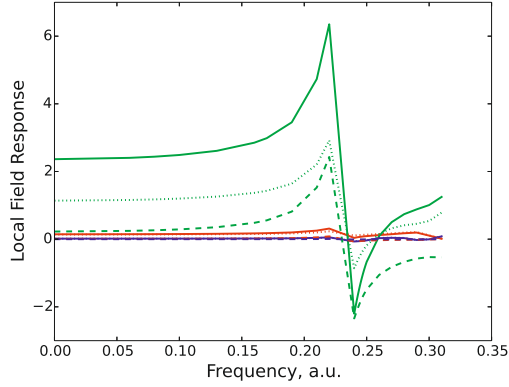


Figure 3: The largest local field response to the y -direction of the external electric field at the hydrogen atom in liquid benzene. The green line is $\frac{\partial E_{I,y}^{\text{loc}}}{\partial E_x^{\text{ext}}}$ and the red and blue lines are $\frac{\partial E_{I,x}^{\text{loc}}}{\partial E_y^{\text{ext}}}$ and $\frac{\partial E_{I,z}^{\text{loc}}}{\partial E_y^{\text{ext}}}$, respectively. The dashed line is the charge contribution and the dotted line is the dipole contribution. (1 a.u. = 27.21 eV)

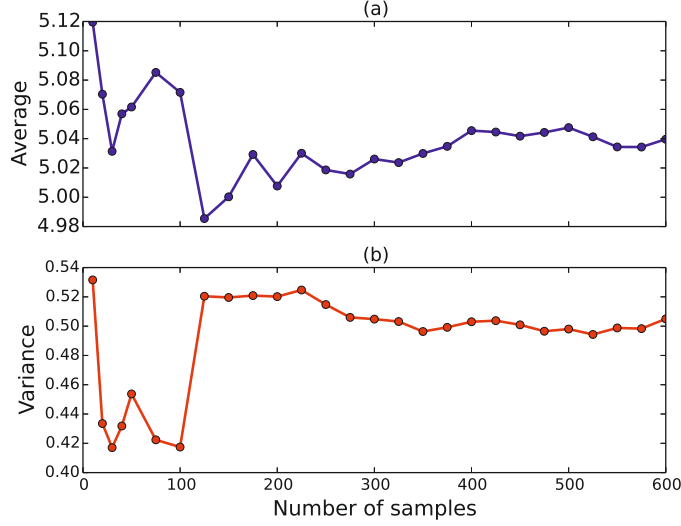


Figure 4: The average (a) and the variance (b) of the local field factor, $\frac{\partial E_{x,y}^{\text{loc}}}{\partial E_y^{\text{ext}}}$, at the hydrogen atom at the absorption frequency as a function of the number of samples.

where N_d is the number density and $\langle \alpha_{\alpha\beta}^{\text{mol}} \rangle = \frac{1}{3}(\alpha_{xx} + \alpha_{yy} + \alpha_{zz})$ is the isotropic molecular polarizability. The linear susceptibility, $\chi_{zz}^{(1)}$ is defined as^{15,50,51}

$$\chi_{zz}^{(1)} = \frac{\partial P_z}{\partial E_z^{\text{ext}}} = \frac{N_d \langle \alpha_{\alpha\beta}^{\text{mol}} \rangle}{1 - \frac{4\pi}{3} N_d \langle \alpha_{\alpha\beta}^{\text{mol}} \rangle} \quad (4)$$

The dielectric constant, ϵ , is obtained as^{15,50,51}

$$\epsilon = 1 + 4\pi \chi_{zz}^{(1)} \quad (5)$$

The refractive index is thereby calculated from the square root of the dielectric constant.¹⁵ As shown elsewhere, the Clausius-Mossotti relation can be improved by replacing the gas phase value of $\langle \alpha_{\alpha\beta}^{\text{mol}} \rangle$ by the value obtained for a molecule in a cluster using a classical force-field model.⁴⁹

Figure 5 shows the distribution of the linear susceptibility at zero and the absorption frequency, respectively, and the dielectric constant as a function of frequency. The linear susceptibility is distributed around 0.1 at zero frequency, while it is around 0.4 at the absorption frequency. The real part of the dielectric constant is 2.3 at zero frequency in good agreement with the experimental value of 2.2⁵² and it increases to 6.3 at the absorption frequency. The imaginary part of the dielectric constant is around 6.6 at the absorption frequency. From the imaginary part, one can find the dielectric loss of the liquid which is an important factor in for example insulation applications in high-voltage devices.

To summarize, we have applied a model for the calculation of the local field factor which

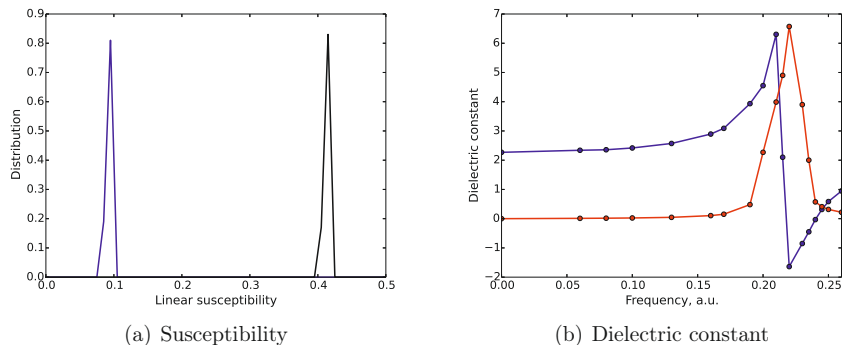


Figure 5: (a) The susceptibility distribution of liquid benzene at zero (blue) and the absorption (black) frequencies. (b) The dielectric constant of liquid benzene. The real and imaginary parts are shown in blue and red, respectively.

can be used for relatively large systems such as molecular clusters and macromolecules. For liquid benzene, the decomposition of the local field factor into charge and dipole terms indicates that the static local field is dominated by the dipole term, while at the absorption frequency, they contribute almost equally. At the carbon atom, the difference between the average local field factor at zero and the absorption frequency is around 0 for $\partial E_{I,y}^{\text{loc}}/\partial E_y^{\text{ext}}$, $\partial E_{I,x}^{\text{loc}}/\partial E_y^{\text{ext}}$ and $\partial E_{I,z}^{\text{loc}}/\partial E_z^{\text{ext}}$, respectively, while it is around 1.6 for $\partial E_{I,x}^{\text{loc}}/\partial E_x^{\text{ext}}$. At the hydrogen atom, the differences are around 3, 0, 0, and 3.3 for $\partial E_{I,y}^{\text{loc}}/\partial E_y^{\text{ext}}$, $\partial E_{I,x}^{\text{loc}}/\partial E_y^{\text{ext}}$, $\partial E_{I,z}^{\text{loc}}/\partial E_z^{\text{ext}}$ and $\partial E_{I,x}^{\text{loc}}/\partial E_x^{\text{ext}}$, respectively. The smaller difference at the carbon atom compared to the hydrogen atom is related to the cancellation of charge and dipole terms at the absorption frequency which leads to a local field factor comparable to the static one. An advantage of a force-field model is the division into different contributions, in this case a charge and a dipole contribution. Therefore we can classify the local field factors in two groups, either the charge and dipole terms add up to a substantial contribution or they to a large extent cancel each other.

In addition to the local field factor, the model gives other static and optical properties at both the microscopic and the macroscopic scales such as the polarizability, susceptibility, dielectric constant and absorption spectrum. It has been demonstrated that the CT-PDI model is capable of predicting the shift in excitation energies in good agreement with TDDFT for systems with different chain lengths, for example alkanes and polyenes and also for aromatic molecules and azo dyes with different substituents.^{20,25} The $\pi \rightarrow \pi^*$ excitation energy of benzene in liquid phase is calculated to be around 6.0 eV, while it is around 6.3 eV in the gas phase. The experimental liquid-phase excitation energy is around 6.5 eV, while it is around 6.9 eV in the gas phase.⁵³ Thus, the CT-PDI shift in excitation energy when comparing the gas and liquid phases is in good agreement with the experimental shift.

Developing the model further by including higher-order terms such as hyperpolarizabilities, nonlinear susceptibilities and quadrupole moments can substantially improve the physics of the model and provide a useful tool for the calculation of numerous optical properties used

in different applications.

Acknowledgement

The authors are grateful for a research grant “Modeling of electrical pre-breakdown and breakdown phenomena in insulating liquids” (200631/560) from the Norwegian Research Council, ABB and Statnett and a grant of computer time (account nn2920k) from the NOTUR project.

References

- (1) Metiu, H.; ; Das, P. *Ann. Rev. Phys. Chem.* **1984**, *35*, 507–536.
- (2) Moskovits, M. *Rev. Mod. Phys.* **1985**, *57*, 783–826.
- (3) Kedziora, G. S.; Schatz, G. C. *Spectrochim. Acta A* **1999**, *55*, 625–638.
- (4) Futamata, M.; Maruyama, Y.; Ishikawa, M. *J. Phys. Chem. B* **2003**, *107*, 7607–7617.
- (5) Zhang, J. Z. *J. Phys. Chem. Lett.* **2010**, *1*, 686–695.
- (6) Rycenga, M.; Camargo, P. H. C.; Li, W.; Moran, C. H.; Xia, Y. *J. Phys. Chem. Lett.* **2010**, *1*, 696–703.
- (7) Sarkar, S.; Pradhan, M.; Sinha, A. K.; Basu, M.; Chelate Pal, T. *J. Phys. Chem. Lett.* **2010**, *1*, 439–444.
- (8) Guidez, E. B.; Aikens, C. M. *J. Phys. Chem. C* **2013**, *117*, 21466–21475.
- (9) Johnson, A. E.; Myers, A. B. *J. Phys. Chem.* **1996**, *100*, 7778–7788.
- (10) Shimada, R.; Hamaguchi, H. *J. Chem. Phys.* **2014**, *140*, 204506.
- (11) Shimada, R.; Kano, H.; Hamaguchi, H. *J. Raman Spect.* **2006**, *37*, 469–471.
- (12) Orozco, M.; Luque, F. J. *Chem. Rev.* **2000**, *100*, 4187–4225, Erratum in **101**, 203, 2001.
- (13) Mennucci, B.; Cappelli, C.; Cammi, R.; Tomasi, J. *Chirality* **2011**, *23*, 717–729.
- (14) Egidi, F.; Giovannini, T.; Piccardo, M.; Bloino, J.; Cappelli, C.; Barone, V. *J. Chem. Theory Comput.* **2014**, *10*, 2456–2464.
- (15) Jackson, J. D. *Classical Electrodynamics*, 2nd ed.; John Wiley and Sons: New York, 1975.
- (16) Devins, J. C.; Rzed, S. J.; Schwabe, R. J. *J. Appl. Phys.* **1981**, *52*, 4531–4545.
- (17) Lazzeretti, P.; Zanasi, R. *Chem. Phys. Lett.* **1980**, *71*, 529–533.

- (18) Lazzeretti, P.; Zanasi, R. *Phys. Rev. A* **1981**, *24*, 1696–1704.
- (19) Soncini, A.; Lazzeretti, P.; Bakken, V.; Helgaker, T. *J. Chem. Phys.* **2004**, *120*, 3142–3151.
- (20) Davari, N.; Haghdani, S.; Åstrand, P.-O.; Schatz, G. C. submitted.
- (21) Yamashita, H.; Amano, H. *IEEE Trans. Elect. Insul.* **1988**, *23*, 739–750.
- (22) Tortai, J. H.; Bonifaci, N.; Denat, A. *IEEE Trans. Dielect. Elect. Insul.* **2002**, *9*, 3–9.
- (23) Smalø, H. S.; Åstrand, P.-O.; Jensen, L. *J. Chem. Phys.* **2009**, *131*, 044101.
- (24) Smalø, H. S.; Åstrand, P.-O.; Mayer, A. *Mol. Phys.* **2013**, *111*, 1470.
- (25) Haghdani, S.; Davari, N.; Sandnes, R.; Åstrand, P.-O. *J. Phys. Chem. A* **2014**, *118*, 11282–11292.
- (26) Mortier, W. J.; van Genechten, K.; Gasteiger, J. *J. Am. Chem. Soc.* **1985**, *107*, 829–835.
- (27) Rappé, A. K.; Goddard III, W. A. *J. Phys. Chem.* **1991**, *95*, 3358–3363.
- (28) Stern, H. A.; Kaminski, G. A.; Banks, J. L.; Zhou, R.; Berne, B. J.; Friesner, R. A. *J. Phys. Chem. B* **1999**, *103*, 4730–4737.
- (29) Chelli, R.; Procacci, P.; Righini, R.; Califano, S. *J. Chem. Phys.* **1999**, *111*, 8569–8575.
- (30) Silberstein, L. *Phil. Mag.* **1917**, *33*, 92–128.
- (31) Silberstein, L. *Phil. Mag.* **1917**, *33*, 521–533.
- (32) Applequist, J.; Carl, J. R.; Fung, K.-F. *J. Am. Chem. Soc.* **1972**, *94*, 2952–2960.
- (33) Applequist, J. *Acc. Chem. Res.* **1977**, *10*, 79–85.
- (34) Bode, K. A.; Applequist, J. *J. Phys. Chem.* **1996**, *100*, 17820–17824.
- (35) Jensen, L.; Åstrand, P.-O.; Osted, A.; Kongsted, J.; Mikkelsen, K. V. *J. Chem. Phys.* **2002**, *116*, 4001–4010.
- (36) Mayer, A.; Lambin, P.; Åstrand, P.-O. *Nanotechnology* **2008**, *19*, 025203.
- (37) Runge, E.; Gross, E. K. U. *Phys. Rev. Lett.* **1984**, *52*, 997–1000.
- (38) Gross, E. K. U.; Dobson, J. F.; Petersilka, M. *Top. Curr. Chem.* **1996**, *181*, 81–172.
- (39) Marques, M. A. L.; Gross, E. K. U. *Ann. Rev. Phys. Chem.* **2004**, *55*, 427–455.
- (40) Norman, P.; Bishop, D. M.; Jensen, H. J. Aa.; Oddershede, J. *J. Chem. Phys.* **2001**, *115*, 10323–10334.

- (41) Jensen, L.; Autschbach, J.; Schatz, G. C. *J. Chem. Phys.* **2005**, *122*, 224115.
- (42) Plimpton, S. *J. Comput. Phys.* **1995**, *117*, 1–19.
- (43) Jorgensen, W. L.; Tirado-Rives, J. *J. Am. Chem. Soc.* **1988**, *110*, 1657–1666.
- (44) Jorgensen, W. L.; Severance, D. L. *J. Am. Chem. Soc.* **1990**, *112*, 4768–4774.
- (45) Fu, C.-F.; Tian, S. X. *J. Chem. Theory Comput.* **2011**, *7*, 2240–2252.
- (46) Nosé, S. *Mol. Phys.* **1984**, *52*, 255–268.
- (47) Hoover, W. G. *Phys. Rev. A* **1985**, *31*, 1695–1697.
- (48) Narten, A. H. *J. Chem. Phys.* **1977**, *67*, 2102.
- (49) Jensen, L.; Åstrand, P.-O.; Mikkelsen, K. V. *J. Phys. Chem. B* **2004**, *108*, 8226–8233.
- (50) Boyd, R. W. *Nonlinear Optics*; Academic Press: San Diego, CA, 1992.
- (51) Böttcher, C. J. F. *Theory of Electric Polarization*, 2nd ed.; Elsevier: Amsterdam, Netherlands, 1973; Vol. 1.
- (52) Mardolcar, U.; Nieto de Castro, C. A.; Santos, F. J. V. *Fluid Phase Equil.* **1992**, *79*, 255–264.
- (53) Inagaki, T. *J. Chem. Phys.* **1972**, *57*, 2526–2530.

